

Estimate of particle rates for
elastic and inelastic
parity-violating electron scattering
off different spin 0 nuclei

by

Shahin Sepanlou

Bachelor thesis in physics
submitted to the Department of Physics, Mathematics and
Computer Science (FB 08)
of Johannes Gutenberg-University Mainz
on 10. May 2021

1. Reviewer: Prof. Dr. Frank Maas
2. Reviewer: Prof. Dr. Josef Pochodzalla

I certify that I have written this paper independently and that I have not used any sources or aids other than those indicated, and that I have marked quotations.

S. Sepanlou

Mainz, 10.05.2021

Abstract: In this thesis we estimate the measuring time for the parity-violating asymmetry in elastic and inelastic electron scattering off different spin 0 nuclei for the P2 experiment at the MESA accelerator in Mainz. With the usage of measured cross sections for ^{12}C , ^{40}Ca , ^{42}Ca , ^{48}Ca and ^{208}Pb from different experiments the electric form factor is calculated and the measuring time is estimated. In order to achieve an analytical expression for the electric form factor different parameterisations for the form factor e.g. the Helm form factor, the Sum of Gaussian or the Fourier Bessel form factors are used. For different precisions of the parity-violating asymmetry different measuring times are calculated. For an accuracy of $\Delta A = 0.1\%$ the measuring time for the cross section averaged asymmetry is between $T = 3260$ h and $T = 45295$ h depending on the nucleus, the parameterisation for the form factor and the polarization of the electron beam.

Contents

1	Introduction	5
2	Theory of parity-violating electron scattering off nuclei with spin 0	6
2.1	Mott scattering and electric form factor of nuclei	6
2.2	Parameterisation of the electric form factor of nuclei	7
2.2.1	The Helm form factor parameterisation	7
2.2.2	The sum of Gaussian functions parameterisation	8
2.2.3	The Fourier-Bessel parameterisation	9
2.2.4	Polynomial function parameterisation	9
2.2.5	Gaussian function parameterisation	10
2.3	Parity-violating asymmetry of electron scattering off spin 0 nuclei	10
2.4	Estimate of the measuring time	12
3	The P2-experiment	14
4	Preparatory work	16
4.1	Compilation of scattering cross section world data	16
4.2	Overview of ROOT to analyse data	16
4.3	Usage of the ROOT macros in this work	16
5	Fit of form factors and calculation of world data	18
5.1	Plots of the cross section	18
5.1.1	Elastic scattering on ^{12}C	18
5.1.2	Inelastic scattering on ^{12}C	19
5.1.3	Elastic scattering on ^{40}Ca	22
5.1.4	Elastic scattering on ^{42}Ca	23
5.1.5	Elastic scattering on ^{48}Ca	24
5.1.6	Elastic scattering on ^{208}Pb	24
5.1.7	Inelastic scattering on ^{208}Pb	25
5.2	Plots of the electric form factors	28
5.2.1	Elastic scattering on ^{12}C	28
5.2.2	Inelastic scattering on ^{12}C	29
5.2.3	Elastic scattering on ^{40}Ca	31
5.2.4	Elastic scattering on ^{42}Ca	31
5.2.5	Elastic scattering on ^{48}Ca	33
5.2.6	Elastic scattering on ^{208}Pb	33
5.2.7	Inelastic scattering on ^{208}Pb	33
5.3	Parameterisation of the form factor for elastic electron scattering	35
5.3.1	Helm form factor parameterisation	35
5.3.2	Sum of Gaussian functions form factor parameterisation .	40
5.3.3	The Fourier-Bessel parameterisation	47
5.3.4	Polynomial function parameterisation	52
5.3.5	Gaussian function parameterisation	57

5.4	Form factor parameterisation inelastic scattering	66
5.5	Results for the parity-violating asymmetry	71
5.6	Results for the measuring time	72
6	Results and discussion	82
6.1	Summary of the parity-violating asymmetry and measuring time	82
6.2	Discussion of the parity-violating asymmetry and measuring time	83
7	References	84
8	Personal Acknowledgements	85
9	Appendix	86
9.1	C++ code used for the calculations	86
9.2	Plots of the measured cross sections for different nuclei	93

1 Introduction

The goal of physics is to understand and explain the world. Currently we can only explain 5% of matter-energy in the universe with the Standard Model of particle physics. Thus to get a better understanding of the underlying principles of our universe physicists have to search for physics beyond the Standard Model.

One way of searching for physics beyond the Standard Model is to perform high precision measurements of different parameters of the Standard Model. One of these parameters is the weak mixing angle $\sin^2(\theta_w)$. By measuring the weak mixing angle with a high precision, the Standard Model is tested and hints for physics beyond the Standard Model can be found. The weak mixing angle provides information on fundamental properties of the interaction between the different particles in the Standard Model. It is a parameter that occurs when combining the weak interaction with the electromagnetic interaction to the electroweak interaction. Furthermore the measurement of the weak mixing angle could help us understand dark matter or be a hint for new fundamental forces.

With the P2-experiment at MESA ("Mainz Energy-Recovering Superconducting Accelerator") in Mainz the weak mixing angle will be measured with unmatched precision of 0.14%. The P2-experiment will use a liquid hydrogen target. At the P2-experiment parity-violating electron-proton scattering experiments at low momentum transfer values Q^2 are going to be performed.

In the future, experiments with other targets can be performed. This thesis is about a first estimation for the measuring time for ^{12}C , ^{40}Ca , ^{42}Ca , ^{48}Ca and ^{208}Pb as other possible targets.

In Chapter 2 the theory of parity-violating electron scattering off nuclei with spin 0 will be described. Chapter 3 covers the P2-experiment and chapter 4 deals with the preparatory work that was necessary for the thesis. In chapter 5 the result are displayed. Chapter 6 covers the discussion of the results.

2 Theory of parity-violating electron scattering off nuclei with spin 0

This theory section sticks close to [1] by Bogdan Povh, Klaus Rith, Christoph Scholz, Frank Zetsche and Werner Rodejohann.

2.1 Mott scattering and electric form factor of nuclei

The Mott scattering describes the scattering of a point-like spin-1/2 particle, also known as fermion, off a point-like, non moving, electric charge. The incoming electron has the momentum p and the energy E . After the scattering the electron has the momentum p' and energy E' .

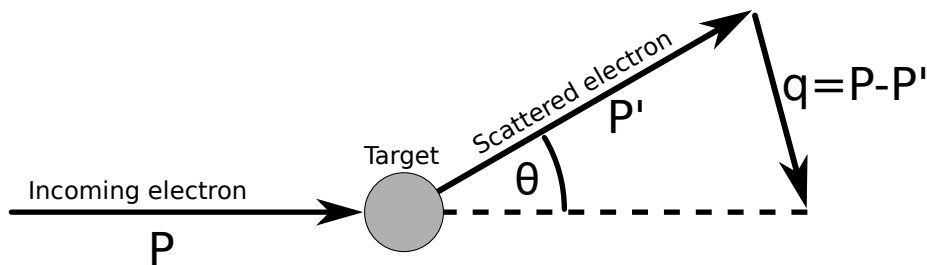


Figure 1: Sketch of the kinematics for electron scattering off a non-moving target

Electron scattering is used to determine the structure of nucleons. The Mott scattering formula is a modification of the Rosenbluth formula due to the spin of the scattering particle and is given by:

$$\left(\frac{d\sigma}{d\Omega}\right)_{\text{Mott}} = \left(\frac{ZZ'e^2}{4\pi\epsilon_0 4E}\right)^2 \cdot \frac{E'}{E} \cdot \frac{1}{\sin^4\left(\frac{\theta}{2}\right)} \cdot \left[1 - \beta^2 \cdot \sin^2\left(\frac{\theta}{2}\right)\right]. \quad (1)$$

The parameter $\beta = \frac{v}{c}$ is the velocity of the particle relative to the speed of light c . Z is the charge of the nucleus and Z' is the charge of the particle. $\epsilon_0 = 8.854187 \cdot 10^{-12} \frac{\text{A}\cdot\text{s}}{\text{V}\cdot\text{m}}$ is the electric field constant. The parameter $e = 1.602176 \cdot 10^{-19} \text{ C}$ is the elementary charge, θ is the scattering angle, which can be seen in figure 1. E is the energy of the particle before the scattering and E' is the energy of the scattered particle. E' is given by:

$$E' = \frac{E}{1 + \frac{E}{Mc^2}(1 - \cos(\theta))}. \quad (2)$$

M is the mass of the nucleus. The momentum transfer $Q^2 = -q^2$ is defined by the four-vectors of the incoming and outgoing electron and is shown in figure 1:

$$Q^2 = -q^2 = -(p - p')^2. \quad (3)$$

If we neglect the electron mass, we get for the momentum transfer:

$$Q^2 = \frac{4EE'}{c^2} \cdot \sin^2\left(\frac{\theta}{2}\right). \quad (4)$$

2.2 Parameterisation of the electric form factor of nuclei

In order to take into account that nuclei are extended and not point-like particles, the Mott cross section is modified with the electric form factor. In simplified terms, the electric form factor can be viewed as the Fourier transform of the charge density of the nuclei and is dependent on the momentum transfer. The experimentally measured cross section and the Mott cross section are related by the electric form factor as follows:

$$\left(\frac{d\sigma}{d\Omega}\right)_{\text{Exp}} = \left(\frac{d\sigma}{d\Omega}\right)_{\text{Mott}} \cdot |F(q^2)|^2. \quad (5)$$

In order to achieve an analytical expression for the electric form factor, different parameterisations can be used. The advantage of a parameterisation is that it can be used in calculations better than single measurement points. The description of the following parameterisations in section 3.2.1, 3.2.2 and 3.2.3 follows from [2].

2.2.1 The Helm form factor parameterisation

The Helm form factor is a modification of the nucleus as a solid sphere [2]. It describes the charge density of the nuclei as constant inside with a decrease at the edge. The charge distribution is given as:

$$\rho_H(\vec{r}) = \int \rho_U(\vec{r}') \rho_G(\vec{r} - \vec{r}') d^3r'. \quad (6)$$

ρ_U is the charge density of the solid sphere and is given by:

$$\rho_U(\vec{r}) = \frac{3Ze}{4\pi R^3} \text{ for } r \leq R. \quad (7)$$

up to a cutoff radius R . To account for the soft edge of the nucleus a Gaussian function is multiplied. The charge density of the Gaussian surface smearing is

given by:

$$\rho_G(\vec{r}) = \frac{1}{(2\pi g^2)^{\frac{3}{2}}} \cdot e^{-\frac{r^2}{2g^2}}. \quad (8)$$

Here, the parameter g is related to the Gaussian smearing surface. The Helm form factor is using the spherical Bessel functions of the first order $j_1(x)$:

$$j_1(x) = \frac{\sin(x)}{x^2} - \frac{\cos(x)}{x}. \quad (9)$$

The form factor parameterisation is given by:

$$|F(q)|^2 = \left(\frac{3j_1(qR)}{qR} \right)^2 \cdot e^{-q^2 g^2}. \quad (10)$$

We get:

$$|F(q)|^2 = \left(3 \left(\frac{\sin(qR)}{(qR)^3} - \frac{\cos(qR)}{(qR)^2} \right) \right)^2 \cdot e^{-q^2 g^2}. \quad (11)$$

Here the parameter R is called the effective nuclear radius. The parameter g is called the nuclear skin thickness. These parameters are different for every nucleus.

2.2.2 The sum of Gaussian functions parameterisation

The sum of Gaussian parameterisation [2] models the charge density of nuclei as series of Gaussian functions. The charge density is given by:

$$\rho(r) = \sum_{i=1}^N A_i \left(e^{-\left(\frac{r-R_i}{\gamma}\right)^2} + e^{-\left(\frac{r+R_i}{\gamma}\right)^2} \right), \quad (12)$$

where A_i is given by:

$$A_i = \frac{ZeQ_i}{2\pi^{\frac{3}{2}}\gamma^3\left(1 + 2\frac{R_i^2}{\gamma^2}\right)}. \quad (13)$$

With the assumption of a spherical symmetry, we get a parameterisation for the form factor of the form:

$$F(q) = e^{-\frac{q^2\gamma^2}{\hbar^2c^24}} \sum_{i=1}^N \frac{Q_i}{1 + \frac{2R_i^2}{\gamma^2}} \left(\cos\left(\frac{qR_i}{\hbar c}\right) + \frac{2R_i^2 \sin\left(\frac{qR_i}{\hbar c}\right)}{\gamma^2 \frac{qR_i}{\hbar c}} \right). \quad (14)$$

Here, the parameter γ is the width of the Gaussian functions. It is the smallest

width of the peaks in the nuclear wave functions that are calculated with the Hartree-Fock calculations. The parameters Q_i are the fractional charges carried by each Gaussian. The charges are normalized such that:

$$\sum_{i=1}^N Q_i = 1. \quad (15)$$

The parameter R_i is the effective nuclear radius of each Gaussian.

2.2.3 The Fourier-Bessel parameterisation

The Fourier-Bessel parameterisation [2] models the charge density as a sum of Bessel functions of zeroth-order up to a cutoff radius R :

$$j_0(x) = \frac{\sin(x)}{x}. \quad (16)$$

The charge density is given by:

$$\rho(r) = \sum_{\nu=1}^N a_{\nu} j_0\left(\frac{\nu\pi r}{R}\right) \text{ for } r \leq R. \quad (17)$$

The density is assumed to be zero afterwards. If we assume a spherical symmetry, we obtain an expression for the form factor:

$$F(q) = \frac{\sin\left(\frac{qR}{\hbar c}\right)}{\frac{qR}{\hbar c}} \frac{\sum_{\nu=1}^N \frac{(-1)^{\nu} a_{\nu}}{\nu^2 \pi^2 - \frac{q^2 R^2}{\hbar^2 c^2}}}{\sum_{\nu=1}^N \frac{(-1)^{\nu} a_{\nu}}{\nu^2 \pi^2}}. \quad (18)$$

The expression in the denominator normalizes the form factor to $F(0) = 1$.

2.2.4 Polynomial function parameterisation

This parameterisation models the form factor as a polynomial multiplied by a decaying exponential to fit the experimental data. The idea is that we can expand every function as a power series. It also has the advantage that it can be nonzero at every value of x in contrast to the other parameterisation that got introduced before. This parameterisation is given by:

$$F(x) = e^{-a_0 x} (a_1 + a_2 x + a_3 x^2 + a_3 x^3 + a_4 x^4 + a_5 x^5 + a_6 x^6). \quad (19)$$

We get:

$$|F(Q^2)|^2 = \left(e^{-a_0 Q^2} (a_1 + a_2 Q^2 + a_3 Q^4 + a_3 Q^6 + a_4 Q^8 + a_5 Q^{10} + a_6 Q^{12}) \right)^2. \quad (20)$$

2.2.5 Gaussian function parameterisation

The Gaussian function parameterisation describes the form factor as the sum of Gaussian functions. This parameterisation is similar to the sum of Gaussian parameterisation but the parameters can be chosen more freely. This parameterisation is advantageous because this parameterisation can be nonzero at x -values where the other parameterisations are zero. It is given by:

$$F(x) = a_1 \cdot e^{a_2 \cdot (x-a_3)^2} + a_4 \cdot e^{a_5 \cdot (x-a_6)^2} + a_7 \cdot e^{a_8 \cdot (x-a_9)^2}. \quad (21)$$

We get:

$$|F(Q^2)|^2 = \left(a_1 \cdot e^{a_2 \cdot (Q^2-a_3)^2} + a_4 \cdot e^{a_5 \cdot (Q^2-a_6)^2} + a_7 \cdot e^{a_8 \cdot (Q^2-a_9)^2} \right)^2. \quad (22)$$

2.3 Parity-violating asymmetry of electron scattering off spin 0 nuclei

The Standard Model of particle physics describes three of the four fundamental forces and classifies the known particles into a scheme. The weak interaction is the only force that violates parity. Parity violation was postulated by Lee and Yang in 1956 [3] and proven by Wu in 1957 [4] with an experiment that analysed the β -decay of ^{60}Co . Parity-violating experiments are used to measure different parameters of the Standard Model. For the formulas used in the theory parts before an exchange of a photon was assumed during the electron scattering. During the scattering, a Z_0 can also be exchanged. These two processes are represented as Feynman diagrams in figure 2. The interference between the exchange of a virtual photon and a Z_0 leads to an asymmetry. The parity violation in electron scattering can be measured with [5]:

$$A_{exp}^{PV} = \frac{N^+ - N^-}{N^+ + N^-}. \quad (23)$$

Here, N^+ describes the number of elastically scattered electrons with a positive helicity and N^- describes the number of elastically scattered electrons with a negative helicity. Helicity is defined as:

$$h = \vec{S} \cdot \frac{\vec{p}}{|\vec{p}|}. \quad (24)$$

A particle with positive helicity is called right handed and a particle with negative helicity is called left handed. This means that for positive helicity the spin

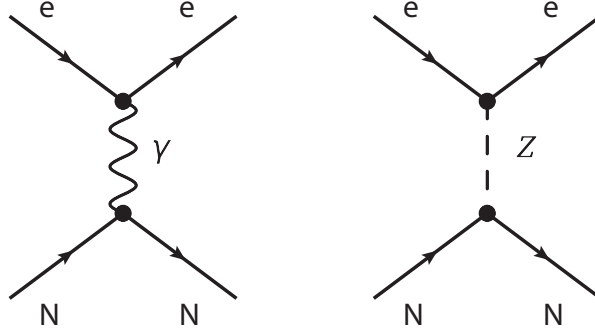


Figure 2: Feynman diagrams of elastic electron scattering under the exchange of a photon (left) and Z_0 (right) [5]

and the momentum of the particle point in the same direction. For negative helicity the spin and the momentum point in opposite directions.

We can express the parity-violating asymmetry with the cross sections σ^+ and σ^- from scattering of electrons with positive and negative helicity and the integrated luminosity $\tilde{L} = \int L dt$. Since the number of events is given by:

$$N = \int L dt \cdot \sigma, \quad (25)$$

the asymmetry can be calculated with [5]:

$$A = \frac{\tilde{L} \cdot \sigma^+ - \tilde{L} \cdot \sigma^-}{\tilde{L} \cdot \sigma^+ + \tilde{L} \cdot \sigma^-}. \quad (26)$$

We neglect the axial form factor for nuclei with negative parity. For a spin-zero nucleus with nuclear charge Z the parity-violating asymmetry in leading order is given by [6]:

$$A = -\frac{G_F \cdot Q^2}{4\sqrt{2}\pi\alpha} \cdot \frac{Q_w}{Z} \quad (27)$$

and using:

$$Q_w = Z(1 - 4\sin^2(\theta_w)) - N. \quad (28)$$

The parameter G_F is the Fermi coupling constant. It is given by $\frac{G_F}{(\hbar c)^3} = 1.166378 \cdot 10^{-3} \text{ GeV}^{-2}$. The Fermi coupling constant determines how strong the Fermi interaction is. The Fermi interaction is an effective description of the weak interaction. It was suggested by Enrico Fermi and it describes 4 directly

interacting fermions. The parameter Z is the number of protons and the parameter N is the number of neutrons. The parameter Q_w is the weak nuclear charge where $\sin^2(\theta_w) = 0.231$ is called the weak mixing angle. The scale dependence of the weak mixing angle $\sin^2(\theta_w)$ and measured values are shown in figure 3.

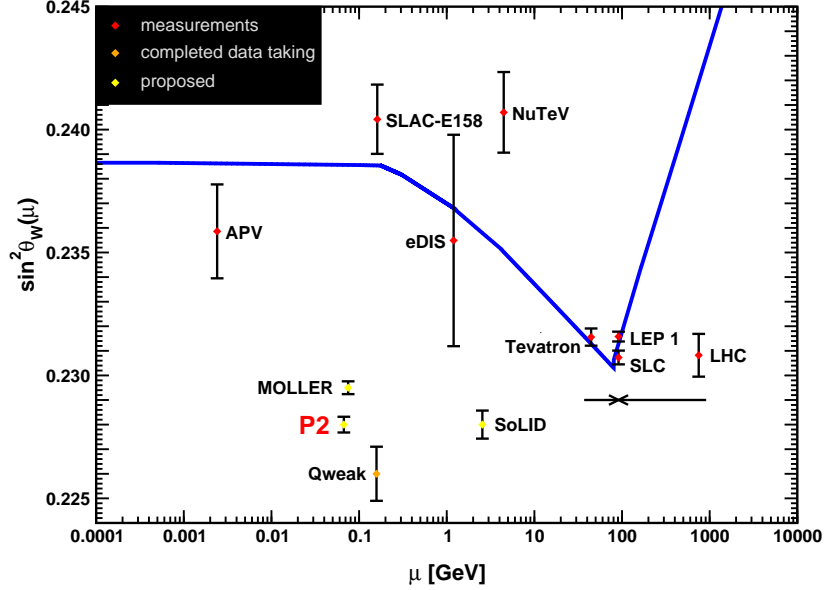


Figure 3: Scale dependence of the weak mixing angle $\sin^2(\theta_w)$ (blue line) together with the measured values (red) as well as proposed future measurements (yellow) [5].

It is important to note that this formula does not take into account corrections that derive from the fact that the nucleus is not a point-like particle.

2.4 Estimate of the measuring time

In section 2.3 the parity-violating asymmetry was explained. The parity-violating asymmetry, cross section averaged over the acceptance of the detector, is given by:

$$\langle A \rangle = \frac{\int A \frac{d\sigma}{d\Omega} d\Omega}{\int \frac{d\sigma}{d\Omega} d\Omega}, \quad (29)$$

with :

$$\int \frac{d\sigma}{d\Omega} d\Omega = \int |F(q^2)|^2 \cdot \left(\frac{d\sigma}{d\Omega} \right)_{Mott} d\Omega = \int_0^{2\pi} \int_{\theta_1}^{\theta_2} \sin(\theta) \cdot |F(q^2)|^2 \cdot \left(\frac{d\sigma}{d\Omega} \right)_{Mott} d\theta d\phi. \quad (30)$$

The cross section-averaged parity-violating asymmetry has the advantage that it takes into account the change in Q^2 for different scattering angle.

For the uncertainty of the parity-violating asymmetry we have to calculate:

$$\Delta A^2 = \sum_{i=+,-} \left(\frac{\partial A(N^+, N^-)}{\partial N^i} \Delta N^i \right)^2, \quad (31)$$

using the asymmetry from equation (23) and:

$$\Delta N^{+,-} = \sqrt{N^{+,-}}. \quad (32)$$

Since the parity-violating asymmetry is very small, we can assume that the number of scattered events $N^{+,-}$ for both helicities are the same and thus we introduce the total number of events $N = N^+ + N^-$. This leads to:

$$\Delta A = \frac{1}{\sqrt{N}}. \quad (33)$$

In order to estimate the measurement time, we have to solve:

$$N = \int L dt \cdot \sigma = \int L dt \cdot \int \frac{d\sigma}{d\Omega} d\Omega. \quad (34)$$

In this case the integration over the time is performed from $t = 0$ to $t = T$. If we solve this equation for the measuring time and assume that the luminosity is time independent we get:

$$T = \frac{N}{L \cdot \int \frac{d\sigma}{d\Omega} d\Omega}. \quad (35)$$

The luminosity for a fixed target experiment is given by the product of the incoming particle flux ϕ and the target density n_T :

$$L = \phi \cdot n_T. \quad (36)$$

The parameter n_T depends on the target density ρ , the target length l and the molar mass m_{Mol} with $N_A = 6.02214076 \cdot 10^{23} \text{ mol}^{-1}$ being the Avogadro constant.

$$n_T = \rho l \frac{N_A}{m_{Mol}}. \quad (37)$$

The parameter ϕ is given by the beam current I of the particle accelerator:

$$\phi = \frac{I}{e}, \quad (38)$$

where e the electron charge $e = 1.602176634 \cdot 10^{-19}$ C.

3 The P2-experiment

The P2-experiment is designed to measure the parity-violating asymmetry in electron-proton scattering. It aims to determine the weak mixing angle, an important parameter in the Standard Model, with a relative precision of 0.14% [5]. The P2-experiment can also be used to measure the parity-violating asymmetry in electron-nucleus scattering. A sketch of the P2-experiment is shown in figure 4.

In the P2-experiments a lH_2 -target is going to be used off which the beam electrons will be scattered elastically. The P2-experiment will use longitudinally polarized electrons. These electrons will be polarized up to 85% and have an energy up to $E_{Beam} = 155$ MeV. The beam current is planned to be $I_{Beam} = 150$ μ A. The helicity of the beam will be switched at a frequency of $f \approx 1$ kHz. The lH_2 -target will have the length of $l = 600$ mm and is aligned along the beam. The scattered electrons will be detected in a Cherenkov detector. The detector consists of 82 wedged fused silica bars (quartz bars) that will cover the whole azimuth angle. The bars also guide the Cherenkov light to the photomultiplier tube. The angular acceptance for the P2-experiment ranges from $\theta = 25^\circ$ to $\theta = 45^\circ$. Figure 5 shows the Cherenkov ring detector in the experimental setup of the P2-experiment. Because of the high luminosity the detector has to detect up to 100 GHz of scattered electrons. The luminosity for the P2-experiment is going to be:

$$L = \frac{I_{Beam}}{e} \rho l \frac{N_A}{m_{Mol}} = 2.38 \cdot 10^{39} \text{ cm}^{-2} \text{ s}^{-1}. \quad (39)$$

Here, e is the electron charge, ρ the density of protons in the liquid hydrogen target (lH_2 -target), N_A the Avogadro constant and m_{Mol} the molar mass of the target. It is important to note that the luminosity given here is the luminosity for a lH_2 -target. For the calculation of the measuring time later on the luminosity for each target is calculated separately.

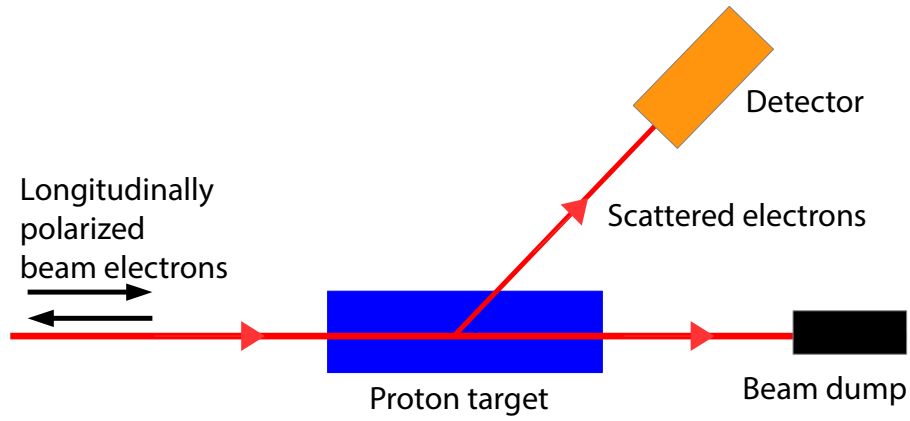


Figure 4: Sketch of the experimental method used at the P2-experiment: A longitudinally polarized electron beam impinges on the proton target. The scattered electrons are detected in the detector. [5]

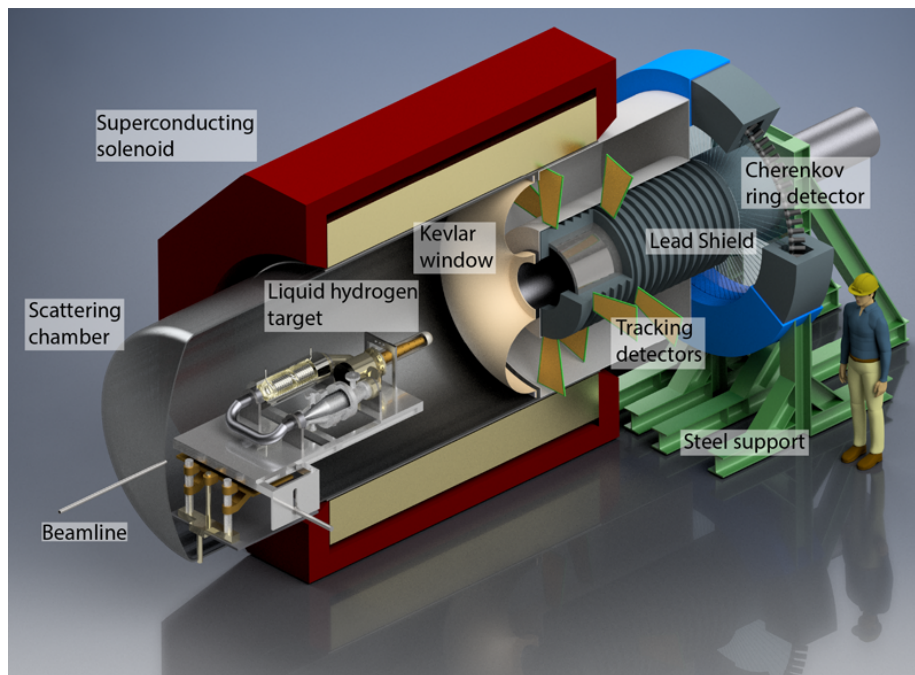


Figure 5: CAD drawing of the experimental setup of the P2-experiment. [5]

4 Preparatory work

4.1 Compilation of scattering cross section world data

At first, the database from nuclear data tables [7] was used. On this site the energy levels of the different elements are given. So we had to search for the following nuclei: ^{12}C , ^{40}Ca , ^{42}Ca , ^{48}Ca and ^{208}Pb . The search provided a list for the electron scattering data.

In this section, papers are listed on where measured electron nucleus scattering cross sections can be found. These cross sections were written into a text file for later use in the calculations [10], [11], [12], [13], [14], [15], [16], [17], [18], [19], [20], [21], [22], [23], [24], [25].

To extend the data set found in the nuclear data tables, the references within the papers were used. The cross section values found were added to the text files.

In addition to the nuclear data tables, a search on inspirehep [8] for additional papers was performed. A lot of papers from this search were already found before. The newly found cross section were also added to text files.

4.2 Overview of ROOT to analyse data

ROOT [9] is an open-source data analysis framework designed by CERN which was primarily designed for analysis in the field of particle physics. Later on ROOT was used for more different applications for example in astronomy. The Higgs boson was found with the help of ROOT.

ROOT enables the analysis and the display of large amount of data which are recorded at the large hadron collider. To process this large amount of data ROOT is written in C++. ROOT can be used on Windows, macOS or Linux and is open source. ROOT integrates also with Python.

For this thesis the following functionalities of ROOT are important:

- 1) Plotting histograms and graphs to visualize distributions and functions
- 2) Curve fitting
- 3) Standard mathematical functions
- 4) Creating files like PDF, PNG etc.

4.3 Usage of the ROOT macros in this work

Different ROOT macros are used to estimate the measuring time for a given statistical uncertainty and a given nucleus. Depending on the nucleus the codes of the macros can be adjusted.

First of all the important header files get included as well as the "Constants.hh" file that contains the needed physical constants and a system of units, which enables the conversion of different units into one consistent set. The "read_data" macro is used such that the text files with the cross sections can be imported into ROOT. The function "Sum_of_Gaussian" and "Fourier_Bessel" are the param-

eterisation for the electric form factor and are defined outside the "read_data" macro for later use in the code. The functions "Sigma", "Asymmetrie" and "AsymInt" are defined after the parameterisations. These functions will later be used to calculate the measuring time.

In the "PlotC12" macro first of all the Mott cross section from equation (1), the electric form factor from equation (5) and the momentum transfer from equation (4) are calculated. After the calculations of the form factor and momentum transfer new canvases are defined. Then the measured cross section as well as the Mott cross section are plotted against the angles. Furthermore, the form factor was plotted against the momentum transfer. Then the different form factor parameterisations from section 2.2 are fitted to the plotted form factors. The parameterisation is also plotted into the same plot.

At last, the estimate of the measuring time was performed. To do this the parameterisation of the form factors is used. Then the asymmetry from equation (27) and the cross section averaged asymmetry from equation (29) are calculated to estimate the measuring time from equation (35). The code of the macros used for the calculations can be found in the appendix in section 9.

5 Fit of form factors and calculation of world data

5.1 Plots of the cross section

The cross sections given in the papers were read in ROOT and plotted against the scattering angle. The Mott cross section was also plotted into the same plot. The Mott cross section was calculated using equation (1) from the theory part. The Mott cross section is always larger than the measured cross section because the electric form factor is smaller than 1. It takes the electric charge distribution into account.

5.1.1 Elastic scattering on ^{12}C

The available data for the measured cross sections from experiments [10], [11], [12], [13], [14], [15], [16] were plotted separately as a function of the scattering angle. For comparison, the calculated Mott cross section is also shown in the same plot. One example is shown in figure 6. Plots of the other experiments are found in section 9.

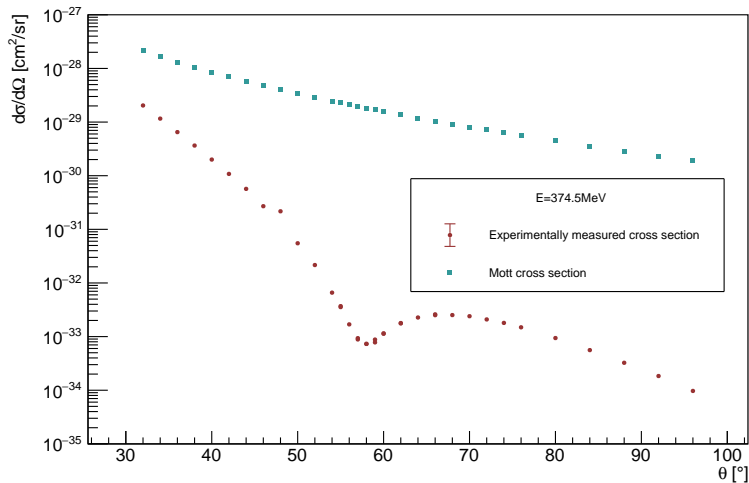


Figure 6: Cross section for elastic electron scattering off the ground state of ^{12}C at a beam energy of $E = 374.5$ MeV [12]. Error bars are too small to be visible due to the marker size. The angular acceptance for the P2-experiment ranges from $\theta = 25^\circ$ to $\theta = 45^\circ$ with a beam energy of $E = 155$ MeV [5].

For a comparison of all the data sets, the cross section is plotted against the scattering angle in figure 7. The measured cross sections range from $\frac{d\sigma}{d\Omega} \approx 10^{-27} \frac{\text{cm}^2}{\text{sr}}$ to $\frac{d\sigma}{d\Omega} \approx 10^{-34} \frac{\text{cm}^2}{\text{sr}}$ depending on the scattering angle as well as the

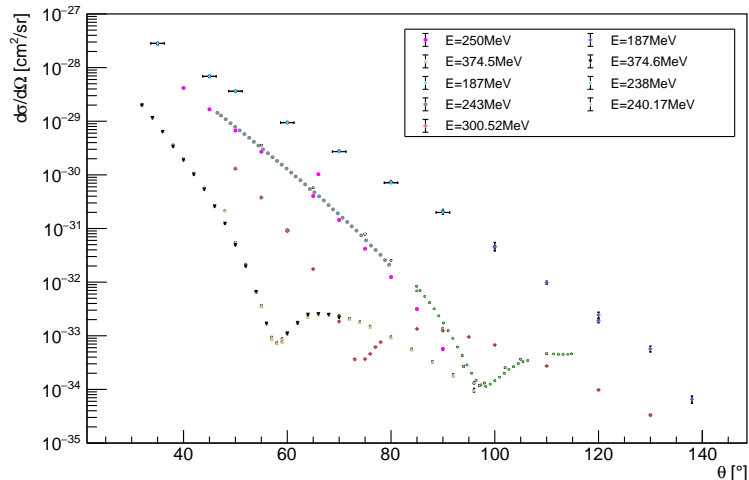


Figure 7: Cross section for elastic electron scattering off the ground state of ^{12}C at various beam energies [10], [11], [12], [13], [14], [15], [16]. Error bars are hardly visible due to the marker size. The angular acceptance for the P2-experiment ranges from $\theta = 25^\circ$ to $\theta = 45^\circ$ with a beam energy of $E = 155$ MeV [5].

energy of the electrons. There are some data points where the cross section is smaller than $\frac{d\sigma}{d\Omega} \approx 10^{-34} \frac{\text{cm}^2}{\text{sr}}$. Generally, cross section values for experiments with similar energies tend to have similar dependence of the scattering angle. The minima of the different graphs are shifted on the x-axis. For higher beam energies the minima of the cross section values shift towards lower θ values. For $E \approx 374$ MeV the minimum is at $\theta \approx 55^\circ$, for $E \approx 300$ MeV the minimum is at $\theta \approx 75^\circ$ and for $E \approx 240$ MeV the minimum is at $\theta \approx 100^\circ$.

5.1.2 Inelastic scattering on ^{12}C

In the case of inelastic scattering the nucleus gets into an excited state. We look at the three lowest energy levels $E_x = 4.43$ MeV, $E_x = 7.66$ MeV and $E_x = 9.64$ MeV. A level scheme for the lowest nuclear energy levels in ^{12}C is displayed in figure 8.

For inelastic scattering similar plots were created as for elastic scattering. The individual measured cross sections from [10], [11] and [15] for the first three energy levels $E_x = 4.43$ MeV, $E_x = 7.66$ MeV and $E_x = 9.64$ MeV were plotted as a function of the scattering angle. In figure 9-11 all cross section values were plotted as a function of the scattering angle θ . The individual experiments are found in section 9. Figure 9 shows the measured cross sections

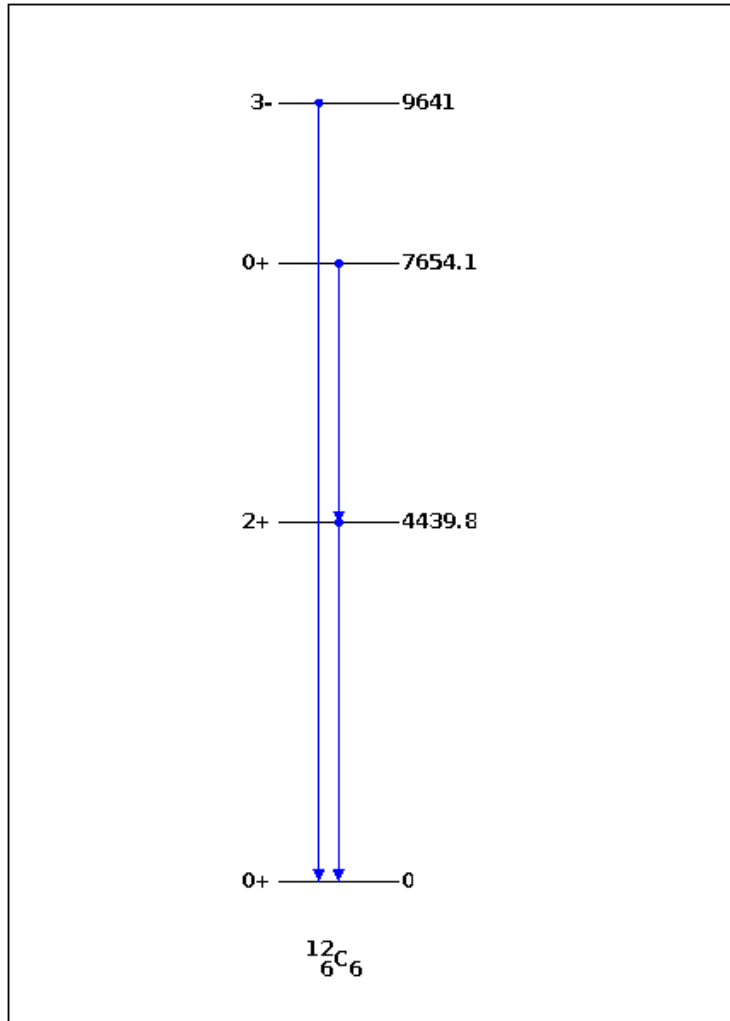


Figure 8: Level scheme for the lowest nuclear energy levels in ^{12}C [7]. On the left side the spins and parity of the different levels are shown. On the right side the excitation energy E_x of the different levels is shown in keV.

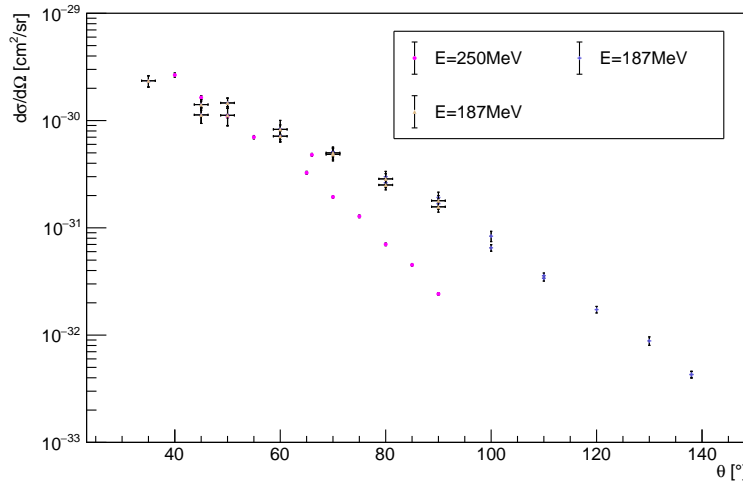


Figure 9: Cross section for inelastic electron scattering off the first excited state $E_x = 4.43$ MeV of ^{12}C at different beam energies [10], [11], [15]. The angular acceptance for the P2-experiment ranges from $\theta = 25^\circ$ to $\theta = 45^\circ$ with a beam energy of $E = 155$ MeV [5].

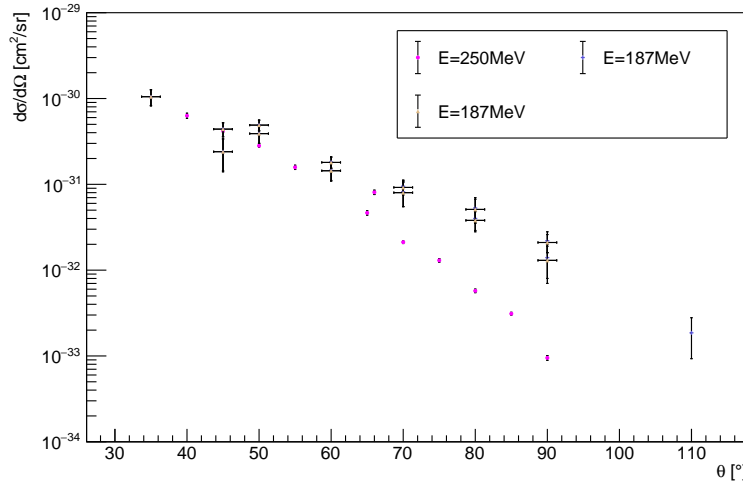


Figure 10: Cross section for inelastic electron scattering off the second excited state $E_x = 7.66$ MeV of ^{12}C at different beam energies [10], [11], [15]. The angular acceptance for the P2-experiment ranges from $\theta = 25^\circ$ to $\theta = 45^\circ$ with a beam energy of $E = 155$ MeV [5].

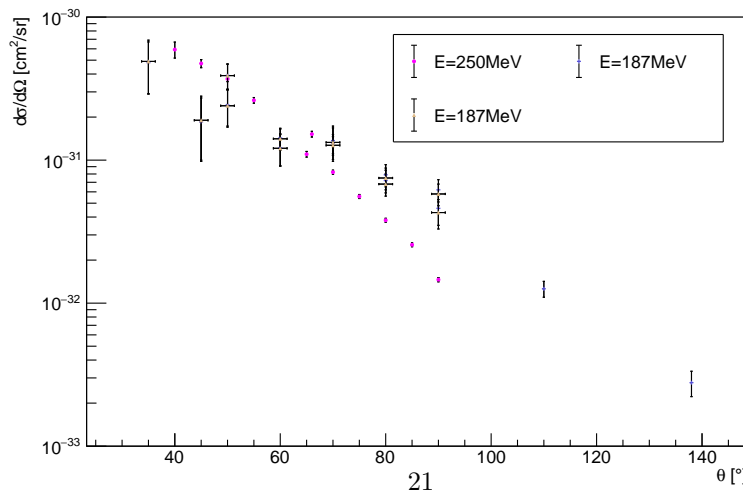


Figure 11: Cross section for inelastic electron scattering off the third excited state $E_x = 9.64$ MeV of ^{12}C at different beam energies [10], [11], [15]. The angular acceptance for the P2-experiment ranges from $\theta = 25^\circ$ to $\theta = 45^\circ$ with a beam energy of $E = 155$ MeV [5].

for $E_x = 4.43$ MeV as a function of the scattering angle θ . The energy level $E_x = 7.66$ MeV is shown in figure 10 and in figure 11 the energy level $E_x = 9.64$ MeV is plotted as a function of θ .

Generally, we can see that the measured cross section values decrease similar to the elastic scattering ones. The cross sections range from $\frac{d\sigma}{d\Omega} \approx 10^{-29} \frac{\text{cm}^2}{\text{sr}}$ to $\frac{d\sigma}{d\Omega} \approx 10^{-33} \frac{\text{cm}^2}{\text{sr}}$ depending on the scattering angle as well as the energy of the electrons. Cross sections for the scattering to the third energy level $E_x = 9.64$ MeV are smaller than the others. They range from $\frac{d\sigma}{d\Omega} \approx 10^{-30} \frac{\text{cm}^2}{\text{sr}}$ to $\frac{d\sigma}{d\Omega} \approx 10^{-33} \frac{\text{cm}^2}{\text{sr}}$. For forward scattering, we can see that the cross section for the elastic scattering is larger than the cross section for the inelastic scattering. For backward scattering the cross section of the inelastic scattering is equal or even larger than the cross section of the elastic scattering.

5.1.3 Elastic scattering on ^{40}Ca

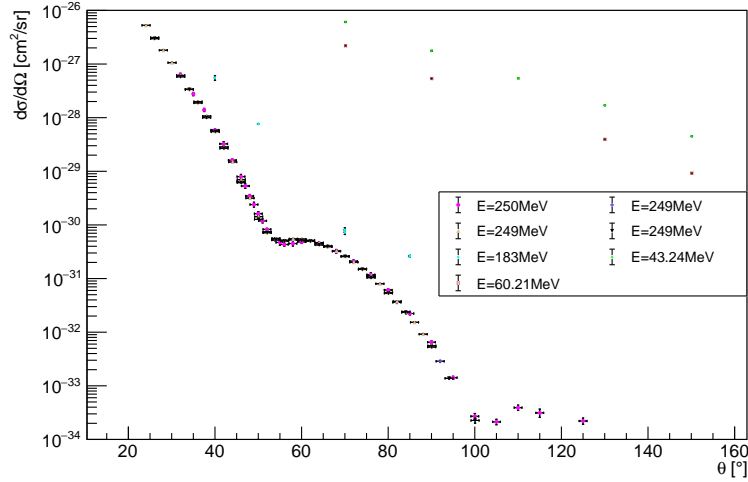


Figure 12: Cross section for elastic electron scattering off the ground state of ^{40}Ca at various beam energies [17], [18], [19], [20]. Error bars are hardly visible due to marker size. The angular acceptance for the P2-experiment ranges from $\theta = 25^\circ$ to $\theta = 45^\circ$ with a beam energy of $E = 155$ MeV [5].

The approach for the elastic electron scattering on ^{40}Ca was the same as for ^{12}C . The available measured cross sections for ^{40}Ca from [17], [18], [19] and [20] are plotted as a function of the scattering angle and can be found in section 9. Figure 12 shows the measured cross sections as a function of the scattering angle θ .

Generally, we see that the cross section values range from $\frac{d\sigma}{d\Omega} \approx 10^{-26} \frac{\text{cm}^2}{\text{sr}}$ to

$\frac{d\sigma}{d\Omega} \approx 10^{-34} \frac{\text{cm}^2}{\text{sr}}$ so they are approximately in the same order of magnitude as the cross section values for elastic scattering off ^{12}C . For the smaller energies and angles the cross section of ^{40}Ca is bigger than ^{12}C . We see that the measurements at lower beam energies ($E = 43.24 \text{ MeV}$ and $E = 60.21 \text{ MeV}$) deviate a lot from the measurements at higher beam energies. The cross section values for $E \approx 250 \text{ MeV}$ decrease till $\theta = 55^\circ$. From approximately $\theta = 55^\circ$ to $\theta = 65^\circ$ the cross section values have a plateau. Then the values of the cross section decrease again. Between $\theta = 100^\circ$ and $\theta = 105^\circ$ the cross section values have their minimum.

5.1.4 Elastic scattering on ^{42}Ca

For the available measured cross sections [17] and [21] the approach for ^{42}Ca was the same as for the nuclei before. In section 9 the individual measured cross sections are plotted against the scattering angle. In figure 13 the measured cross sections are shown as a function of the scattering angle θ .

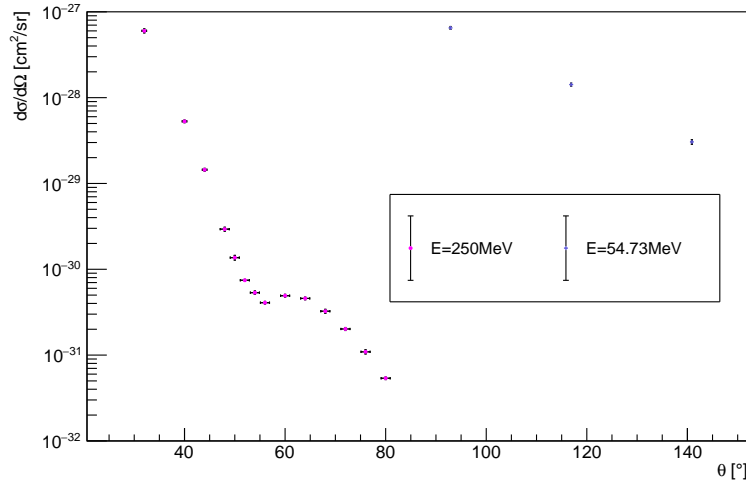


Figure 13: Cross section for elastic electron scattering off the ground state of ^{42}Ca at different beam energies [17], [21]. Error bars are hardly visible due to marker size. The angular acceptance for the P2-experiment ranges from $\theta = 25^\circ$ to $\theta = 45^\circ$ with a beam energy of $E = 155 \text{ MeV}$ [5].

The cross section values range from $\frac{d\sigma}{d\Omega} \approx 10^{-28} \frac{\text{cm}^2}{\text{sr}}$ to $\frac{d\sigma}{d\Omega} \approx 10^{-32} \frac{\text{cm}^2}{\text{sr}}$. The smaller energy data deviate from the higher energy data. The cross section values for $E \approx 250 \text{ MeV}$ decrease until $\theta = 55^\circ$ where the data points have their minimum. Then the cross section increase up to the value of $\theta = 65^\circ$ and start decreasing to the second minimum of the cross section data.

5.1.5 Elastic scattering on ^{48}Ca

For ^{48}Ca the plots were made the same way as before. The plots for the individual experiments [17] and [18] can be found in section 9. In figure 14 the measured cross sections are plotted as a function of the scattering angle θ .

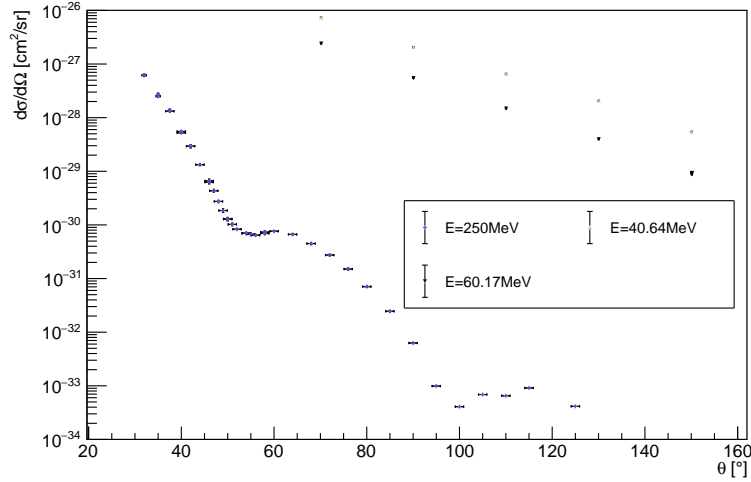


Figure 14: Cross section for elastic electron scattering off the ground state of ^{48}Ca at different beam energies [17], [18]. Error bars are hardly visible due to marker size. The angular acceptance for the P2-experiment ranges from $\theta = 25^\circ$ to $\theta = 45^\circ$ with a beam energy of $E = 155$ MeV [5].

The cross section ranges from $\frac{d\sigma}{d\Omega} \approx 10^{-27} \frac{\text{cm}^2}{\text{sr}}$ to $\frac{d\sigma}{d\Omega} \approx 10^{-34} \frac{\text{cm}^2}{\text{sr}}$ similar to the values of the cross section for ^{40}Ca . The shapes of the graphs of ^{48}Ca and ^{40}Ca are almost identical. As for the cross section of ^{40}Ca the cross section values at lower beam energies ($E = 40.64$ MeV, $E = 60.17$ MeV) deviate from the cross section values at higher beam energies ($E = 250$ MeV). The decrease of the cross section values to the first minimum at $\theta = 50^\circ$ is similar to the decrease for ^{40}Ca . In contrast to the plateau for ^{40}Ca the cross section values for ^{48}Ca increase up to approximately $\theta = 65^\circ$. The cross section values start decreasing to the second minimum at about $\theta = 100^\circ$.

5.1.6 Elastic scattering on ^{208}Pb

For the ^{208}Pb data sets [22], [23], [25] the same approach as before is used. In figure 15 the measured cross sections are plotted against the scattering angle θ . The cross section ranges from $\frac{d\sigma}{d\Omega} \approx 10^{-25} \frac{\text{cm}^2}{\text{sr}}$ to $\frac{d\sigma}{d\Omega} \approx 10^{-34} \frac{\text{cm}^2}{\text{sr}}$. We can see that the cross sections measured at lower beam energies deviate from the cross sections at higher beam energies. Generally, we see that the cross section values

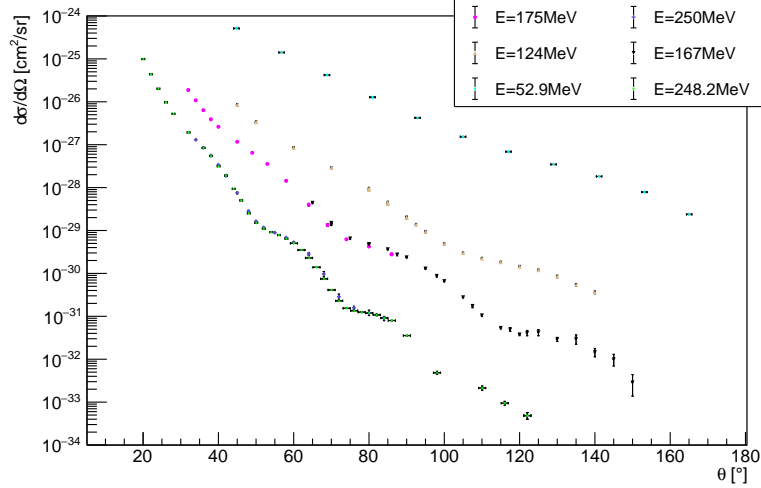


Figure 15: Cross section for elastic electron scattering off ^{208}Pb , [22], [23], [25]. Error bars are hardly visible due to marker size. The angular acceptance for the P2-experiment ranges from $\theta = 25^\circ$ to $\theta = 45^\circ$ with a beam energy of $E = 155$ MeV [5].

at lower beam energies are shifted on the x-axis towards larger scattering angles θ . For $E \approx 250$ MeV the cross section values decrease until $\theta = 50^\circ$ although the slope decreases from $\theta \approx 30^\circ$ to $\theta \approx 50^\circ$. From $\theta = 50^\circ$ to $\theta = 60^\circ$ the cross section has a plateau before it drops again until $\theta = 75^\circ$. Then the cross section has a plateau again until $\theta = 85^\circ$ before they start dropping off again.

5.1.7 Inelastic scattering on ^{208}Pb

For the inelastic scattering off ^{208}Pb [24] we looked at the two lowest energy levels $E_x = 2.6$ MeV and $E_x = 3.2$ MeV. The level scheme of ^{208}Pb is displayed in figure 16. The same approach as for the inelastic scattering off ^{12}C from section 5.1.2 is used. Figure 17 shows the cross section values for $E_x = 2.6$ MeV plotted against θ and figure 18 shows the cross section values for $E_x = 3.2$ MeV plotted against θ .

Generally, we see that the cross section range for the first energy level is bigger than the cross section range for the second energy level. The range for the cross section of the first energy level $E_x = 2.6$ MeV is from $\frac{d\sigma}{d\Omega} \approx 10^{-29} \frac{\text{cm}^2}{\text{sr}}$ to $\frac{d\sigma}{d\Omega} \approx 10^{-33} \frac{\text{cm}^2}{\text{sr}}$. For the second energy level $E_x = 3.2$ MeV the cross section ranges from $\frac{d\sigma}{d\Omega} \approx 10^{-31} \frac{\text{cm}^2}{\text{sr}}$ to $\frac{d\sigma}{d\Omega} \approx 10^{-33} \frac{\text{cm}^2}{\text{sr}}$. For the $E_x = 2.6$ MeV level and a beam energy of $E = 167$ MeV a plateau is visible from approximately $\theta = 65^\circ$ to $\theta = 80^\circ$. Then the cross section values decrease until $\theta = 110^\circ$ where

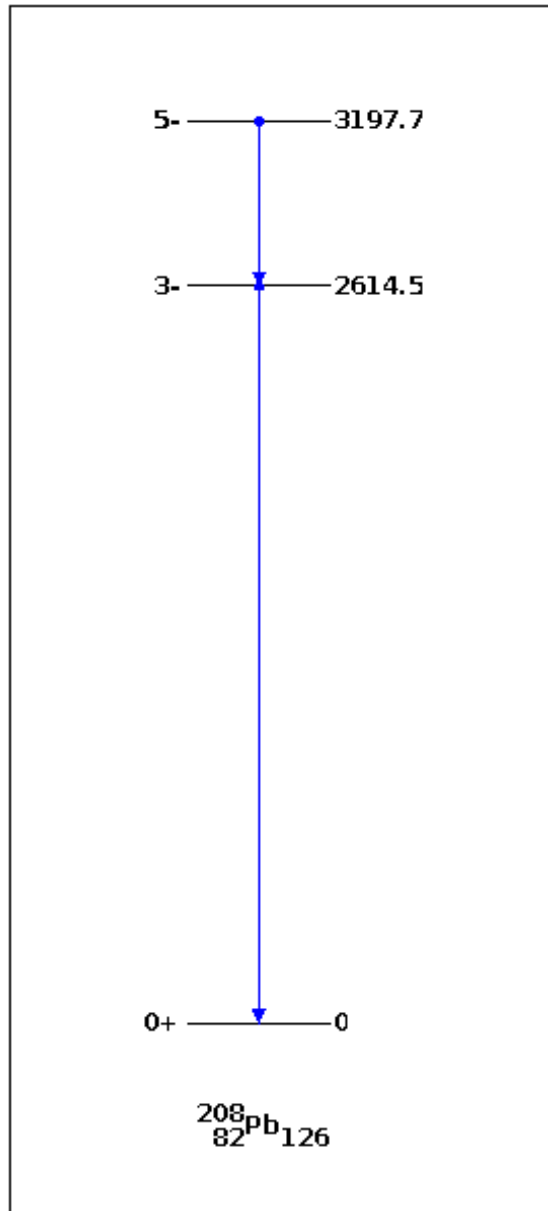


Figure 16: Level scheme for the lowest nuclear energy levels in ^{208}Pb [7]. On the left side the spin and parity of the different levels are shown. On the right side the excitation energies E_x of the different levels are displayed in keV.

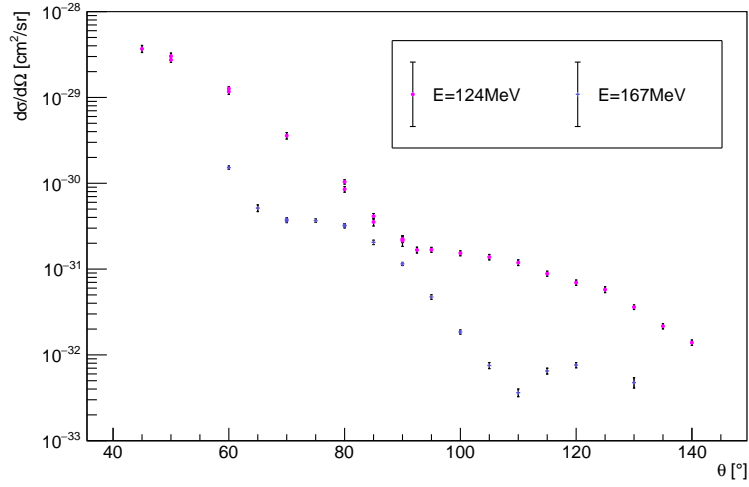


Figure 17: Cross section for inelastic electron scattering off the first excited state $E_x = 2.6$ MeV of ^{208}Pb at different beam energies [24]. The angular acceptance for the P2-experiment ranges from $\theta = 25^\circ$ to $\theta = 45^\circ$ with a beam energy of $E = 155$ MeV [5].

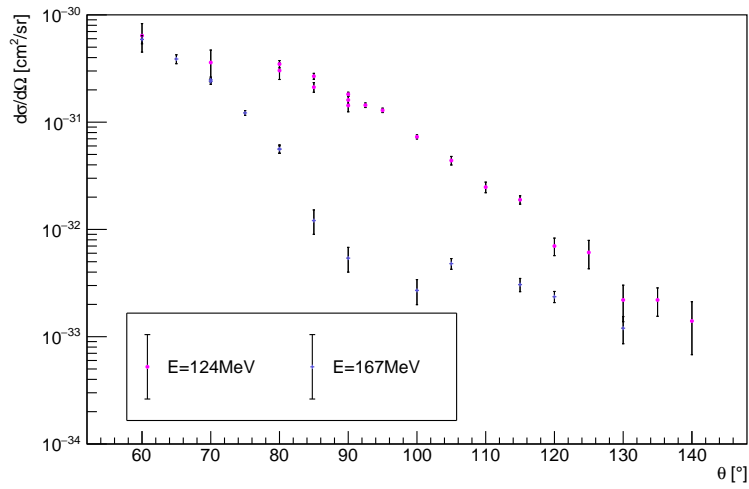


Figure 18: Cross section for inelastic electron scattering off the second excited state $E_x = 3.2$ MeV of ^{208}Pb at different beam energies [24]. The angular acceptance for the P2-experiment ranges from $\theta = 25^\circ$ to $\theta = 45^\circ$ with a beam energy of $E = 155$ MeV [5].

the data points have a minimum. For the second energy level $E_x = 3.2$ MeV and a beam energy of $E = 167$ MeV the cross section values decrease until approximately $\theta = 95^\circ$ where the minimum is.

5.2 Plots of the electric form factors

The electric form factor can be interpreted as the Fourier transform of the charge distribution of the nucleus. The form factor can be obtained from the measured cross section using a parameterisation for the Mott cross section. Using (5) from the theory part we get for the form factor:

$$|F(q^2)|^2 = \frac{\left(\frac{d\sigma}{d\Omega}\right)_{\text{Exp}}}{\left(\frac{d\sigma}{d\Omega}\right)_{\text{Mott}}}. \quad (40)$$

To calculate the uncertainty the Gaussian error propagation is used. We assume that only the measured cross section is an error-prone value. We get:

$$\Delta|F(q^2)|^2 = \frac{1}{\left(\frac{d\sigma}{d\Omega}\right)_{\text{Mott}}} \Delta \left(\frac{d\sigma}{d\Omega}\right)_{\text{Exp}}. \quad (41)$$

The electric form factor depends on the momentum transfer Q^2 . The momentum transfer can be calculated using equation (4). The momentum transfer uncertainty is also calculated with the Gaussian error propagation. It is given by:

$$\Delta Q^2 = \left(\frac{4EE'}{c^2} \cos\left(\frac{\theta}{2}\right) \cdot \sin\left(\frac{\theta}{2}\right) + \frac{4E}{c^2} \cdot \sin^2\left(\frac{\theta}{2}\right) \cdot \frac{\frac{E}{Mc^2} \sin(\theta)}{\left(\frac{E}{Mc^2} (1 - \cos(\theta)) + 1\right)^2} \right) \Delta\theta. \quad (42)$$

In the following sections the form factor of the different nuclei is presented.

5.2.1 Elastic scattering on ^{12}C

The calculated form factors are shown in figure 19 as a function of the momentum transfer Q^2 . All experiments are distinguishable in the plot by using different colors and different symbols for the markers.

Generally, we see that all data points fit well together. We see that 2 data points deviate strongly from the other data points. These two data points are at $Q^2 \approx 70 \cdot 10^3 \frac{\text{MeV}^2}{c^2}$ and at $Q^2 \approx 90 \cdot 10^3 \frac{\text{MeV}^2}{c^2}$. Between $Q^2 \approx 110 \cdot 10^3 \frac{\text{MeV}^2}{c^2}$ and $Q^2 \approx 140 \cdot 10^3 \frac{\text{MeV}^2}{c^2}$ the data points for the experiments with $E = 374.5$ MeV and $E = 374.6$ MeV do not agree well with the data points of the other experiments.

In general, the calculated form factor is getting smaller for larger momentum transfers Q^2 . The electric form factor ranges from $|F(Q^2)|^2 \approx 1$ to $|F(Q^2)|^2 \approx 10^{-5}$ depending on the momentum transfer Q^2 . At $Q^2 \approx 125 \cdot 10^3 \frac{\text{MeV}^2}{c^2}$ the form

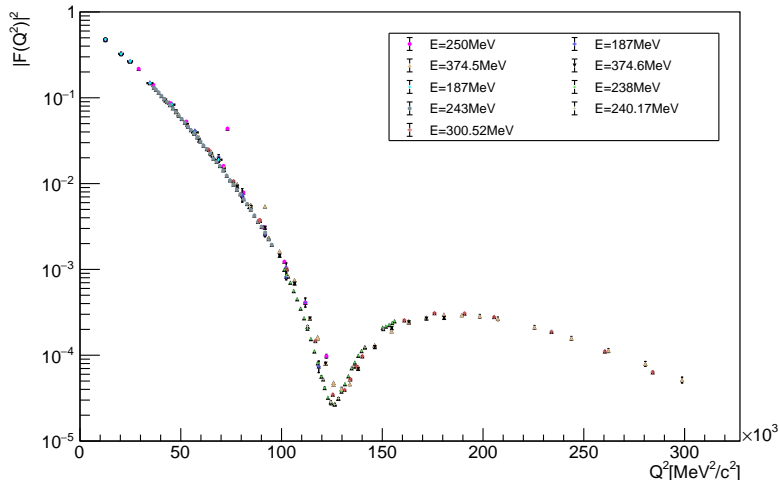


Figure 19: Form factor for elastic electron scattering off the ground state of ^{12}C for various beam energies. The errors are mostly not visible due to marker size.

factor has its local minimum. The form factor rises until $Q^2 \approx 190 \cdot 10^3 \frac{\text{MeV}^2}{c^2}$ and drops off afterwards towards the second minimum.

5.2.2 Inelastic scattering on ^{12}C

For the inelastic scattering we distinguish between the 3 lowest energy levels $E_x = 4.43 \text{ MeV}$, $E_x = 7.66 \text{ MeV}$ and $E_x = 9.64 \text{ MeV}$. The form factors for $E_x = 4.43 \text{ MeV}$ are plotted against the momentum transfer Q^2 in figure 20. In figure 21 the form factor for $E_x = 7.66 \text{ MeV}$ is plotted as a function of Q^2 and in figure 22 the form factor for $E_x = 9.64 \text{ MeV}$ is plotted against the momentum transfer Q^2 . All experiments are distinguishable in the plot by using different colors and different symbols for the markers.

We see that the form factor for the inelastic scattering by exciting the $E_x = 4.43 \text{ MeV}$ level is approximately 10 times bigger than the form factors for the inelastic scattering to the $E_x = 7.66 \text{ MeV}$ and $E_x = 9.64 \text{ MeV}$ level. Comparing the maxima of the $E_x = 7.66 \text{ MeV}$ and the $E_x = 9.64 \text{ MeV}$ we see that the maximum for the $E_x = 9.64 \text{ MeV}$ level is larger than the $E_x = 7.66 \text{ MeV}$ level. The form factors in figure 20, 21 and 22 have generally the shape of a Gaussian function. These Gaussian functions have different parameters for the position and height but approximately the same variance.

For the calculations of the measuring time later on the inelastic scattering contributions will be neglected because the form factor for inelastic scattering under forward angles is between 100 times for the $E_x = 4.43 \text{ MeV}$ level and 1000 times

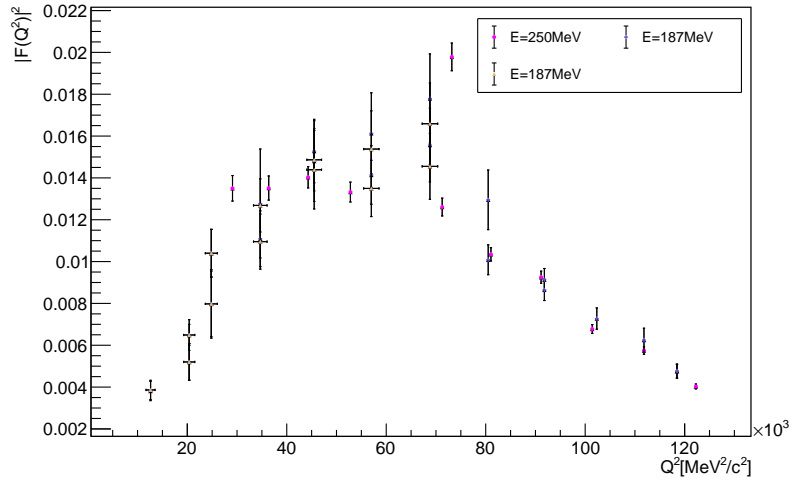


Figure 20: Form factor for inelastic electron scattering off the first excited state $E_x = 4.43\text{MeV}$ of ^{12}C at various beam energies.

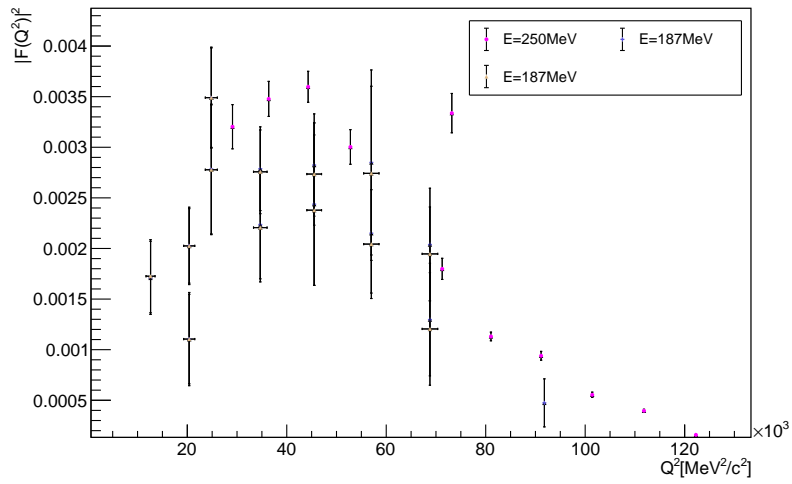


Figure 21: Form factor for inelastic electron scattering off the second excited state $E_x = 7.66\text{MeV}$ of ^{12}C at various beam energies.

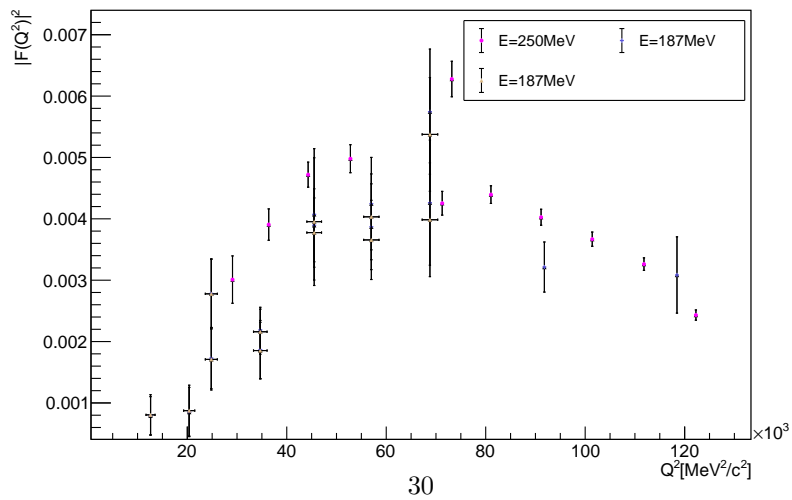


Figure 22: Form factor for inelastic electron scattering off the third excited state $E_x = 9.64\text{MeV}$ of ^{12}C at various beam energies.

for the $E_x = 7.66$ MeV level and $E_x = 9.64$ MeV level smaller than the form factor for elastic scattering.

5.2.3 Elastic scattering on ^{40}Ca

In figure 23 the calculated form factor is plotted as a function of the momentum transfer Q^2 . The different experiments are distinguishable by the different markers that were used.

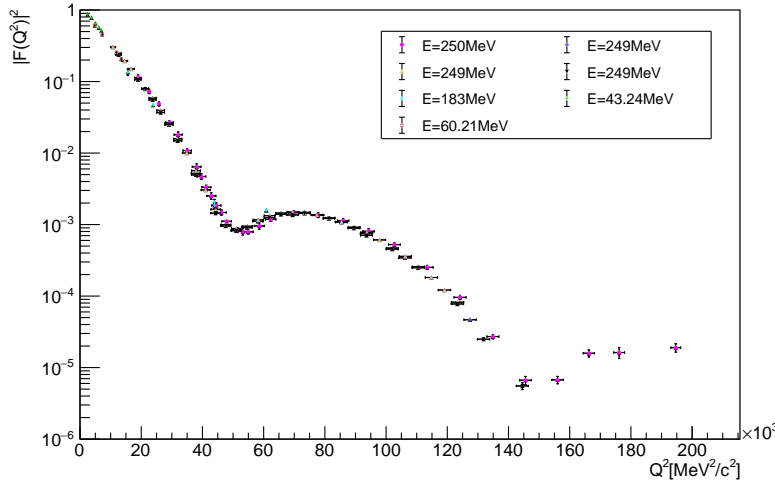


Figure 23: Form factor for elastic electron scattering off the ground state of ^{40}Ca at various beam energies. The error bars are mostly not visible due to the marker size.

Generally, the data points fit well together. The form factor values range from $|F(Q^2)|^2 \approx 1$ to $|F(Q^2)|^2 \approx 10^{-5}$. The form factor values decrease until the first minimum at $Q^2 \approx 50 \cdot 10^3 \frac{\text{MeV}^2}{c^2}$. From $Q^2 = 50 \cdot 10^3 \frac{\text{MeV}^2}{c^2}$ to $Q^2 = 75 \cdot 10^3 \frac{\text{MeV}^2}{c^2}$ the form factor values increase towards their local maximum. From there the form factor values decrease until the second local minimum at $Q^2 \approx 150 \cdot 10^3 \frac{\text{MeV}^2}{c^2}$. For higher values of Q^2 the cross section values increase slightly again.

5.2.4 Elastic scattering on ^{42}Ca

In figure 24 the form factor of ^{42}Ca are shown as a function of the momentum transfer Q^2 . The 2 experiments are distinguishable by the different markers.

We see that the form factor values range from $|F(Q^2)|^2 \approx 1$ to $|F(Q^2)|^2 \approx 10^{-4}$.

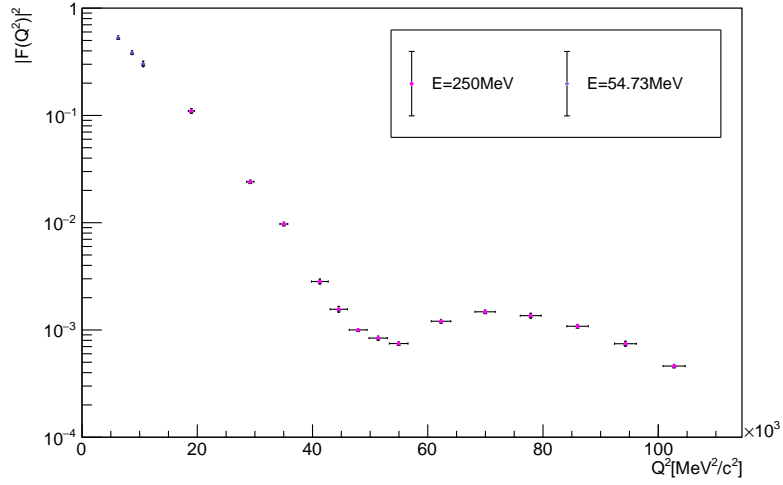


Figure 24: Form factor for elastic electron scattering off the ground state of ^{42}Ca at different beam energies. The error bars are mostly not visible due to marker size

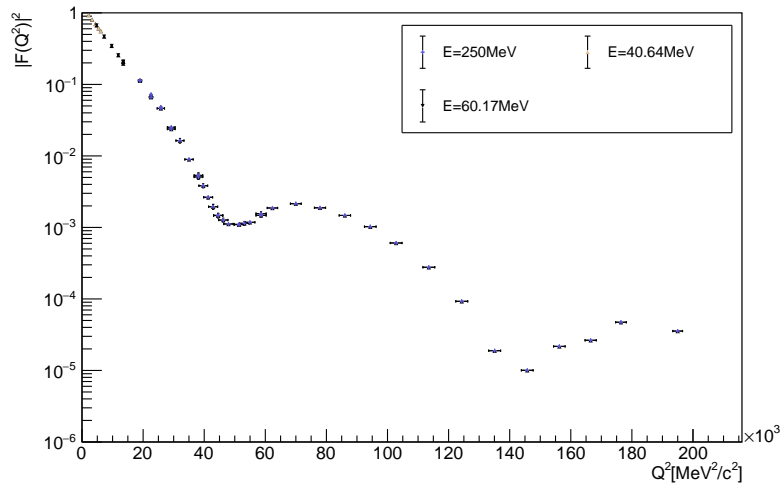


Figure 25: Form factor for elastic electron scattering off the ground state of ^{48}Ca at different beam energies. The error bars are mostly not visible due to marker size.

It is important to note that the range of the Q^2 -values is smaller than for the plots before. It only ranges up to $Q^2 = 100 \cdot 10^3 \frac{\text{MeV}^2}{c^2}$. The form factor values decrease until the first minimum at $Q^2 \approx 55 \cdot 10^3 \frac{\text{MeV}^2}{c^2}$. Then the form factor values increase until $Q^2 = 70 \cdot 10^3 \frac{\text{MeV}^2}{c^2}$. For Q^2 values larger than $Q^2 = 70 \cdot 10^3 \frac{\text{MeV}^2}{c^2}$ the drop off of the form factor values to the second minimum is visible.

5.2.5 Elastic scattering on ^{48}Ca

The form factor values for ^{48}Ca are shown in figure 25 as a function of the momentum transfer.

We see that the plot for ^{48}Ca looks similar the plot for ^{40}Ca . The form factor ranges from $|F(Q^2)|^2 \approx 1$ to $|F(Q^2)|^2 \approx 10^{-5}$. The form factor values decrease until $Q^2 \approx 55 \cdot 10^3 \frac{\text{MeV}^2}{c^2}$ where the form factor values have their first minimum. From $Q^2 = 55 \cdot 10^3 \frac{\text{MeV}^2}{c^2}$ the form factor values increase until $Q^2 = 70 \cdot 10^3 \frac{\text{MeV}^2}{c^2}$ before they decrease until $Q^2 = 145 \cdot 10^3 \frac{\text{MeV}^2}{c^2}$ where the form factor values have their second minimum. After the second minimum the form factor values increase until $Q^2 \approx 180 \cdot 10^3 \frac{\text{MeV}^2}{c^2}$ before they start decreasing towards the third minimum.

5.2.6 Elastic scattering on ^{208}Pb

In figure 26 the form factor values for ^{208}Pb are shown as a function of the momentum transfer Q^2 .

We see that the form factor values range from $F^2(Q^2) \approx 1$ to $F^2(Q^2) \approx 10^{-6}$. The form factor values no longer correlate well for $Q^2 > 30 \cdot 10^3 \frac{\text{MeV}^2}{c^2}$. This is not observed for the other nuclei and is the reason that ROOT has problems with the fits for ^{208}Pb later on.

We can see that the form factor values decrease until $Q^2 = 40 \cdot 10^3 \frac{\text{MeV}^2}{c^2}$. In the interval from $Q^2 \approx 40 \cdot 10^3 \frac{\text{MeV}^2}{c^2}$ to $Q^2 \approx 60 \cdot 10^3 \frac{\text{MeV}^2}{c^2}$ the form factor values form a plateau before they start decreasing until $Q^2 = 80 \cdot 10^3 \frac{\text{MeV}^2}{c^2}$. From there the form factor values form a plateau until $Q^2 = 120 \cdot 10^3 \frac{\text{MeV}^2}{c^2}$ before they start decreasing.

5.2.7 Inelastic scattering on ^{208}Pb

For the inelastic scattering we distinguish between the two lowest energy levels $E_x = 2.6 \text{ MeV}$ and $E_x = 3.2 \text{ MeV}$. In figure 27 the form factor for the inelastic scattering to $E_x = 2.6 \text{ MeV}$ is shown as a function of the momentum transfer Q^2 . The form factor of the inelastic scattering to $E_x = 3.2 \text{ MeV}$ is shown as a function of the momentum transfer Q^2 in figure 28.

The form factor values for the inelastic scattering to $E_x = 2.6 \text{ MeV}$ are one order of magnitude larger than the form factor values for the inelastic scattering to $E_x = 3.2 \text{ MeV}$. The form factor values generally have the shape of two

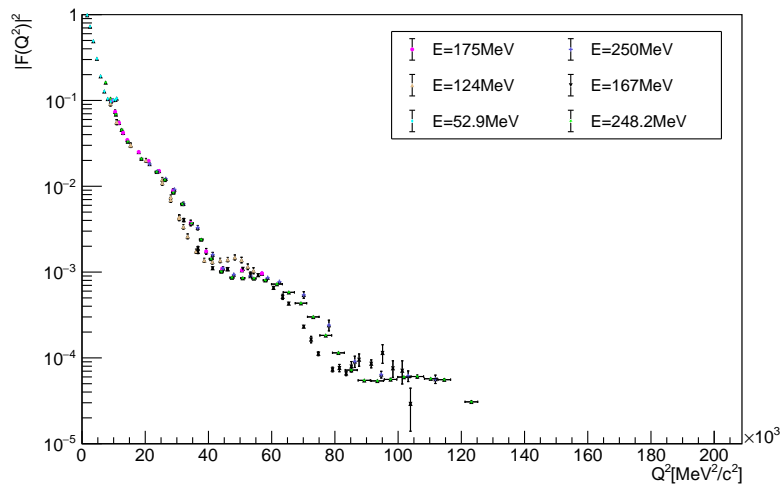


Figure 26: Form factor for elastic electron scattering off the ground state of ^{208}Pb at various beam energies. The error bars are hardly visible due to marker size.

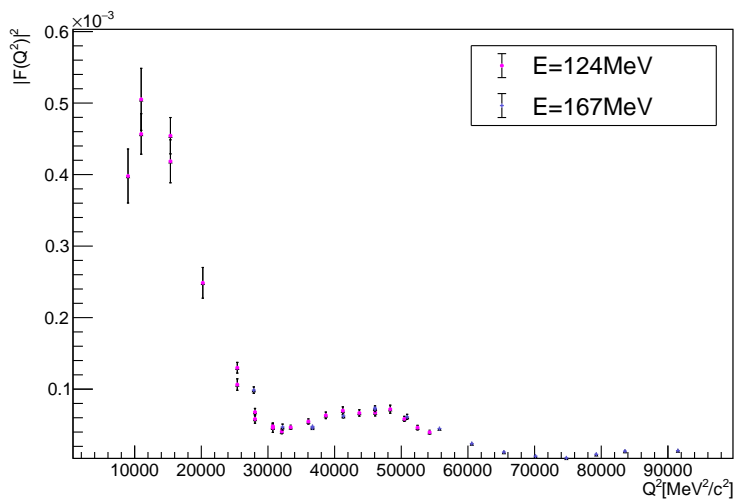


Figure 27: Form factor for inelastic electron scattering off the first excited state $E_x = 2.6$ MeV of ^{208}Pb at different beam energies.

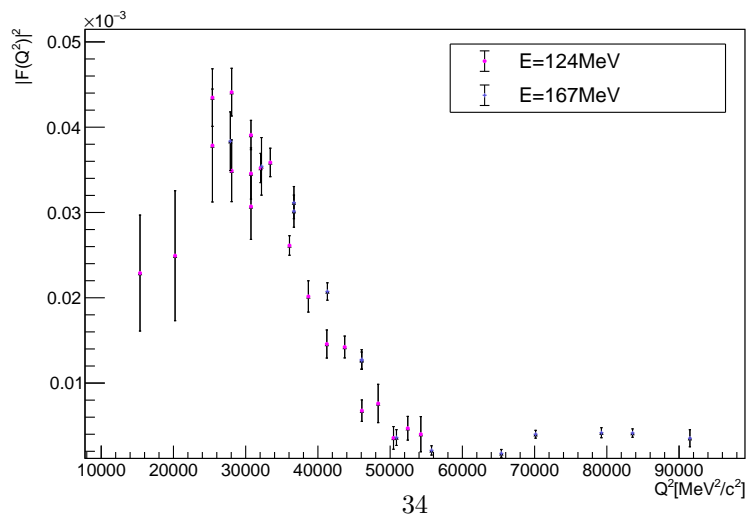


Figure 28: Form factor for inelastic electron scattering off the second excited state $E_x = 3.2$ MeV of ^{208}Pb at different beam energies.

Gaussian functions. The difference is that the height as well as the expected value for the Gaussian functions differ from each other.

Like for ^{12}C the form factor values for inelastic scattering get neglected for the later computations of the measuring time because the form factors for inelastic scattering under forward angles are much smaller than for forward elastic scattering.

5.3 Parameterisation of the form factor for elastic electron scattering

In this section the different parameterisations introduced in section 2.2 are used to fit the form factor plots made in section 5.2.

5.3.1 Helm form factor parameterisation

The Helm form factor parameterisation introduced in equation (11) is used to fit the form factor data for each nucleus.

To start fitting the Helm form factor to the data points, the starting parameters had to be guessed. To do these guesses the fit panel of ROOT was used. The fit panel visualizes the fit of the data points for a given set of parameters. This way by guessing different sets of parameters we can try to approximate the fit function. If one set of parameters matches the data point the parameters were set as starting parameters for the fit function of ROOT. If ROOT does not find a good solution with the given parameters new sets of parameters are tested with the help of the fit panel. This is done for each nucleus.

In figure 29 the Helm form factor fit function for the form factor of ^{12}C is plotted together with the data from figure 19. Figure 30 shows the Helm form factor parameterisation for the specific Q^2 interval of the P2-experiment. The Q^2 interval ranges from $Q^2 = 3000 \frac{\text{MeV}^2}{c^2}$ to $Q^2 = 7000 \frac{\text{MeV}^2}{c^2}$.

The fit function agrees well with the form factor value up to $Q^2 = 110 \cdot 10^3 \frac{\text{MeV}^2}{c^2}$. After that the fit deviates up to the minimum of the data points. From $Q^2 = 130 \cdot 10^3 \frac{\text{MeV}^2}{c^2}$ to $Q^2 = 190 \cdot 10^3 \frac{\text{MeV}^2}{c^2}$ the fit agrees well with the form factor values. For the data points $Q^2 > 190 \cdot 10^3 \frac{\text{MeV}^2}{c^2}$ the form factor values and the fit function deviate greatly.

The fit parameters for the Helm parameterisation are listed in table 1.

Parameter	Value
Effective nuclear radius	$0.0127847 \pm 1.1 \cdot 10^{-6} \frac{c}{\text{MeV}}$
Nuclear skin thickness	$0.0041082 \pm 1.7 \cdot 10^{-6} \frac{c}{\text{MeV}}$

Table 1: Fit parameter for the Helm parameterisation for ^{12}C

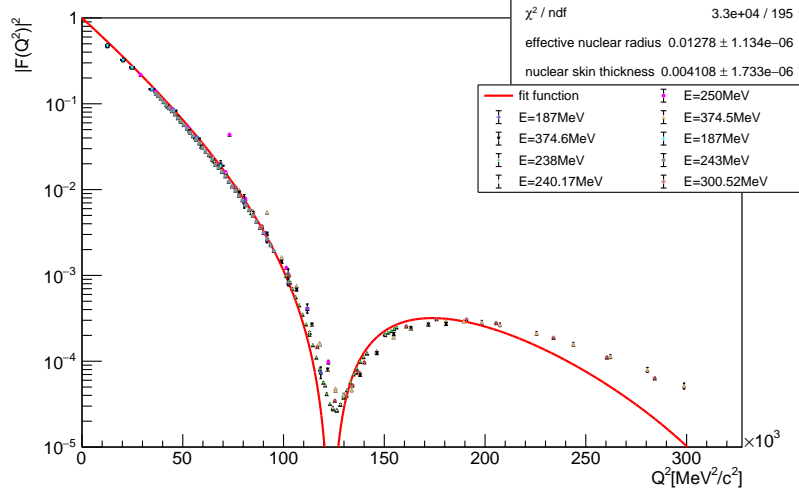


Figure 29: Helm form factor parameterisation for elastic electron scattering off the ground state of ^{12}C .

In figure 31 the fit function for the Helm parameterisation for the form factor of ^{40}Ca is plotted together with the data from figure 23. Figure 32 shows the Helm parameterisation in the Q^2 interval of the P2-experiment.

The fit function matches the data points up to $Q^2 \approx 40 \cdot 10^3 \frac{\text{MeV}^2}{c^2}$. We see that the fit function can not be used to describe the minimum of the data points because the helm function gets zero at $Q^2 \approx 50 \cdot 10^3 \frac{\text{MeV}^2}{c^2}$. From $Q^2 = 60 \cdot 10^3 \frac{\text{MeV}^2}{c^2}$ to $Q^2 = 130 \cdot 10^3 \frac{\text{MeV}^2}{c^2}$ the fit functions matches the data points good. The fit function can also not describe the minimum at $Q^2 = 140 \cdot 10^3 \frac{\text{MeV}^2}{c^2}$. The fit parameters for the Helm parameterisation are given in table 2.

Parameter	Value
Effective nuclear radius	$0.0202456 \pm 4.7 \cdot 10^{-6} \frac{c}{\text{MeV}}$
Nuclear skin thickness	$0.004542 \pm 1.1 \cdot 10^{-5} \frac{c}{\text{MeV}}$

Table 2: Fit parameter for the Helm parameterisation for ^{40}Ca

For ^{42}Ca the Helm form factor fit function is plotted in figure 33 and figure 34 shows the Helm parameterisation for the Q^2 interval of the P2-experiment.

The fit function agrees with the data points up to $Q^2 \approx 30 \cdot 10^3 \frac{\text{MeV}^2}{c^2}$. In the interval from $Q^2 = 30 \cdot 10^3 \frac{\text{MeV}^2}{c^2}$ to $Q^2 = 55 \cdot 10^3 \frac{\text{MeV}^2}{c^2}$ the fit function deviates from the data points. For $Q^2 > 55 \cdot 10^3 \frac{\text{MeV}^2}{c^2}$ the fit function agrees with the form factor values.

The fit parameters are listed in table 3.

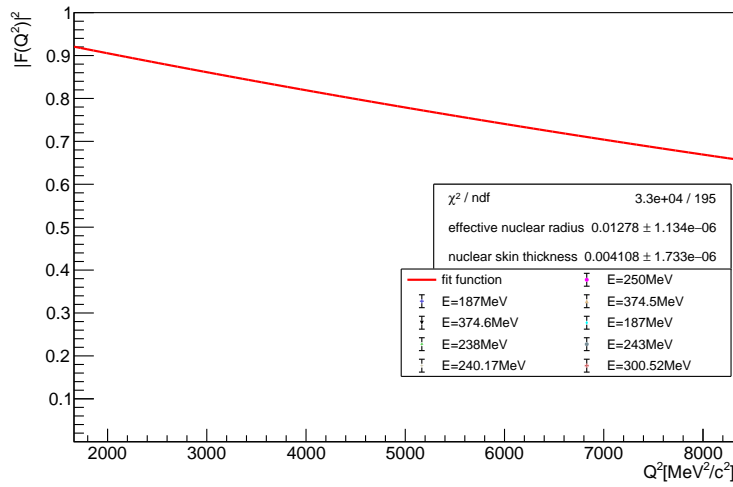


Figure 30: Helm form factor parameterisation for elastic electron scattering off the ground state of ^{12}C in the Q^2 interval of the P2-experiment. The averaged Q^2 for the P2-experiment is $Q^2 = 5000 \frac{\text{MeV}^2}{c^2}$.

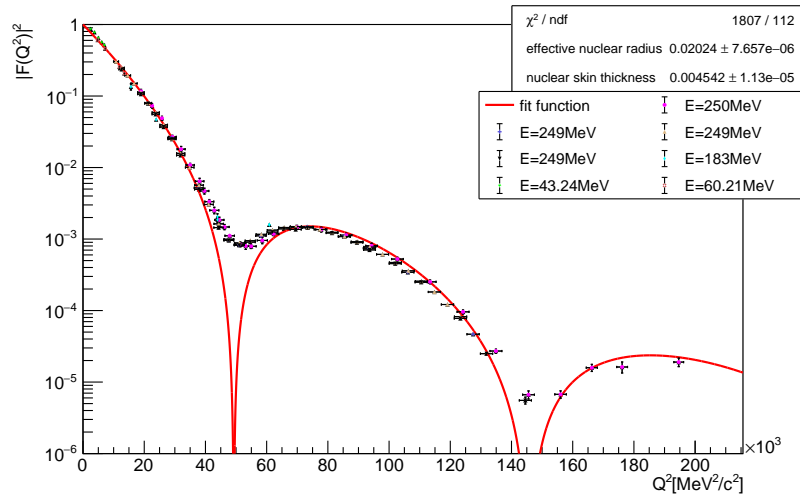


Figure 31: Helm form factor parameterisation for elastic electron scattering off the ground state of ^{40}Ca .

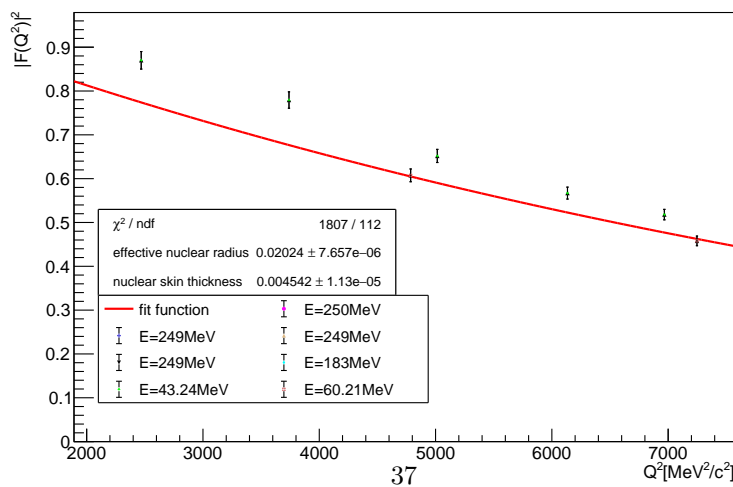


Figure 32: Helm form factor parameterisation for elastic electron scattering off the ground state of ^{40}Ca in the Q^2 interval of the P2-experiment. The averaged Q^2 for the P2-experiment is $Q^2 = 5000 \frac{\text{MeV}^2}{c^2}$.

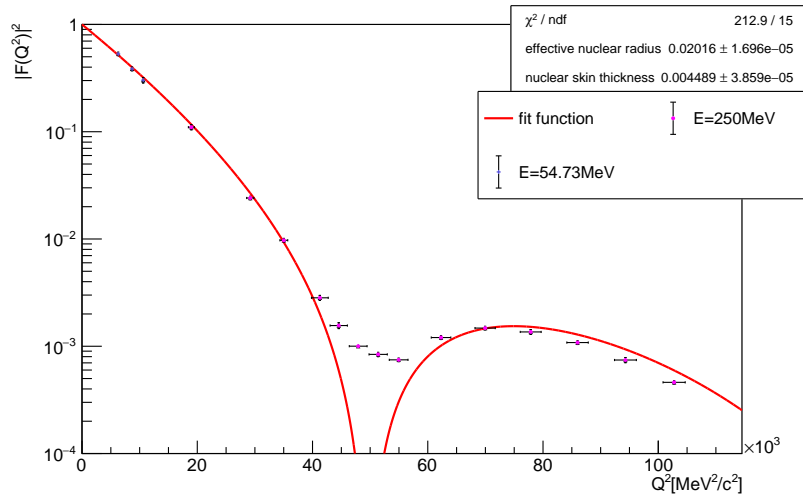


Figure 33: Helm form factor parameterisation for elastic electron scattering off the ground state of ^{42}Ca .

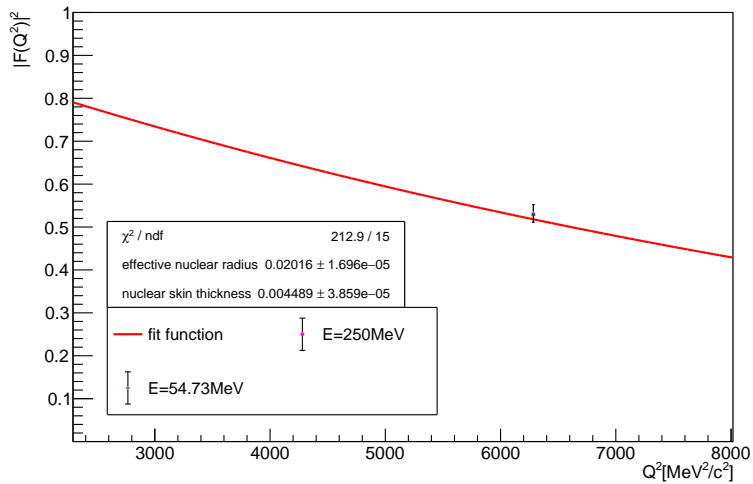


Figure 34: Helm form factor parameterisation for elastic electron scattering off the ground state of ^{42}Ca in the Q^2 interval of the P2-experiment. The averaged Q^2 for the P2-experiment is $Q^2 = 5000 \frac{\text{MeV}^2}{c^2}$.

Parameter	Value
Effective nuclear radius	$0.020161 \pm 1.7 \cdot 10^{-5} \frac{c}{\text{MeV}}$
Nuclear skin thickness	$0.004489 \pm 3.9 \cdot 10^{-5} \frac{c}{\text{MeV}}$

Table 3: Fit parameter for the Helm parameterisation for ^{42}Ca

The Helm form factor parameterisation for ^{48}Ca is shown in figure 35. Figure 36 shows the Helm form factor in the limited interval of Q^2 for the P2-experiment.

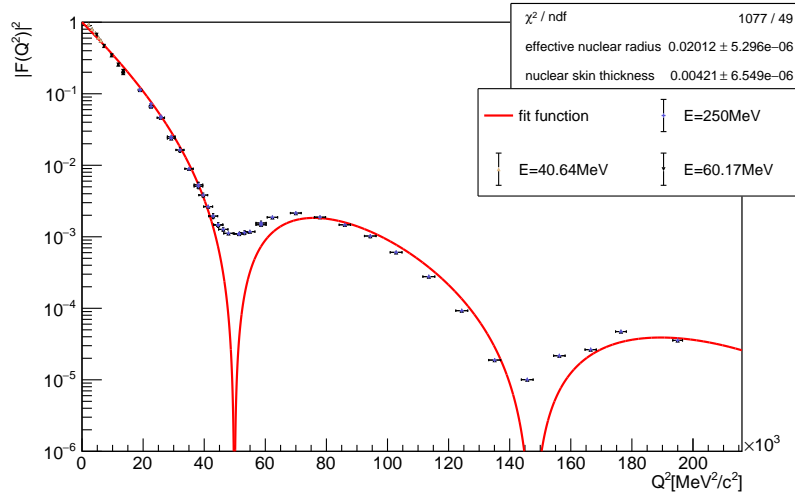


Figure 35: Helm form factor parameterisation for elastic electron scattering off the ground state of ^{48}Ca .

The fit function matches the data points up to $Q^2 = 45 \cdot 10^3 \frac{\text{MeV}^2}{c^2}$. From $Q^2 = 45 \cdot 10^3 \frac{\text{MeV}^2}{c^2}$ to $Q^2 = 70 \cdot 10^3 \frac{\text{MeV}^2}{c^2}$ the fit function does not agree with the form factor values. From $Q^2 = 70 \cdot 10^3 \frac{\text{MeV}^2}{c^2}$ up to $Q^2 = 140 \cdot 10^3 \frac{\text{MeV}^2}{c^2}$ the fit does not precisely agree with the data points. For Q^2 values larger than $Q^2 = 140 \cdot 10^3 \frac{\text{MeV}^2}{c^2}$ the fit function does not agree very well with the data points. In table 4 the fit parameters are listed.

Parameter	Value
Effective nuclear radius	$0.0201175 \pm 5.3 \cdot 10^{-6} \frac{c}{\text{MeV}}$
Nuclear skin thickness	$0.0042099 \pm 6.5 \cdot 10^{-6} \frac{c}{\text{MeV}}$

Table 4: Fit parameter for the Helm parameterisation for ^{48}Ca

For ^{208}Pb ROOT was not able to find a fit function. The problem is that the

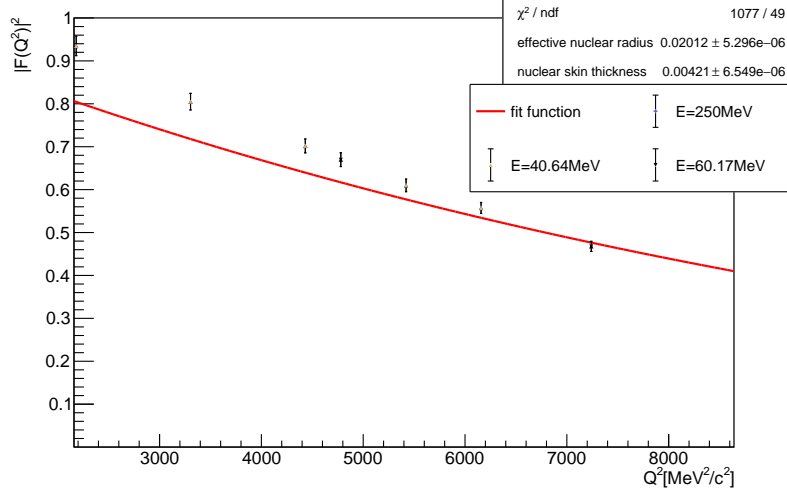


Figure 36: Helm form factor parameterisation for elastic electron scattering off the ground state of ^{48}Ca in the Q^2 interval of the P2-experiment. The averaged Q^2 for the P2-experiment is $Q^2 = 5000 \frac{\text{MeV}^2}{c^2}$.

different data points do not correlate as good as the data points for the other nuclei.

5.3.2 Sum of Gaussian functions form factor parameterisation

The sum of Gaussian parameterisation introduced in equation (14) is used to fit the form factor plots of each nucleus.

To start fitting the data points the starting parameters need to be guessed. For the sum of Gaussian functions parameterisation the values from the "Nuclear Data Tables" [26] were used as starting parameters for the fitting function of ROOT. Therefore, the values that were found by ROOT are not the same as the values from the "Nuclear Data Tables".

The sum of Gaussian parameterisation for ^{12}C is shown in figure 37. Figure 38 shows the sum of Gaussian parameterisation for the limited Q^2 interval of the P2-experiment.

The sum of Gaussian parameterisation is consistent up to $Q^2 = 180 \cdot 10^3 \frac{\text{MeV}^2}{c^2}$ with the Helm form factor parameterisation. For Q^2 values larger than $Q^2 = 180 \cdot 10^3 \frac{\text{MeV}^2}{c^2}$ the sum of Gaussian parameterisation describes the form factor values better than the Helm form factor parameterisation. It is important to note that the sum of Gaussian parameterisation has 4 parameters more than the Helm parameterisation. The sum of the Q_i parameters gives approximately

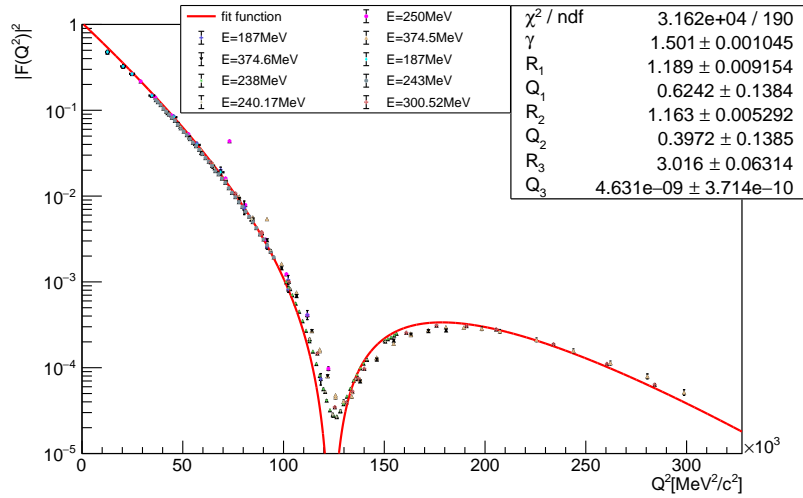


Figure 37: Sum of Gaussian form factor parameterisation for elastic electron scattering off the ground state of ^{12}C .

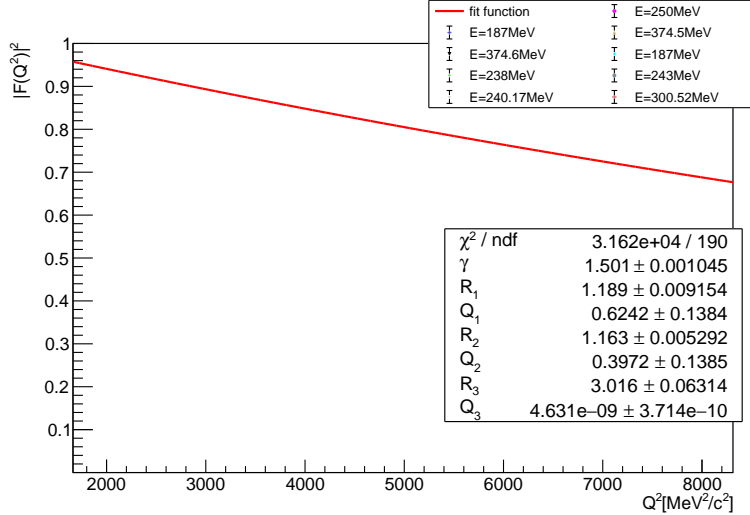


Figure 38: Sum of Gaussian form factor parameterisation parameterisation for elastic electron scattering off the ground state of ^{12}C in the Q^2 interval of the P2-experiment. The averaged Q^2 for the P2-experiment is $Q^2 = 5000 \frac{\text{MeV}^2}{c^2}$.

1. The fit parameters are listed in table 5.

Parameter	Value
γ	$1.501 \pm 1 \cdot 10^{-3}$ fm
R_1	$1.189 \pm 9 \cdot 10^{-3}$ fm
Q_1	0.62 ± 0.14
R_2	$1.163 \pm 5 \cdot 10^{-3}$ fm
Q_2	0.40 ± 0.14
R_3	3.016 ± 0.063 fm
Q_3	$4.63 \cdot 10^{-9} \pm 0.37 \cdot 10^{-9}$

Table 5: Fit parameter for the sum of Gaussian parameterisation for ^{12}C

The sum of Gaussian parameterisation fit function for ^{40}Ca is plotted in figure 39. Figure 40 shows the sum of Gaussian parameterisation in the Q^2 interval of the P2-experiment.

Up to $Q^2 = 30 \cdot 10^3 \frac{\text{MeV}^2}{c^2}$ the fit function matches the data points. The sum of Gaussian parameterisation does not describe the form factor values as good as the Helm parameterisation for Q^2 values between $Q^2 = 30 \cdot 10^3 \frac{\text{MeV}^2}{c^2}$ and $Q^2 = 40 \cdot 10^3 \frac{\text{MeV}^2}{c^2}$. Like the Helm parameterisation the sum of Gaussian parameterisation does not match the data points around the local minimum. From $Q^2 = 55 \cdot 10^3 \frac{\text{MeV}^2}{c^2}$ up to $130 \cdot 10^3 \frac{\text{MeV}^2}{c^2}$ the fit function agrees even better than the Helm parameterisation with the form factor values. For larger momentum transfers than $Q^2 = 130 \cdot 10^3 \frac{\text{MeV}^2}{c^2}$ the fit function deviates from the data points. Just as for ^{12}C the sum of the Q_i parameters gives approximately 1. The fit parameters for the sum of Gaussian function are given in table 6.

Parameter	Value
γ	1.703 ± 0.029 fm
R_1	0.1362 ± 0.0886 fm
Q_1	0.0812 ± 0.0031
R_2	3.88 ± 0.11 fm
Q_2	0.131 ± 0.022
R_3	2.58 ± 0.01 fm
Q_3	0.866 ± 0.018

Table 6: Fit parameter for the sum of Gaussian parameterisation for ^{40}Ca

For ^{42}Ca the fit function is shown in figure 41. Figure 42 shows the sum of Gaussian fit function for ^{42}Ca in the Q^2 interval for the P2-experiment. The fit parameters are listed in table 7.

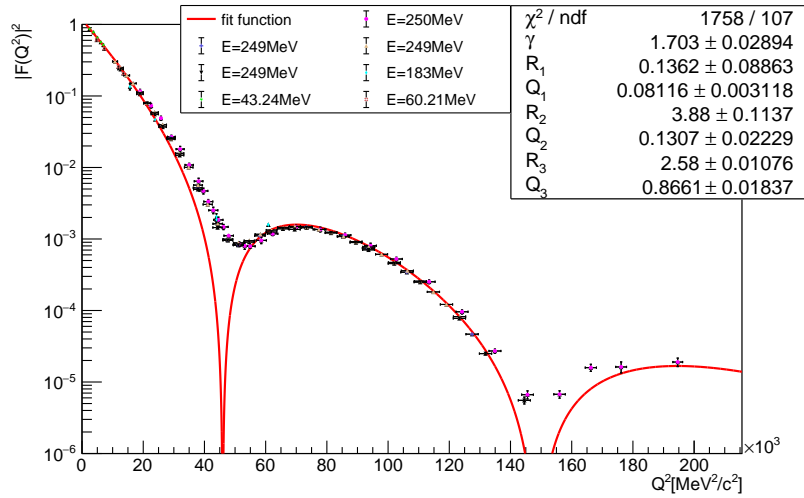


Figure 39: Sum of Gaussian form factor parameterisation for elastic electron scattering off the ground state of ^{40}Ca .

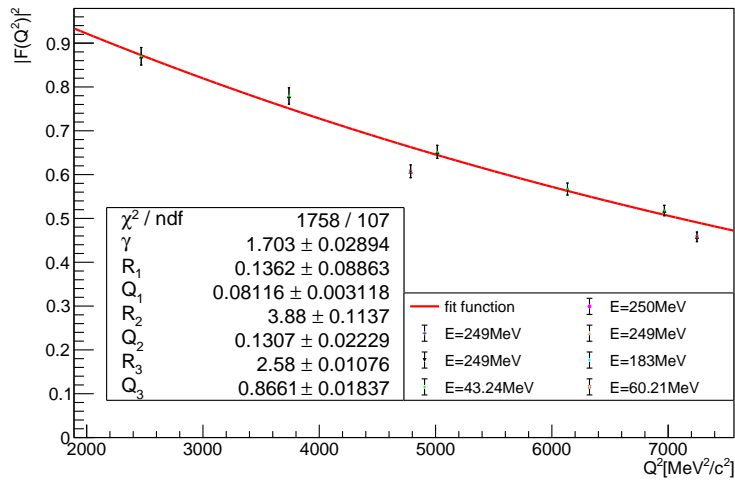


Figure 40: Sum of Gaussian form factor parameterisation for elastic electron scattering off the ground state of ^{40}Ca in the Q^2 interval of the P2-experiment. The averaged Q^2 for the P2-experiment is $Q^2 = 5000 \frac{\text{MeV}^2}{c^2}$.

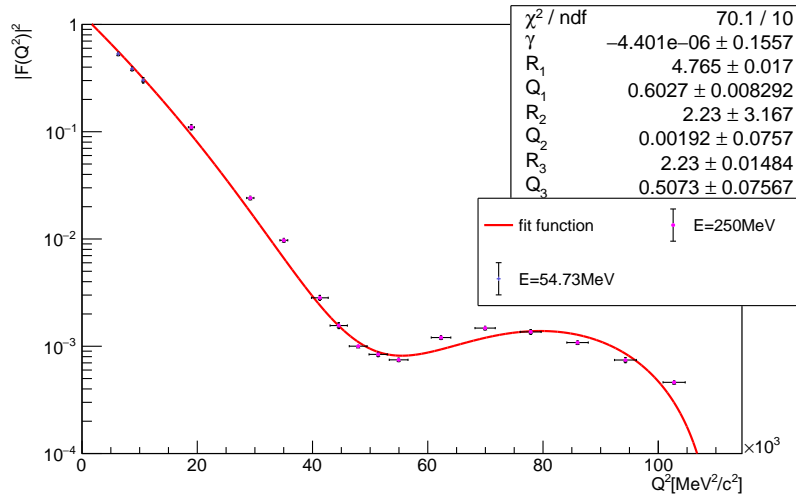


Figure 41: Sum of Gaussian form factor parameterisation for elastic electron scattering off the ground state of ^{42}Ca .

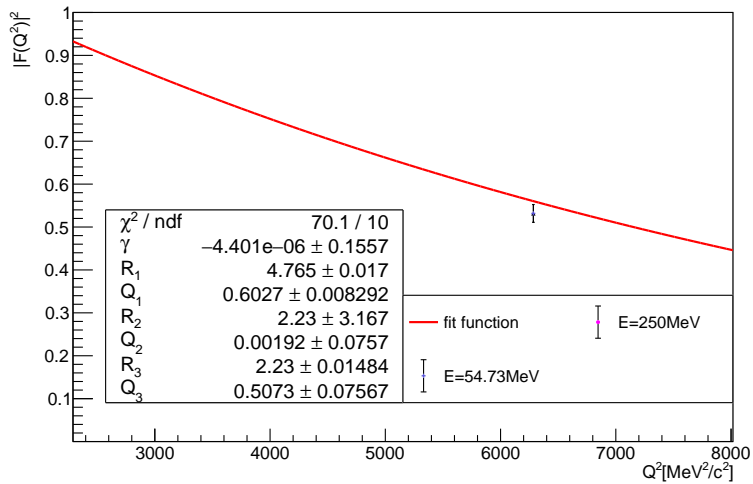


Figure 42: Sum of Gaussian form factor parameterisation for elastic electron scattering off the ground state of ^{42}Ca in the Q^2 interval of the P2-experiment. The averaged Q^2 for the P2-experiment is $Q^2 = 5000 \frac{\text{MeV}^2}{c^2}$.

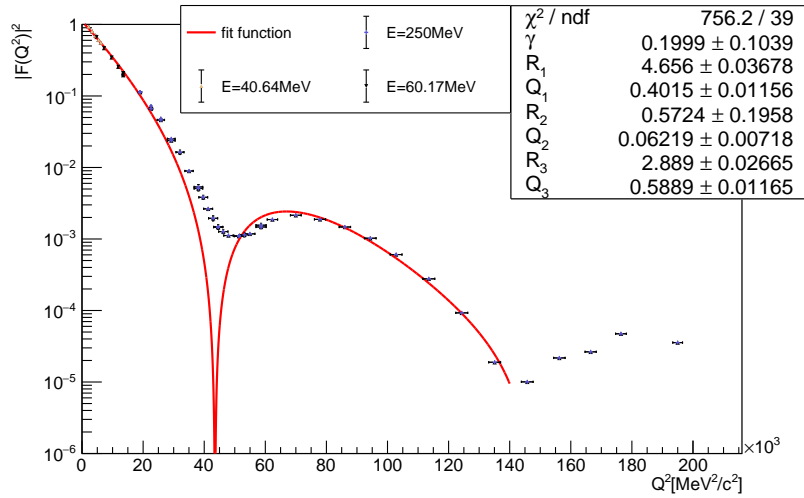


Figure 43: Sum of Gaussian form factor parameterisation for elastic electron scattering off the ground state of ^{48}Ca .

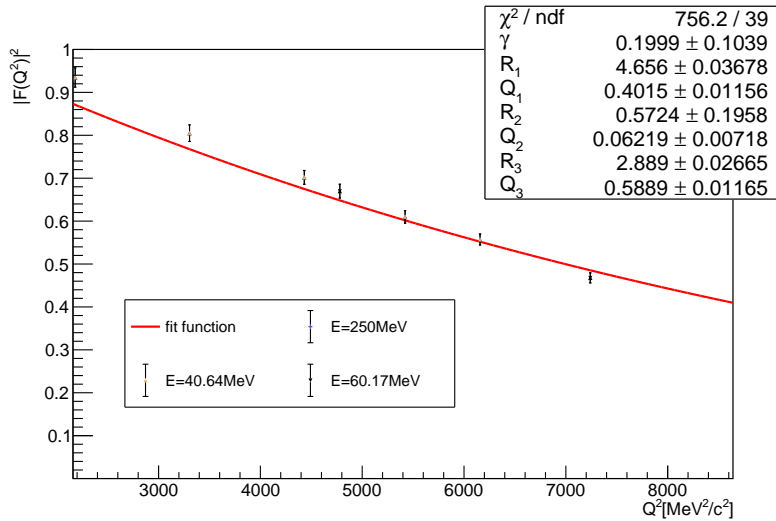


Figure 44: Sum of Gaussian form factor parameterisation for elastic electron scattering off the ground state of ^{48}Ca in the Q^2 interval of the P2-experiment. The averaged Q^2 for the P2-experiment is $Q^2 = 5000 \frac{\text{MeV}^2}{c^2}$.

Parameter	Value
γ	0.00 ± 0.16 fm
R_1	4.765 ± 0.017 fm
Q_1	$0.6027 \pm 8.3 \cdot 10^{-3}$
R_2	2.2 ± 3.2 fm
Q_2	$2 \cdot 10^{-3} \pm 76 \cdot 10^{-3}$
R_3	2.23 ± 0.01 fm
Q_3	0.507 ± 0.076

Table 7: Fit parameter for the sum of Gaussian parameterisation for ^{42}Ca

Generally, the sum of Gaussian parameterisation describes the form factor precisely. The sum of Gaussian parameterisation agrees with the data points better than the Helm parameterisation which was used before. The sum of the Q_i is approximately 1.

In figure 43 the sum of Gaussian fit for ^{48}Ca is plotted. Figure 44 shows the same parameterisation in the Q^2 interval of the P2-experiment.

The function was only fitted up to $Q^2 = 140 \cdot 10^3 \frac{\text{MeV}^2}{c^2}$ because ROOT was not able to fit a function over the whole interval of Q^2 . Therefore, the function is fitted as far as possible.

Up to $Q^2 \approx 30 \cdot 10^3 \frac{\text{MeV}^2}{c^2}$ the fit function matches the form factor values. From $Q^2 = 30 \cdot 10^3 \frac{\text{MeV}^2}{c^2}$ to $Q^2 = 50 \cdot 10^3 \frac{\text{MeV}^2}{c^2}$ the fit function does not agree with the data points. For larger Q^2 up to $Q^2 = 140 \cdot 10^3 \frac{\text{MeV}^2}{c^2}$ the fit function describes the form factor precise. The sum of the parameters Q_i is approximately 1.

The fit parameters are listed in table 8.

Parameter	Value
γ	0.20 ± 0.10 fm
R_1	4.656 ± 0.037 fm
Q_1	0.40 ± 0.01
R_2	0.57 ± 0.20 fm
Q_2	0.0622 ± 0.00072
R_3	2.889 ± 0.027 fm
Q_3	0.589 ± 0.012

Table 8: Fit parameter for the sum of Gaussian parameterisation for ^{48}Ca

For ^{208}Pb the same problem as for the Helm parameterisation occurs. ROOT is not able to fit the function to the data points.

5.3.3 The Fourier-Bessel parameterisation

The Fourier-Bessel parameterisation introduced in equation (18) is used to fit the form factor data of each nucleus.

The start parameters for the fit are again taken from the "Nuclear Data Tables" [26]. The fit for ^{12}C is shown in figure 45. Figure 46 shows the fit for the Q^2 interval of the P2-experiment.

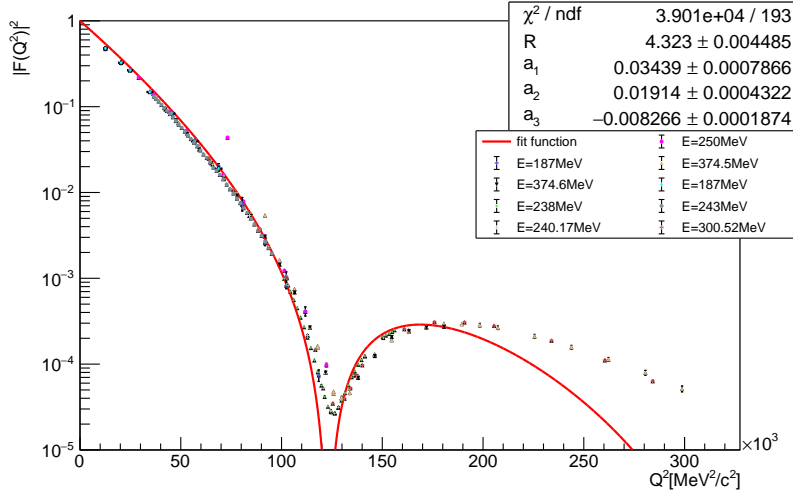


Figure 45: Fourier-Bessel form factor parameterisation for elastic electron scattering off the ground state of ^{12}C .

Generally, we see that even in the range for small values of Q^2 up to $Q^2 = 40 \cdot 10^3 \frac{\text{MeV}^2}{c^2}$ the fit function deviates more from the form factor values than the parameterisations before and describes the form factor for $Q^2 > 180 \cdot 10^3 \frac{\text{MeV}^2}{c^2}$ even worse than the parameterisations before.

The fit parameters are given in table 9.

Parameter	Value
R	$4.3235 \pm 4.5 \cdot 10^{-3} \text{ fm}$
a_1	$0.03439 \pm 7.9 \cdot 10^{-4}$
a_2	$0.01914 \pm 4.3 \cdot 10^{-4}$
a_3	-0.00827 ± 0.00019

Table 9: Fit parameter for the Fourier-Bessel parameterisation for ^{12}C

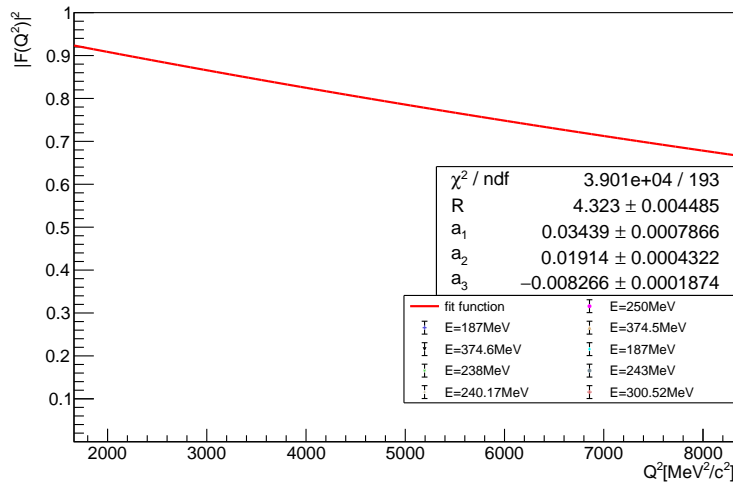


Figure 46: Fourier-Bessel form factor parameterisation for elastic electron scattering off the ground state of ^{12}C in the Q^2 interval of the P2-experiment. The averaged Q^2 for the P2-experiment is $Q^2 = 5000 \frac{\text{MeV}^2}{c^2}$.

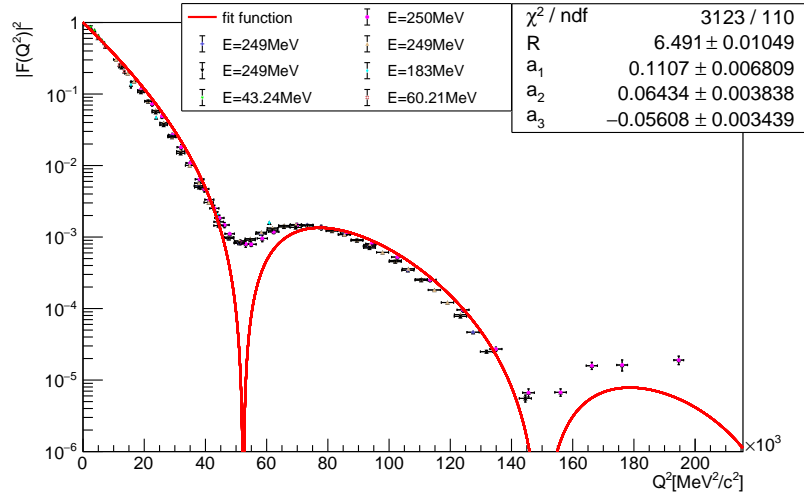


Figure 47: Fourier-Bessel form factor parameterisation for elastic electron scattering off the ground state of ^{40}Ca .

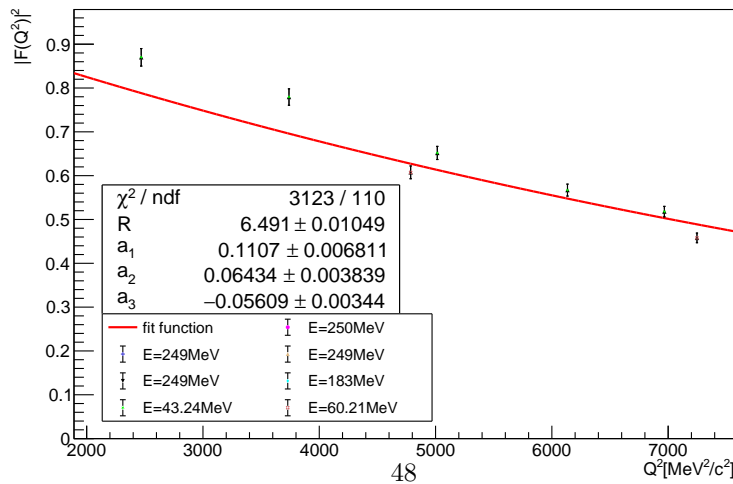


Figure 48: Fourier-Bessel form factor parameterisation for elastic electron scattering off the ground state of ^{40}Ca in the Q^2 interval of the P2-experiment. The averaged Q^2 for the P2-experiment is $Q^2 = 5000 \frac{\text{MeV}^2}{c^2}$.

In figure 47 the Fourier-Bessel parameterisation for ^{40}Ca is plotted. Figure 48 shows the Fourier-Bessel fit function in the Q^2 interval of the P2-experiment. The Fourier-Bessel parameterisation has problems with describing the minimum of the data points at $Q^2 \approx 55 \cdot 10^3 \frac{\text{MeV}^2}{c^2}$. The fit function matches the data points until $Q^2 = 45 \cdot 10^3 \frac{\text{MeV}^2}{c^2}$ and from $Q^2 = 70 \cdot 10^3 \frac{\text{MeV}^2}{c^2}$ to $Q^2 = 140 \cdot 10^3 \frac{\text{MeV}^2}{c^2}$. For larger Q^2 -values then $Q^2 = 140 \cdot 10^3 \frac{\text{MeV}^2}{c^2}$ the function does not match the data points.

The fit parameters are listed in table 10.

Parameter	Value
R	$6.491 \pm 0.010 \text{ fm}$
a_1	$0.1107 \pm 6.8 \cdot 10^{-3}$
a_2	0.0643 ± 0.0038
a_3	-0.0561 ± 0.0034

Table 10: Fit parameter for the Fourier-Bessel parameterisation for ^{40}Ca

For ^{42}Ca the fit function is plotted in figure 49. Figure 50 shows the fit function for ^{42}Ca in the Q^2 interval of the P2-experiment.

The Fourier-Bessel parameterisation again has the problem in matching the minimum of the form factor values at $Q^2 = 50 \cdot 10^3 \frac{\text{MeV}^2}{c^2}$. The fit function agrees with the other form factor values.

The fit parameters are given in table 11.

Parameter	Value
R	$6.915 \pm 0.056 \text{ fm}$
a_1	0.025 ± 0.010
a_2	0.0190 ± 0.0079
a_3	-0.0134 ± 0.0057

Table 11: Fit parameter for the Fourier-Bessel parameterisation for ^{42}Ca

The Fourier-Bessel fit function for ^{48}Ca is plotted in figure 51. Figure 52 shows the fit function in the Q^2 interval of the P2-experiment.

As for the nuclei before the Fourier-Bessel function struggles to describe the minimum at $Q^2 \approx 50 \cdot 10^3 \frac{\text{MeV}^2}{c^2}$. In contrast to the parameterisations used before the Fourier-Bessel parameterisation does not precisely describe the form factor values in the interval from $Q^2 = 70 \cdot 10^3 \frac{\text{MeV}^2}{c^2}$ to $Q^2 = 130 \cdot 10^3 \frac{\text{MeV}^2}{c^2}$.

In table 12 the fit parameter are listed.

For ^{208}Pb the same applies as for the parameterisations used before.

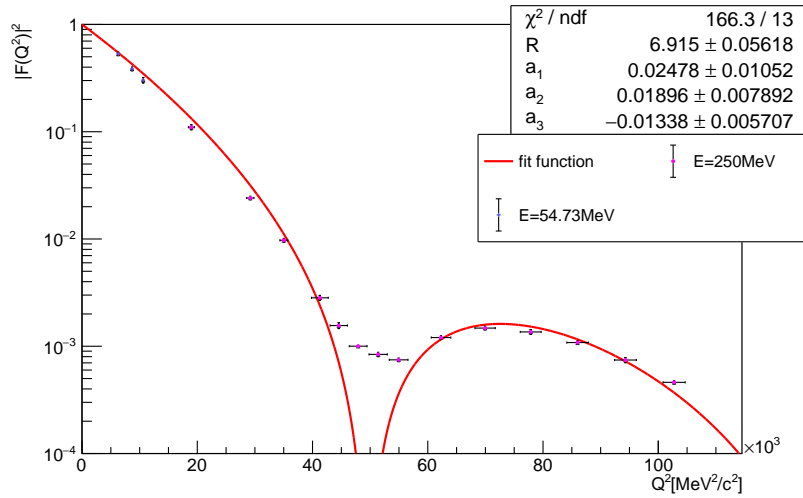


Figure 49: Fourier-Bessel form factor parameterisation for elastic electron scattering off the ground state of ^{42}Ca .

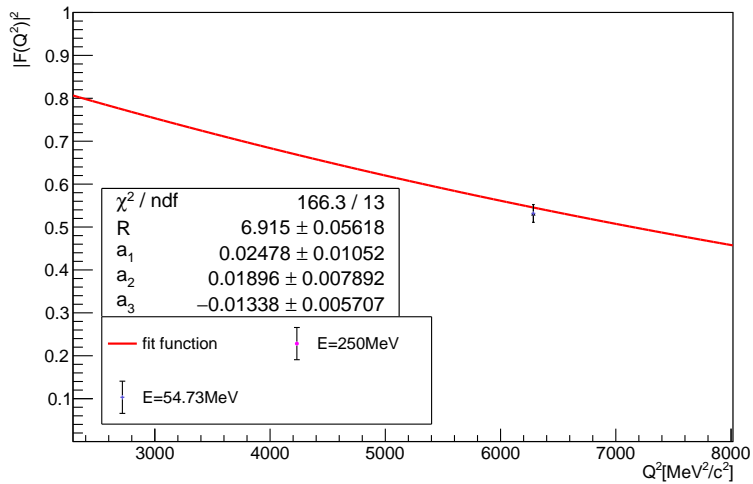


Figure 50: Fourier-Bessel form factor parameterisation for elastic electron scattering off the ground state of ^{42}Ca in the Q^2 interval of the P2-experiment. The averaged Q^2 for the P2-experiment is $Q^2 = 5000 \frac{\text{MeV}^2}{c^2}$.

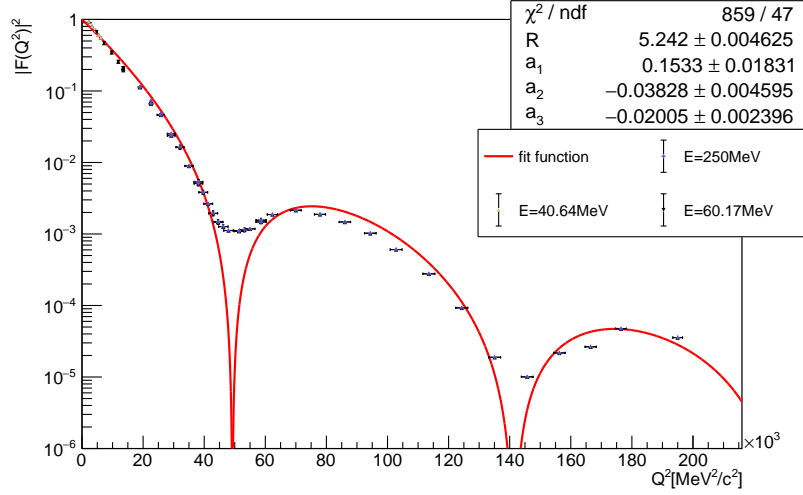


Figure 51: Fourier-Bessel form factor parameterisation for elastic electron scattering off the ground state of ^{48}Ca

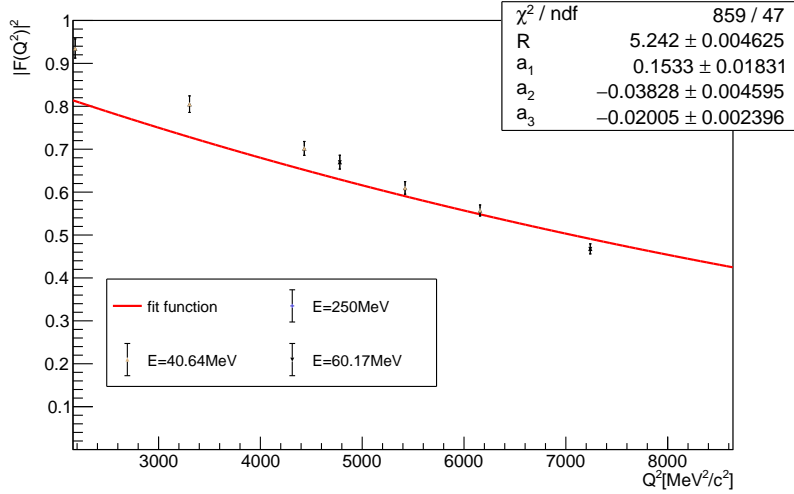


Figure 52: Fourier-Bessel form factor parameterisation for elastic electron scattering off the ground state of ^{48}Ca in the Q^2 interval of the P2-experiment. The averaged Q^2 for the P2-experiment is $Q^2 = 5000 \frac{\text{MeV}^2}{c^2}$.

Parameter	Value
R	$5.2428 \pm 4.6 \cdot 10^{-3}$ fm
a_1	0.153 ± 0.018
a_2	-0.0383 ± 0.0046
a_3	-0.0201 ± 0.0024

Table 12: Fit parameter for the Fourier-Bessel parameterisation for ^{48}Ca

5.3.4 Polynomial function parameterisation

The polynomial function parameterisation introduced in equation (20) is used to fit the form factor data of each nucleus.

To find the start parameters for this parameterisations the fit panel of ROOT was used. The first 4 parameters were found by trying to fit the data points up to the first minimum of the form factor values. The other parameters were calculated by the fit function of ROOT after presetting the 4 parameters.

The fit function for ^{12}C is plotted in figure 53 as a function of the momentum transfer. Figure 54 shows the polynomial fit function in the Q^2 interval of the P2-experiment.

Generally, we see that the fit functions describes the form factor up to $Q^2 = 125 \cdot 10^3 \frac{\text{MeV}^2}{c^2}$ with high precision. For the values of $Q^2 = 125 \cdot 10^3 \frac{\text{MeV}^2}{c^2}$ to $Q^2 = 135 \cdot 10^3 \frac{\text{MeV}^2}{c^2}$ the fit function differs from the measuring data. For the rest of the Q^2 values the fit describes the measuring data better than the Helm form factor parameterisation and the Fourier Bessel parameterisation but worse than the sum of Gaussian parameterisation.

Table 13 lists the fit parameter of the polynomial parameterisation for ^{12}C .

Parameter	Value
a_0	$3.3897 \cdot 10^{-5} \pm 9.3 \cdot 10^{-8} \frac{c^2}{\text{MeV}^2}$
a_1	-0.949 ± 0.018
a_2	$-2.090 \cdot 10^{-5} \pm 5.3 \cdot 10^{-7} \frac{c^2}{\text{MeV}^2}$
a_3	$5.378 \cdot 10^{-10} \pm 5.9 \cdot 10^{-12} \frac{c^4}{\text{MeV}^4}$
a_4	$-7.2535 \cdot 10^{-15} \pm 6.9 \cdot 10^{-18} \frac{c^6}{\text{MeV}^6}$
a_5	$4.023 \cdot 10^{-20} \pm 1.2 \cdot 10^{-22} \frac{c^8}{\text{MeV}^8}$
a_6	$-2.219 \cdot 10^{-26} \pm 8.8 \cdot 10^{-28} \frac{c^{10}}{\text{MeV}^{10}}$

Table 13: Fit parameter for the polynomial function parameterisation for ^{12}C

For ^{40}Ca the polynomial parameterisation fit function is plotted in figure 55. Figure 56 shows the shows the fit function in the Q^2 interval of the P2-experiment.

Here, we only fitted up to $Q^2 = 135 \cdot 10^3 \frac{\text{MeV}^2}{c^2}$ because ROOT was not able to find a good fitting result for larger intervals of Q^2 . The chosen fit functions was

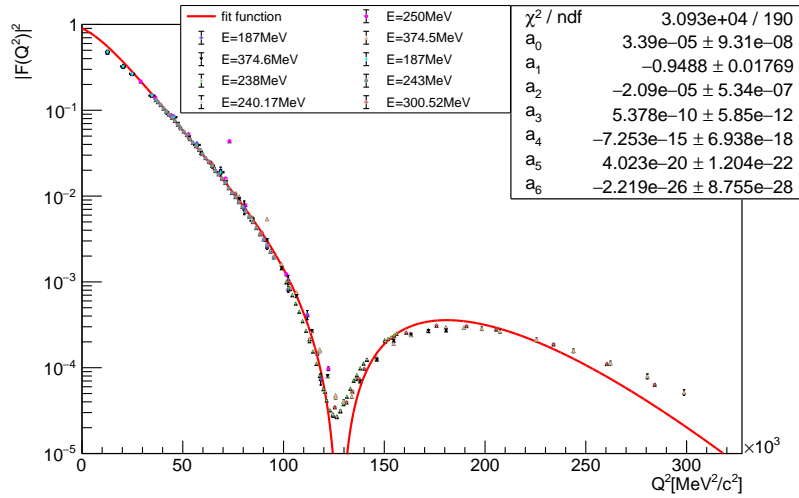


Figure 53: Polynomial function form factor parameterisation for elastic electron scattering off the ground state of ^{12}C .

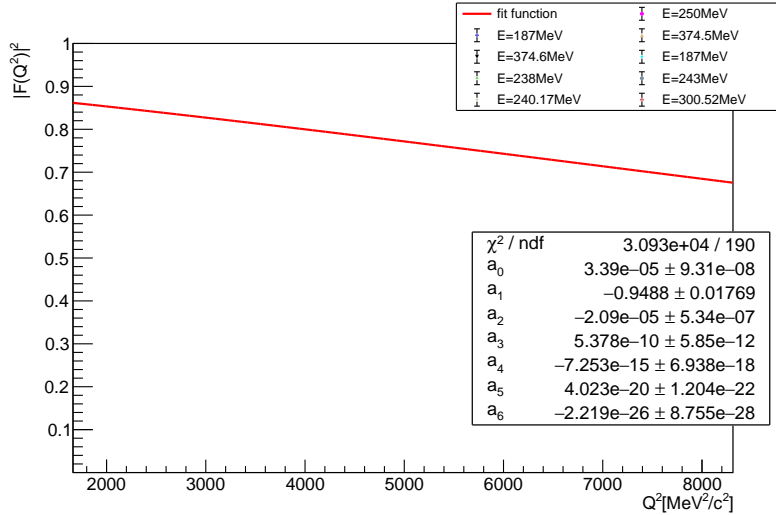


Figure 54: Polynomial function form factor parameterisation for elastic electron scattering off the ground state of ^{12}C in the Q^2 interval of the P2-experiment. The averaged Q^2 for the P2-experiment is $Q^2 = 5000 \frac{\text{MeV}^2}{c^2}$.

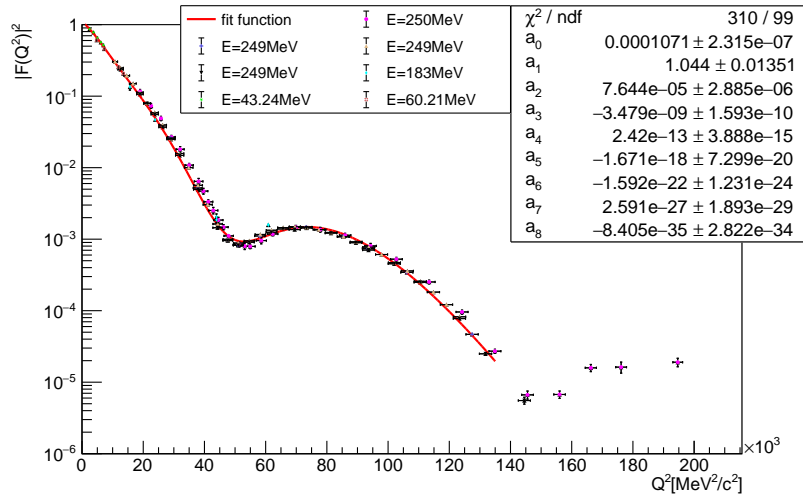


Figure 55: Polynomial function form factor parameterisation for elastic electron scattering off the ground state of ^{40}Ca .

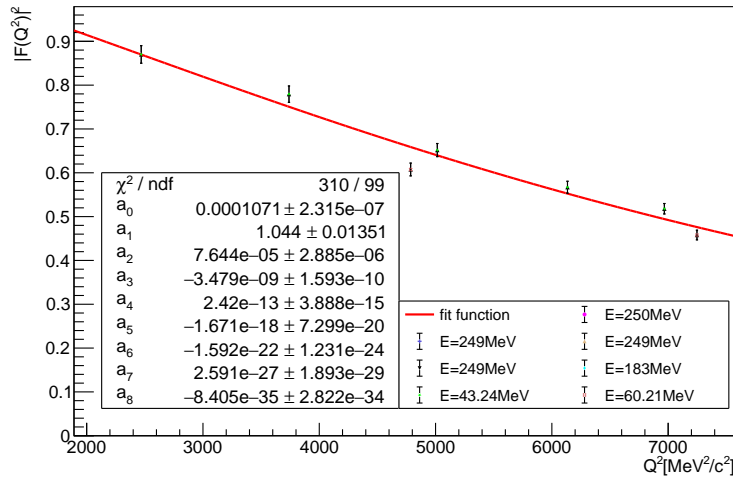


Figure 56: Polynomial function form factor parameterisation for elastic electron scattering off the ground state of ^{40}Ca in the Q^2 interval of the P2-experiment. The averaged Q^2 for the P2-experiment is $Q^2 = 5000 \frac{\text{MeV}^2}{c^2}$.

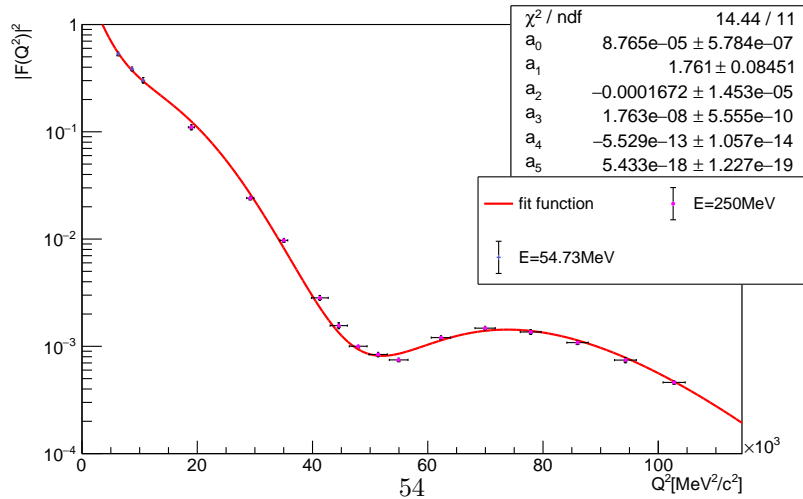


Figure 57: Polynomial function form factor parameterisation for elastic electron scattering off the ground state of ^{42}Ca .

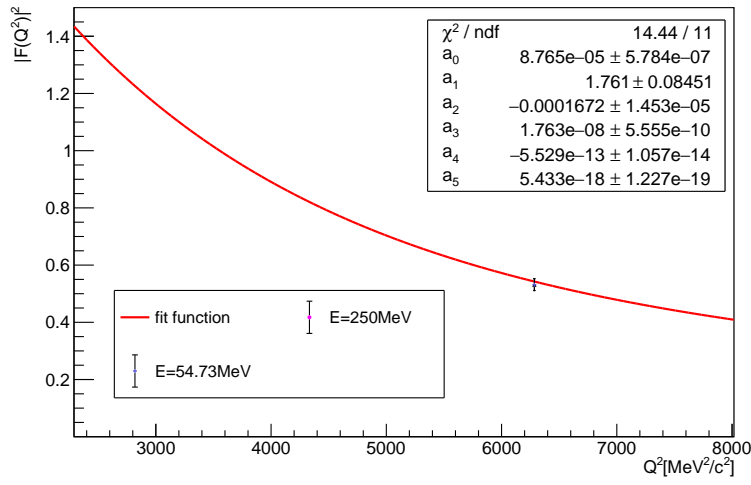


Figure 58: Polynomial function form factor parameterisation for elastic electron scattering off the ground state of ^{42}Ca in the Q^2 interval of the P2-experiment. The averaged Q^2 for the P2-experiment is $Q^2 = 5000 \frac{\text{MeV}^2}{c^2}$.

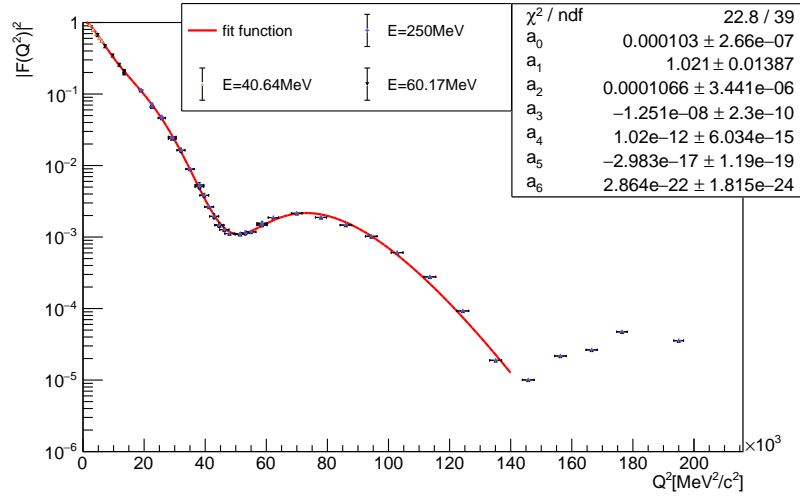


Figure 59: Polynomial function form factor parameterisation for elastic electron scattering off the ground state of ^{48}Ca .

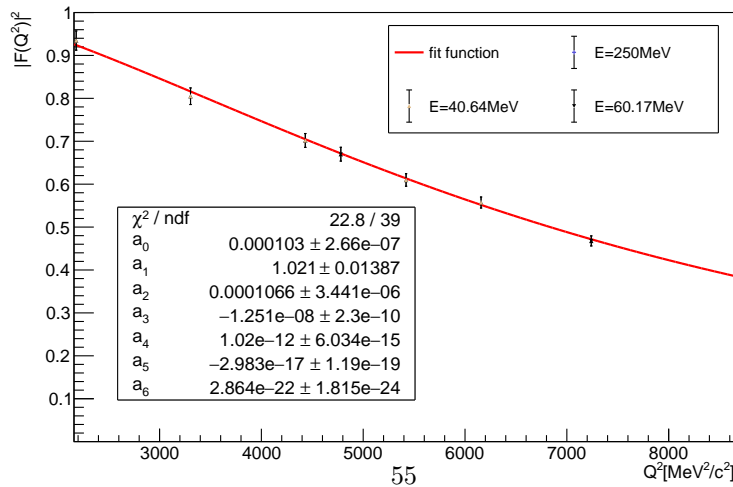


Figure 60: Polynomial function form factor parameterisation for elastic electron scattering off the ground state of ^{48}Ca in the Q^2 interval of the P2-experiment. The averaged Q^2 for the P2-experiment is $Q^2 = 5000 \frac{\text{MeV}^2}{c^2}$.

not able to describe the last local maximum at around $Q^2 = 180 \cdot 10^3 \frac{\text{MeV}^2}{c^2}$. In the given interval the fit function agrees precisely with the form factor values. The fit parameters for ^{40}Ca are given in table 14.

Parameter	Value
a_0	$1.071 \cdot 10^{-4} \pm 2.3 \cdot 10^{-7} \frac{c^2}{\text{MeV}^2}$
a_1	1.044 ± 0.015
a_2	$7.64 \cdot 10^{-5} \pm 0.29 \cdot 10^{-5} \frac{c^2}{\text{MeV}^2}$
a_3	$-3.48 \cdot 10^{-9} \pm 0.16 \cdot 10^{-9} \frac{c^4}{\text{MeV}^4}$
a_4	$2.423 \cdot 10^{-13} \pm 3.9 \cdot 10^{-15} \frac{c^6}{\text{MeV}^6}$
a_5	$-1.671 \cdot 10^{-18} \pm 7.3 \cdot 10^{-20} \frac{c^8}{\text{MeV}^8}$
a_6	$-1.592 \cdot 10^{-22} \pm 1.2 \cdot 10^{-24} \frac{c^{10}}{\text{MeV}^{10}}$
a_7	$2.591 \cdot 10^{-27} \pm 1.9 \cdot 10^{-29} \frac{c^{12}}{\text{MeV}^{12}}$
a_8	$-8.41 \cdot 10^{-35} \pm 28.22 \cdot 10^{-35} \frac{c^{14}}{\text{MeV}^{14}}$

Table 14: Fit parameter for the polynomial function parameterisation for ^{40}Ca

For ^{42}Ca the polynomial parameterisation fit function is shown in figure 57. Figure 58 shows the polynomial fit function in the Q^2 interval of the P2-experiment. Generally, the fit function agrees with the measuring data over the whole Q^2 -interval. In the interval from $Q^2 = 0 \frac{\text{MeV}^2}{c^2}$ to $Q^2 = 5 \cdot 10^3 \frac{\text{MeV}^2}{c^2}$ the fit function has a large slope which leads to form factor values larger than 1. This is contrary to what we would expect. However this fit function is still chosen because it describes the form factor values in the interval from $Q^2 = 5 \cdot 10^3 \frac{\text{MeV}^2}{c^2}$ to $Q^2 = 15 \cdot 10^3 \frac{\text{MeV}^2}{c^2}$ well which is relevant for the P2-experiment. In table 15 the fit parameters for ^{42}Ca are listed.

Parameter	Value
a_0	$8.765 \cdot 10^{-5} \pm 5.8 \cdot 10^{-7} \frac{c^2}{\text{MeV}^2}$
a_1	1.761 ± 0.085
a_2	$-1.67 \cdot 10^{-4} \pm 0.15 \cdot 10^{-4} \frac{c^2}{\text{MeV}^2}$
a_3	$1.763 \cdot 10^{-8} \pm 5.6 \cdot 10^{-10} \frac{c^4}{\text{MeV}^4}$
a_4	$-5.53 \cdot 10^{-13} \pm 0.11 \cdot 10^{-13} \frac{c^6}{\text{MeV}^6}$
a_5	$5.43 \cdot 10^{-18} \pm 0.12 \cdot 10^{-18} \frac{c^8}{\text{MeV}^8}$

Table 15: Fit parameter for the polynomial function parameterisation for ^{42}Ca

For ^{48}Ca the fit function is shown in figure 59. Figure 60 shows the fit function in the Q^2 interval of the P2-experiment. As for ^{40}Ca the fitting interval is adjusted to get a better fitting result. In the whole interval from $Q^2 = 0 \frac{\text{MeV}^2}{c^2}$ to $Q^2 = 140 \cdot 10^3 \frac{\text{MeV}^2}{c^2}$ the fit function agrees with the form factor values.

The fitting parameters for ^{48}Ca are presented in table 16.

Parameter	Value
a_0	$1.0302 \cdot 10^{-4} \pm 2.7 \cdot 10^{-7} \frac{c^2}{\text{MeV}^2}$
a_1	1.021 ± 0.014
a_2	$1.066 \cdot 10^{-4} \pm 3.4 \cdot 10^{-6} \frac{c^2}{\text{MeV}^2}$
a_3	$-1.251 \cdot 10^{-8} \pm 2.3 \cdot 10^{-10} \frac{c^4}{\text{MeV}^4}$
a_4	$1.0204 \cdot 10^{-12} \pm 6.0 \cdot 10^{-15} \frac{c^6}{\text{MeV}^6}$
a_5	$-2.983 \cdot 10^{-17} \pm 1.2 \cdot 10^{-19} \frac{c^8}{\text{MeV}^8}$
a_6	$2.864 \cdot 10^{-22} \pm 1.8 \cdot 10^{-24} \frac{c^{10}}{\text{MeV}^{10}}$

Table 16: Fit parameter for the polynomial function parameterisation for ^{48}Ca

For ^{208}Pb the same applies as for the parameterisations used before.

5.3.5 Gaussian function parameterisation

The polynomial function parameterisation introduced in equation (22) is used to fit the form factor data of each nucleus.

Again the starting parameter are found with the help of the ROOT fit panel. The fit function for the Gaussian function parameterisation for ^{12}C is plotted in figure 61. Figure 62 shows the fit function in the Q^2 interval of the P2-experiment.

We see that up to $Q^2 = 115 \cdot 10^3 \frac{\text{MeV}^2}{c^2}$ the fit function describes the cross section values with good precision. Around the minimum of the cross section values from $Q^2 = 115 \cdot 10^3 \frac{\text{MeV}^2}{c^2}$ to $Q^2 = 130 \cdot 10^3 \frac{\text{MeV}^2}{c^2}$ the function deviates from the cross section values. For $Q^2 > 130 \cdot 10^3 \frac{\text{MeV}^2}{c^2}$ the fit function describes the form factor values precisely. It is important to note that in the interval from $Q^2 = 0 \frac{\text{MeV}^2}{c^2}$ to $Q^2 = 5 \frac{\text{MeV}^2}{c^2}$ the form factor parameterisation is larger than 1 which is contrary to what we would expect. This will lead to a deviation of the measuring time from the other form factor parameterisations for ^{12}C .

The fit parameters of the Gaussian function parameterisation for ^{12}C are listed in table 17.

For ^{40}Ca the fit function is shown in figure 63. Figure 64 shows the fit function in the Q^2 interval of the P2-experiment.

As for the polynomial function parameterisation the fitting interval was shortened in order to get good fitting results. In the whole fitting interval from $Q^2 = 0 \frac{\text{MeV}^2}{c^2}$ to $Q^2 = 135 \cdot 10^3 \frac{\text{MeV}^2}{c^2}$ the form factor values are described by the fitting function precisely.

The fit parameters are displayed in table 18.

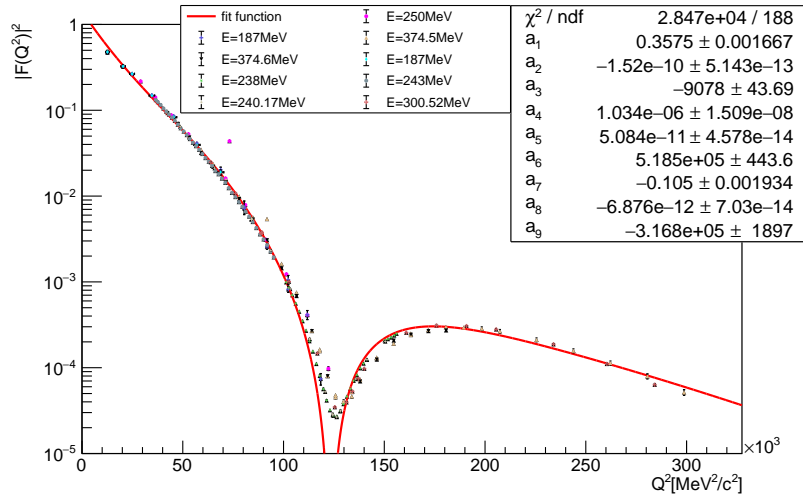


Figure 61: Gaussian function form factor parameterisation for elastic electron scattering off the ground state of ^{12}C .

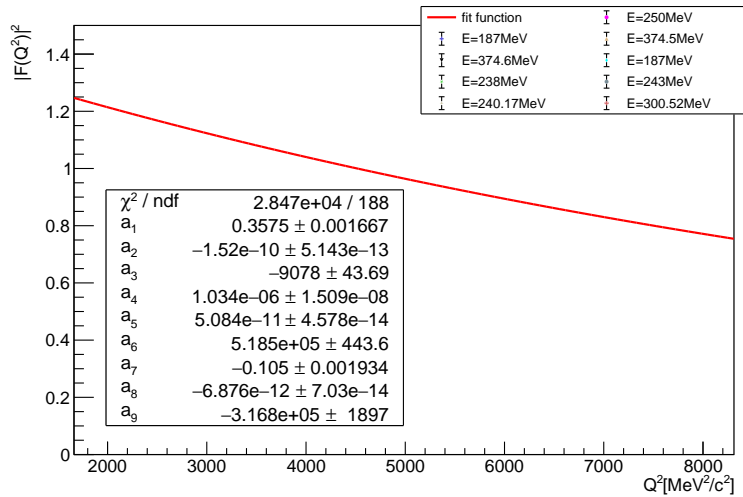


Figure 62: Gaussian function form factor parameterisation for elastic electron scattering off the ground state of ^{12}C in the Q^2 interval of the P2-experiment. The averaged Q^2 for the P2-experiment is $Q^2 = 5000 \frac{\text{MeV}^2}{c^2}$.

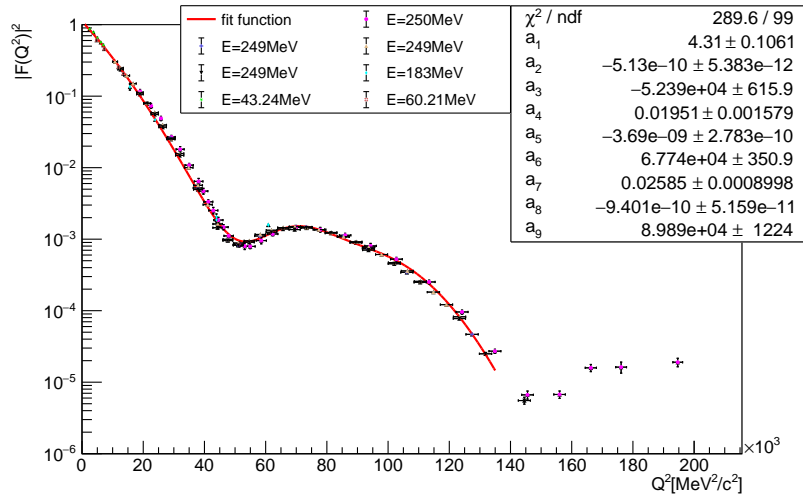


Figure 63: Gaussian function form factor parameterisation for elastic electron scattering off the ground state of ^{40}Ca .

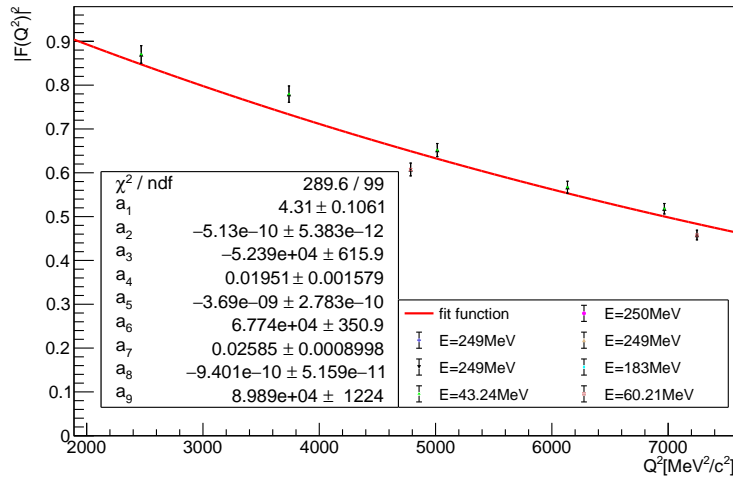


Figure 64: Gaussian function form factor parameterisation for elastic electron scattering off the ground state of ^{40}Ca in the Q^2 interval of the P2-experiment. The averaged Q^2 for the P2-experiment is $Q^2 = 5000 \frac{\text{MeV}^2}{c^2}$.

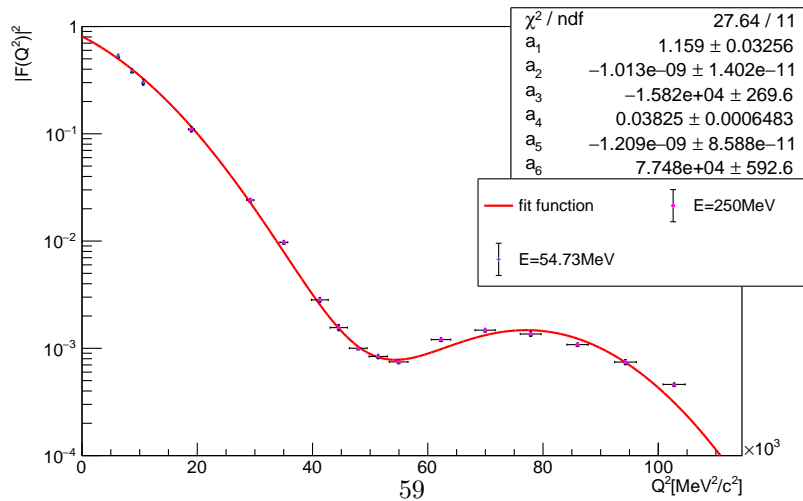


Figure 65: Gaussian function form factor parameterisation for elastic electron scattering off the ground state of ^{42}Ca .

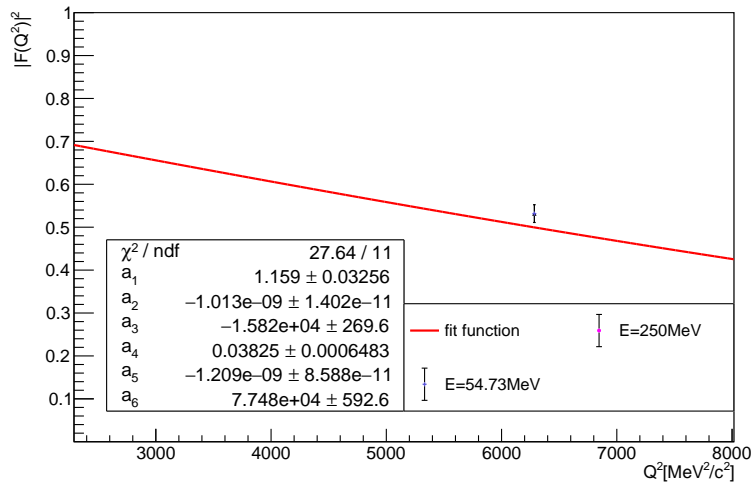


Figure 66: Gaussian function form factor parameterisation for elastic electron scattering off the ground state of ^{42}Ca in the Q^2 interval of the P2-experiment. The averaged Q^2 for the P2-experiment is $Q^2 = 5000 \frac{\text{MeV}^2}{c^2}$.

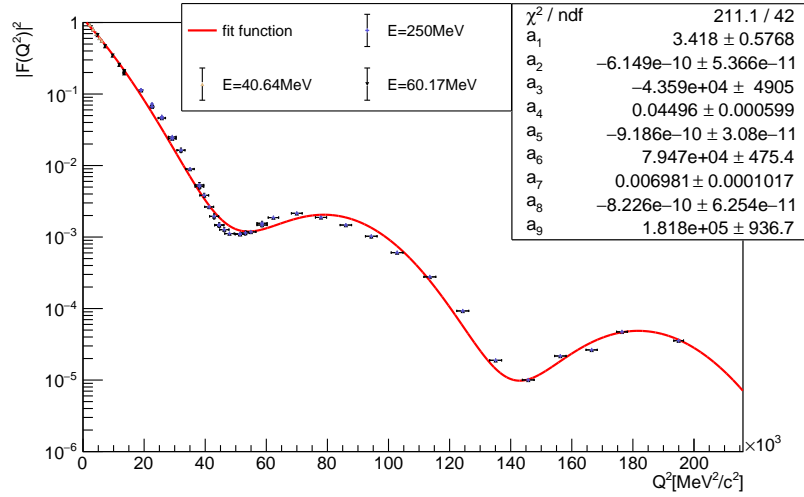


Figure 67: Gaussian function form factor parameterisation for elastic electron scattering off the ground state ^{48}Ca

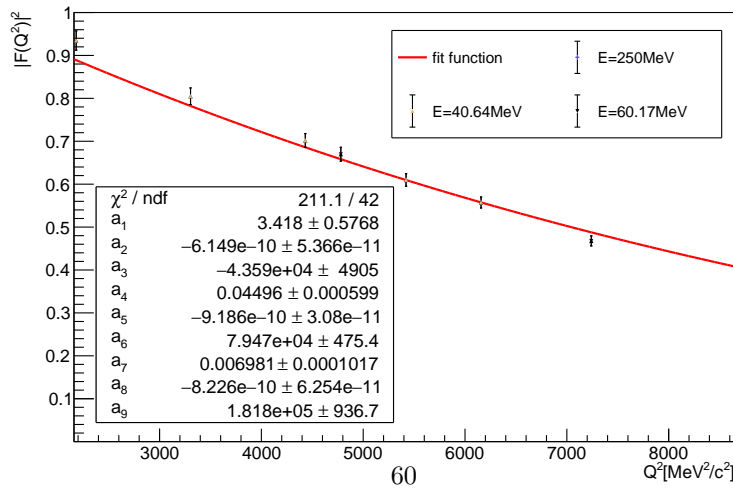


Figure 68: Gaussian function form factor parameterisation for elastic electron scattering off the ground state of ^{48}Ca in the Q^2 interval of the P2-experiment. The averaged Q^2 for the P2-experiment is $Q^2 = 5000 \frac{\text{MeV}^2}{c^2}$.

Parameter	Value
a_1	$0.3575 \pm 1.7 \cdot 10^{-3}$
a_2	$-1.5256 \cdot 10^{-10} \pm 5.1 \cdot 10^{-13} \frac{c^4}{\text{MeV}^4}$
a_3	$-9078 \pm 43 \frac{\text{MeV}^2}{c^2}$
a_4	$1.034 \cdot 10^{-6} \pm 1.5 \cdot 10^{-8}$
a_5	$5.0841 \cdot 10^{-11} \pm 4.6 \cdot 10^{-14} \frac{c^4}{\text{MeV}^4}$
a_6	$5.185 \cdot 10^5 \pm 443 \frac{\text{MeV}^2}{c^2}$
a_7	$-0.1058 \pm 1.9 \cdot 10^{-3}$
a_8	$-6.876 \cdot 10^{-12} \pm 7.0 \cdot 10^{-14} \frac{c^4}{\text{MeV}^4}$
a_9	$-3.168 \cdot 10^5 \pm 1897 \frac{\text{MeV}^2}{c^2}$

Table 17: Fit parameter for the Gaussian function parameterisation for ^{12}C

Parameter	Value
a_1	4.31 ± 0.10
a_2	$-5.136 \cdot 10^{-10} \pm 5.4 \cdot 10^{-12} \frac{c^4}{\text{MeV}^4}$
a_3	$-5.239 \cdot 10^4 \pm 0.062 \cdot 10^4 \frac{\text{MeV}^2}{c^2}$
a_4	0.0195 ± 0.0016
a_5	$-3.69 \cdot 10^{-9} \pm 2.8 \cdot 10^{-10} \frac{c^4}{\text{MeV}^4}$
a_6	$6.774 \cdot 10^4 \pm 0.035 \cdot 10^4 \frac{\text{MeV}^2}{c^2}$
a_7	$0.02585 \pm 9.0 \cdot 10^{-4}$
a_8	$-9.401 \cdot 10^{-10} \pm 0.52 \cdot 10^{-10} \frac{c^4}{\text{MeV}^4}$
a_9	$8.989 \cdot 10^4 \pm 0.12 \cdot 10^4 \frac{\text{MeV}^2}{c^2}$

Table 18: Fit parameter for the Gaussian function parameterisation for ^{40}Ca

In figure 65 the Gaussian parameterisation fit function for ^{42}Ca is shown. Figure 66 shows the Gaussian parameterisation in the Q^2 interval of the P2-experiment. As for ^{40}Ca the fitting functions agrees with the form factor values over the whole fitting interval from $Q^2 = 0 \frac{\text{MeV}^2}{c^2}$ to $Q^2 = 110 \cdot 10^3 \frac{\text{MeV}^2}{c^2}$. Whats notable is that for $Q^2 = 0 \frac{\text{MeV}^2}{c^2}$ the value for the form factor is not exactly 1 which is not observed for most of the other parameterisations. For these the value for the form factor for $Q^2 = 0 \frac{\text{MeV}^2}{c^2}$ is approximately 1.

The fit parameters for the Gaussian function parameterisation for ^{42}Ca are presented in table 19.

For ^{48}Ca the Gaussian parameterisation fit function is displayed in figure 67. Figure 68 shows the fit function in the Q^2 interval of the P2-experiment. We see that up to $Q^2 \approx 40 \cdot 10^3 \frac{\text{MeV}^2}{c^2}$ the fit functions agrees with the data points. In the interval from $Q^2 = 40 \cdot 10^3 \frac{\text{MeV}^2}{c^2}$ to $Q^2 = 100 \cdot 10^3 \frac{\text{MeV}^2}{c^2}$ the fit functions deviates from the data points. For $Q^2 > 100 \cdot 10^3 \frac{\text{MeV}^2}{c^2}$ the fit functions describes the form factor values precise again. If the Q^2 values for the experiment lays in the Q^2 interval where the fit function does not describe the

Parameter	Value
a_1	1.159 ± 0.033
a_2	$-1.013 \cdot 10^{-9} \pm 1.4 \cdot 10^{-11} \frac{c^4}{\text{MeV}^4}$
a_3	$-1.582 \cdot 10^4 \pm 0.027 \cdot 10^4 \frac{\text{MeV}^2}{c^2}$
a_4	$0.03825 \pm 6.5 \cdot 10^{-4}$
a_5	$-1.209 \cdot 10^{-9} \pm 8.6 \cdot 10^{-11} \frac{c^4}{\text{MeV}^4}$
a_6	$7.748 \cdot 10^4 \pm 0.059 \cdot 10^4 \frac{\text{MeV}^2}{c^2}$

Table 19: Fit parameter for the Gaussian function parameterisation for ^{42}Ca

data points precisely we can shorten the fitting interval which is shown in figure 69. The same fit function in the Q^2 interval of the P2-experiment is shown in figure 70.

We see that the interval from $Q^2 = 40 \cdot 10^3 \frac{\text{MeV}^2}{c^2}$ to $Q^2 = 100 \cdot 10^3 \frac{\text{MeV}^2}{c^2}$ is described by the fit function accurately.

The fit parameters for the fit function in figure 48 can be found in table 20 and the fit parameters for the fit function in figure 49 can be found in table 21.

Parameter	Value
a_1	3.42 ± 0.58
a_2	$-6.15 \cdot 10^{-10} \pm 0.54 \cdot 10^{-10} \frac{c^4}{\text{MeV}^4}$
a_3	$-4.36 \cdot 10^4 \pm 0.49 \cdot 10^{-10} \frac{\text{MeV}^2}{c^2}$
a_4	$0.04496 \pm 6.0 \cdot 10^{-4}$
a_5	$-9.19 \cdot 10^{-10} \pm 0.31 \cdot 10^{-10} \frac{c^4}{\text{MeV}^4}$
a_6	$7.947 \cdot 10^4 \pm 0.048 \cdot 10^4 \frac{\text{MeV}^2}{c^2}$
a_7	$6.98 \cdot 10^{-3} \pm 0.1 \cdot 10^{-3}$
a_8	$-8.23 \cdot 10^{-10} \pm 0.63 \cdot 10^{-10} \frac{c^4}{\text{MeV}^4}$
a_9	$1.818 \cdot 10^5 \pm 0.009 \cdot 10^5 \frac{\text{MeV}^2}{c^2}$

Table 20: Fit parameter for the Gaussian function parameterisation for ^{48}Ca in the complete Q^2 interval

For ^{208}Pb the fit function is shown in figure 71. Figure 72 shows the fit function in the Q^2 interval of the P2-experiment.

We can see that the fit function describes the form factor values in the fitting interval from $Q^2 = 0 \frac{\text{MeV}^2}{c^2}$ to $Q^2 = 80 \cdot 10^3 \frac{\text{MeV}^2}{c^2}$. This fit was made by using the fit panel and separately changing the parameters. ROOT itself was not able to find a fit function for the form factor values. This is probably because the different data points do not correlate for Q^2 -values bigger than $Q^2 = 40 \cdot 10^3 \frac{\text{MeV}^2}{c^2}$. The fitting parameter for the Gaussian function parameterisation fit function for ^{208}Pb are displayed in table 22. We see that the errors for the different

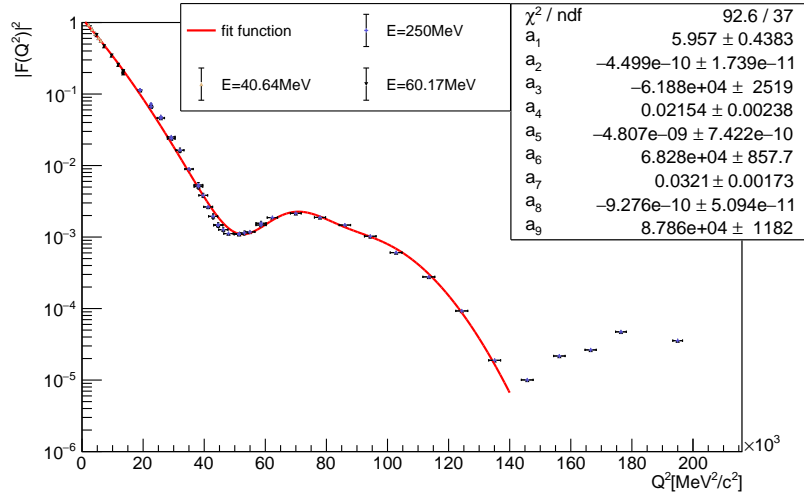


Figure 69: Gaussian function form factor parameterisation for elastic electron scattering off the ground state of ^{48}Ca in a shortened interval.

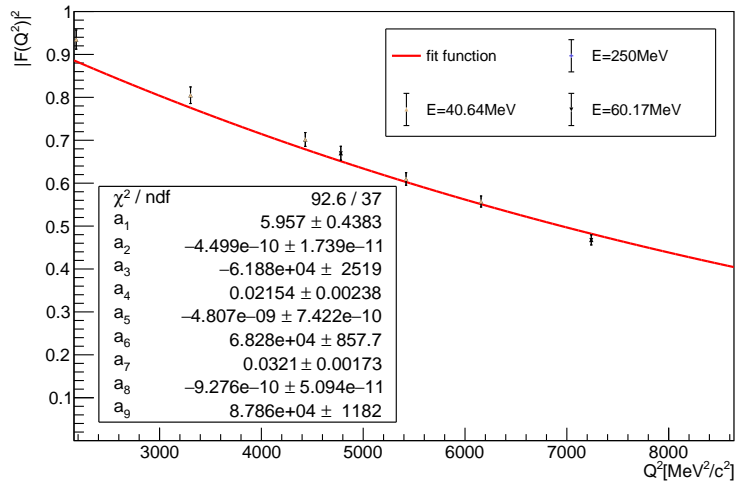


Figure 70: Gaussian function form factor parameterisation in the shortened interval for elastic electron scattering off the ground state of ^{48}Ca in the Q^2 interval of the P2-experiment. The averaged Q^2 for the P2-experiment is $Q^2 = 5000 \frac{\text{MeV}^2}{c^2}$.

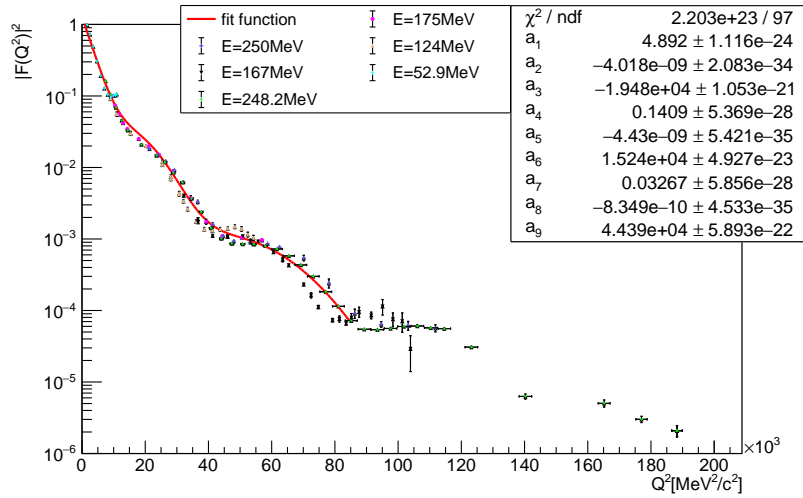


Figure 71: Gaussian function form factor parameterisation for elastic electron scattering off the ground state of ^{208}Pb .

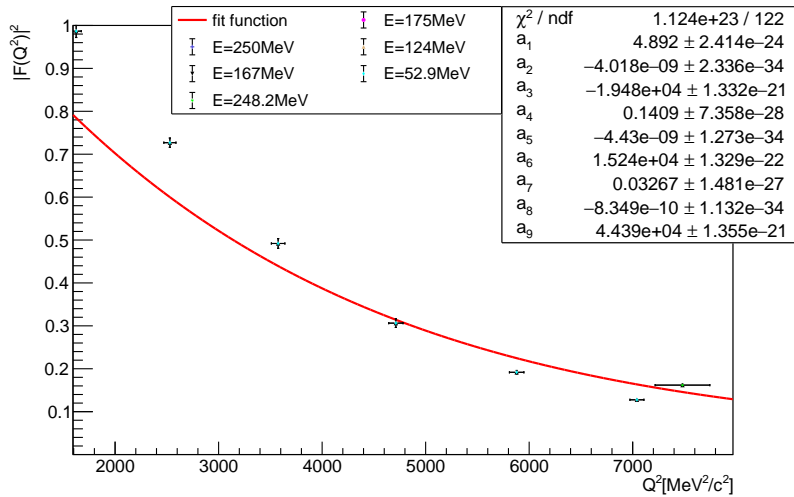


Figure 72: Gaussian function form factor parameterisation for elastic electron scattering off the ground state of ^{208}Pb in the Q^2 interval of the P2-experiment. The averaged Q^2 for the P2-experiment is $Q^2 = 5000 \frac{\text{MeV}^2}{c^2}$.

Parameter	Value
a_1	5.86 ± 0.44
a_2	$-4.5 \cdot 10^{-10} \pm 0.17 \cdot 10^{-10} \frac{c^4}{\text{MeV}^4}$
a_3	$-6.19 \cdot 10^4 \pm 0.25 \cdot 10^4 \frac{\text{MeV}^2}{c^2}$
a_4	$0.02154 \pm 2.38 \cdot 10^{-3}$
a_5	$-4.81 \cdot 10^{-9} \pm 0.74 \cdot 10^{-9} \frac{c^4}{\text{MeV}^4}$
a_6	$6.828 \cdot 10^4 \pm 0.009 \cdot 10^4 \frac{\text{MeV}^2}{c^2}$
a_7	$0.0321 \pm 1.7 \cdot 10^{-3}$
a_8	$-9.28 \cdot 10^{-10} \pm 0.51 \cdot 10^{-10} \frac{c^4}{\text{MeV}^4}$
a_9	$8.79 \cdot 10^4 \pm 0.12 \cdot 10^4 \frac{\text{MeV}^2}{c^2}$

Table 21: Fit parameter for the Gaussian function parameterisation for ^{48}Ca in the shortened Q^2 interval

Parameter	Value
a_1	$4.892 \pm 1.1 \cdot 10^{-24}$
a_2	$-4.018 \cdot 10^{-9} \pm 2.1 \cdot 10^{-34} \frac{c^4}{\text{MeV}^4}$
a_3	$-1.948 \cdot 10^4 \pm 1.1 \cdot 10^{-21} \frac{\text{MeV}^2}{c^2}$
a_4	$0.1409 \pm 5.4 \cdot 10^{-28}$
a_5	$-4.43 \cdot 10^{-9} \pm 5.4 \cdot 10^{-35} \frac{c^4}{\text{MeV}^4}$
a_6	$1.524 \cdot 10^4 \pm 4.9 \cdot 10^{-23} \frac{\text{MeV}^2}{c^2}$
a_7	$0.03268 \pm 5.9 \cdot 10^{-28}$
a_8	$-8.349 \cdot 10^{-10} \pm 4.5 \cdot 10^{-35} \frac{c^4}{\text{MeV}^4}$
a_9	$4.439 \cdot 10^4 \pm 5.9 \cdot 10^{-22} \frac{\text{MeV}^2}{c^2}$

Table 22: Fit parameter for the Gaussian function parameterisation for ^{208}Pb . The errors are not from the fit because the values for the parameters are set by hand.

parameters are very small. This is because the fit was made only by using the fit panel of ROOT.

5.4 Form factor parameterisation inelastic scattering

The Gaussian function parameterisation used before in section 5.3.5 was used to fit the form factor data.

For ^{12}C the fit function for the first energy level $E_x = 4.43$ MeV is displayed in figure 73. The fit function for the second energy level $E_x = 7.66$ MeV is plotted in figure 74 and the fit function for the third energy level $E_x = 9.64$ MeV is plotted in figure 75.

We have to remember that we actually have to fit $2s+1$ form factors where s is the spin of the state. Because we do not have enough data we only fit one form factor. Generally, the form factor for the inelastic scattering off ^{12}C can be described by one simple Gaussian function. We see that the maximum of the form factor values for the $E_x = 4.43$ MeV level is one order of magnitude larger than for the $E_x = 7.66$ MeV and $E_x = 9.64$ MeV levels. The position for each of the Gaussian functions differ from each other because the maxima of each of the form factor value sets are shifted. The variance of the different fit functions are approximately the same.

The fit parameters for $E_x = 4.43$ MeV are listed in table 23. In table 24 the fit parameters for $E_x = 7.66$ MeV and in table 25 the fit parameters for $E_x = 9.64$ MeV are displayed.

Parameter	Value
a_1	$0.11736 \pm 7.7 \cdot 10^{-4}$
a_2	$-1.767 \cdot 10^{-10} \pm 4.6 \cdot 10^{-12} \frac{c^4}{\text{MeV}^4}$
a_3	$6.084 \cdot 10^4 \pm 0.048 \cdot 10^4 \frac{\text{MeV}^2}{c^2}$

Table 23: Fit parameter for the Gaussian function parameterisation for the first excited state $E_x = 4.43$ MeV of ^{12}C .

Parameter	Value
a_1	$0.05445 \pm 6.0 \cdot 10^{-4}$
a_2	$-1.989 \cdot 10^{-10} \pm 8.1 \cdot 10^{-12} \frac{c^4}{\text{MeV}^4}$
a_3	$3.72 \cdot 10^4 \pm 0.14 \cdot 10^4 \frac{\text{MeV}^2}{c^2}$

Table 24: Fit parameter for the Gaussian function parameterisation for the second excited state $E_x = 7.66$ MeV of ^{12}C

The Gaussian function parameterisation fit function for the $E_x = 2.6$ MeV level of ^{208}Pb is plotted in figure 76 and the fit function for the Q^2 interval of the P2-experiment is shown in figure 77. Figure 78 shows the the Gaussian form factor parametersiation for inelastic electron scattering off the second excited state $E_x = 3.2$ MeV level of ^{208}Pb and figure 79 shows the same fit function in the Q^2 interval of the P2-experiment.

In contrast to the inelastic scattering off ^{12}C two Gaussian functions are needed to describe the data points for the first excited state $E_x = 2.6$ MeV. We can

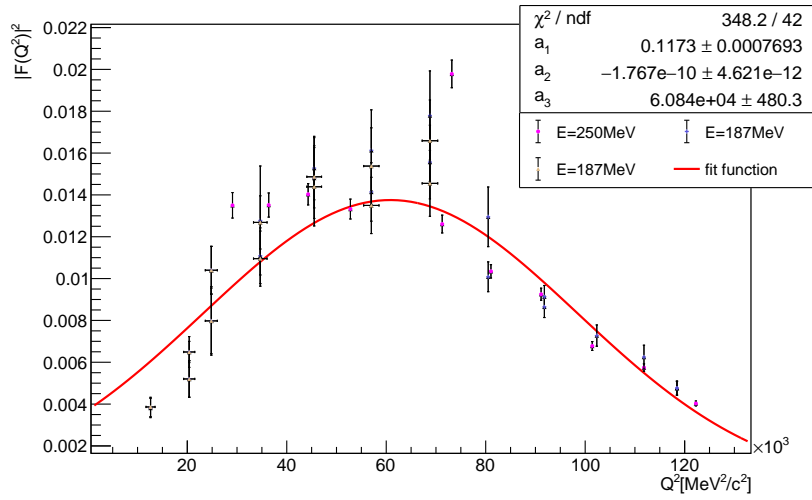


Figure 73: Gaussian function form factor parameterisation for inelastic electron scattering off the first excited state $E_x = 4.43$ MeV of ^{12}C .

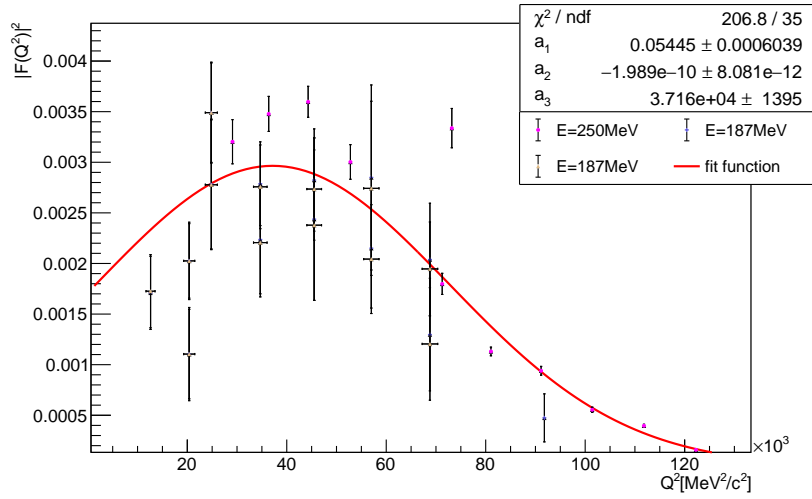


Figure 74: Gaussian function form factor parameterisation for inelastic electron scattering off the second excited state $E_x = 7.66$ MeV of ^{12}C .

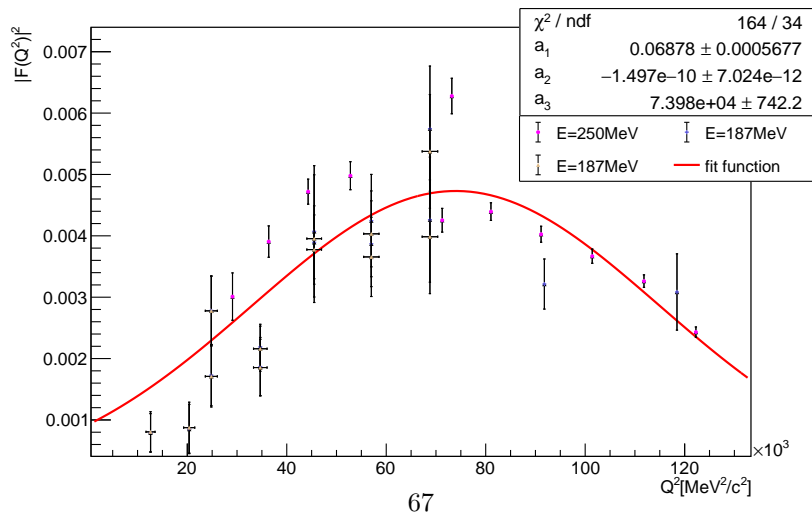


Figure 75: Gaussian function form factor parameterisation for inelastic electron scattering off the third excited state $E_x = 9.64$ MeV of ^{12}C .

Parameter	Value
a_1	$0.06878 \pm 5.7 \cdot 10^{-4}$
a_2	$-1.497 \cdot 10^{-10} \pm 7.0 \cdot 10^{-12} \frac{c^4}{\text{MeV}^4}$
a_3	$7.398 \cdot 10^4 \pm 0.074 \cdot 10^4 \frac{\text{MeV}^2}{c^2}$

Table 25: Fit parameter for the Gaussian function parameterisation for the third excited state $E_x = 9.64$ MeV of ^{12}C

see that the form factor for the $E_x = 2.6$ MeV level is one order of magnitude larger than the form factor for the $E_x = 3.2$ MeV level. The form factor values of the $E_x = 3.2$ MeV level have their maximum at $Q^2 = 20 \cdot 10^3 \frac{\text{MeV}^2}{c^2}$. At this Q^2 value the form factor values of the $E_x = 2.6$ MeV level have their minimum. The fit parameters for the $E_x = 2.6$ MeV level are listed in table 26 and in the fit parameters for the $E_x = 3.2$ MeV level are given in table 27.

Parameter	Value
a_1	$0.02117 \pm 3.4 \cdot 10^{-4}$
a_2	$-7.34 \cdot 10^{-9} \pm 0.42 \cdot 10^{-9} \frac{c^4}{\text{MeV}^4}$
a_3	$1.304 \cdot 10^4 \pm 0.035 \cdot 10^4 \frac{\text{MeV}^2}{c^2}$
a_4	$8.007 \cdot 10^{-3} \pm 6.9 \cdot 10^{-5}$
a_5	$-1.978 \cdot 10^{-9} \pm 7.8 \cdot 10^{-11} \frac{c^4}{\text{MeV}^4}$
a_6	$4.572 \cdot 10^4 \pm 0.028 \cdot 10^4 \frac{\text{MeV}^2}{c^2}$

Table 26: Fit parameter for the Gaussian function parameterisation for the first excited state $E_x = 2.6$ MeV of ^{208}Pb

Parameter	Value
a_1	$6.327 \cdot 10^{-3} \pm 0.104 \cdot 10^{-3}$
a_2	$-1.66 \cdot 10^{-9} \pm 0.15 \cdot 10^{-9} \frac{c^4}{\text{MeV}^4}$
a_3	$2.61 \cdot 10^4 \pm 0.99 \cdot 10^4 \frac{\text{MeV}^2}{c^2}$

Table 27: Fit parameter for the Gaussian function parameterisation for the second excited state $E_x = 3.2$ MeV of ^{208}Pb

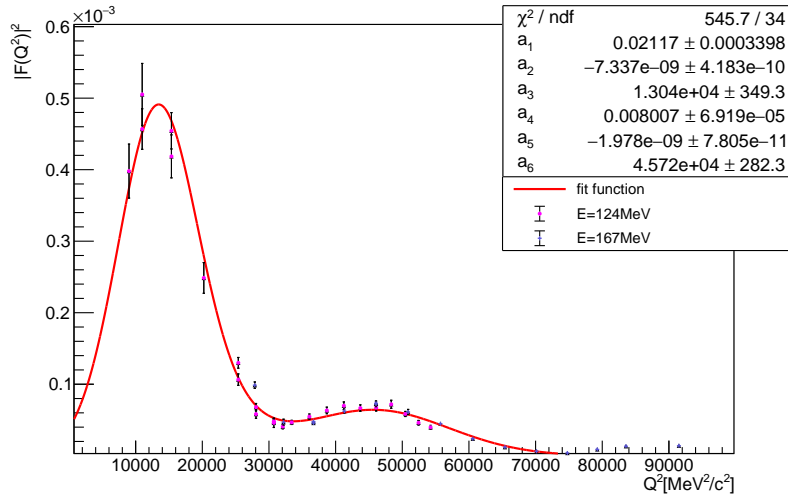


Figure 76: Gaussian function form factor parameterisation for inelastic electron scattering off the first excited state $E_x = 2.6$ MeV of ^{208}Pb .

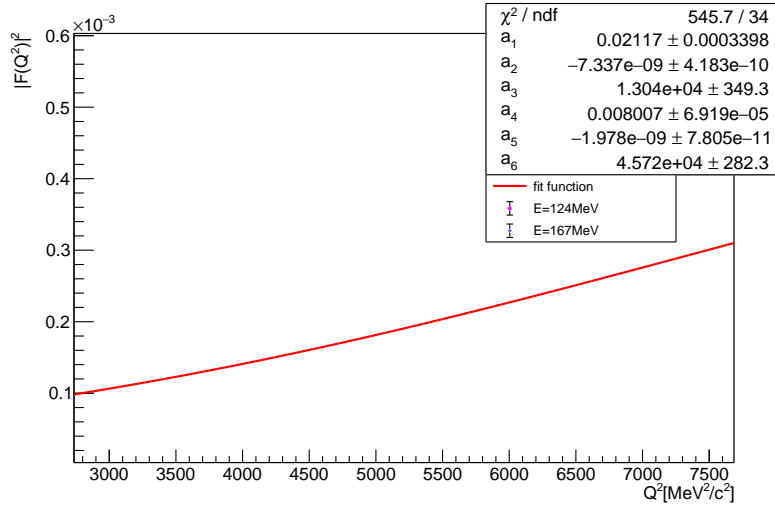


Figure 77: Gaussian function form factor parameterisation for inelastic electron scattering off the first excited state $E_x = 2.6$ MeV of ^{208}Pb in the Q^2 interval of the P2-experiment. The averaged Q^2 for the P2-experiment is $Q^2 = 5000 \frac{\text{MeV}^2}{c^2}$.

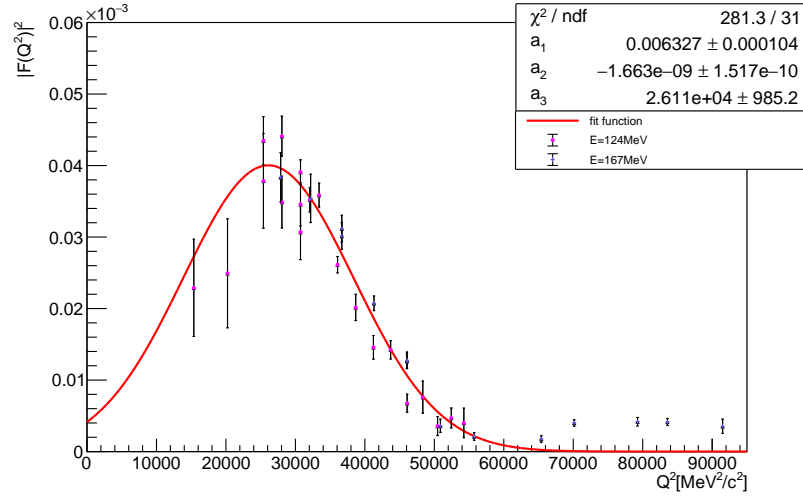


Figure 78: Gaussian function form factor parameterisation for inelastic electron scattering off the second excited state $E_x = 3.2$ MeV of ^{208}Pb .

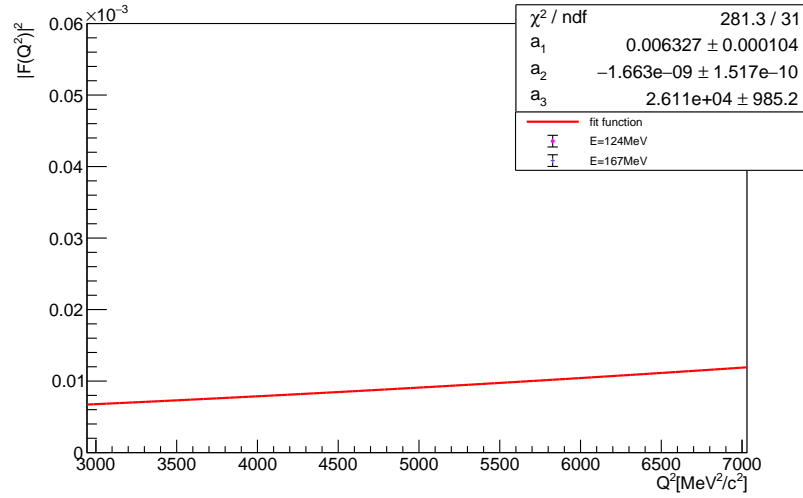


Figure 79: Gaussian function form factor parameterisation for inelastic electron scattering off the second excited state $E_x = 3.2$ MeV of ^{208}Pb in the Q^2 interval of the P2-experiment. The averaged Q^2 for the P2-experiment is $Q^2 = 5000 \frac{\text{MeV}^2}{c^2}$.

5.5 Results for the parity-violating asymmetry

The parity-violating asymmetry is calculated with equation (27) from section 2.3. The weak nuclear charge Q_w is calculated using equation (28) from section 2.3. The value of the parity-violating asymmetry is different for each nucleus. The parity-violating asymmetries calculated for each nucleus by assuming $Q^2 = 4.5 \cdot 10^{-3} \frac{\text{GeV}^2}{c^2}$ which is the Q^2 value for the P2-experiment using a lH_2 -target are shown in table 28.

Nucleus	A
^{12}C	$3.74 \cdot 10^{-7}$
^{40}Ca	$3.74 \cdot 10^{-7}$
^{42}Ca	$4.15 \cdot 10^{-7}$
^{48}Ca	$5.36 \cdot 10^{-7}$
^{208}Pb	$5.91 \cdot 10^{-7}$

Table 28: Parity-violating asymmetry A for $Q^2 = 4.5 \cdot 10^{-3} \text{ GeV}^2$

These values are problematic because they assumes that the Q^2 -values for the different targets are the same as for the lH_2 -target.

If we want to take these differences into account we need to calculate the cross section averaged asymmetry. We averaged the asymmetry over the angle acceptance of the P2-experiment. The angle acceptance for the P2-experiment ranges from $\theta = 25^\circ$ to $\theta = 45^\circ$. The cross section averaged asymmetry was calculated using equation (29) from section 2.4.

This way the Q^2 dependence for each nucleus is correctly taken into account. With the help of the previously introduced parameterisations we can calculate $\frac{d\sigma}{d\Omega}$. This way we get for each parameterisation a different value for the cross section averaged asymmetry. The values for the different asymmetries for ^{12}C , ^{40}Ca , ^{42}Ca and ^{48}Ca can be found in tables 29-32.

Parameterisation	$\langle A \rangle$
Polynomial	$5.98 \cdot 10^{-7}$
Gaussian	$5.85 \cdot 10^{-7}$
Helm	$5.95 \cdot 10^{-7}$
Sum of Gaussian	$5.94 \cdot 10^{-7}$
Fourier-Bessel	$5.96 \cdot 10^{-7}$

Table 29: Cross section averaged parity-violating asymmetry $\langle A \rangle$ for ^{12}C

For ^{208}Pb we only had one parameterisation. We get for the cross section averaged parity-violating asymmetry:

$$\langle A \rangle = 8.31 \cdot 10^{-7}$$

Parameterisation	$\langle A \rangle$
Polynomial	$5.61 \cdot 10^{-7}$
Gaussian	$5.65 \cdot 10^{-7}$
Helm	$5.70 \cdot 10^{-7}$
Sum of Gaussian	$5.65 \cdot 10^{-7}$
Fourier-Bessel	$5.73 \cdot 10^{-7}$

Table 30: Cross section averaged parity-violating asymmetry $\langle A \rangle$ for ^{40}Ca

Parameterisation	$\langle A \rangle$
Polynomial	$6.15 \cdot 10^{-7}$
Gaussian	$6.38 \cdot 10^{-7}$
Helm	$6.32 \cdot 10^{-7}$
Sum of Gaussian	$6.22 \cdot 10^{-7}$
Fourier-Bessel	$6.35 \cdot 10^{-7}$

Table 31: Cross section averaged parity-violating asymmetry $\langle A \rangle$ for ^{42}Ca

Parameterisation	$\langle A \rangle$
Polynomial	$8.01 \cdot 10^{-7}$
Gaussian	$8.08 \cdot 10^{-7}$
Helm	$8.18 \cdot 10^{-7}$
Sum of Gaussian	$8.11 \cdot 10^{-7}$
Fourier-Bessel	$8.21 \cdot 10^{-7}$

Table 32: Cross section averaged parity-violating asymmetry $\langle A \rangle$ for ^{48}Ca

5.6 Results for the measuring time

To calculate the measuring time first of all the luminosity L has to be calculated. The luminosity can be calculated with equation (36) from section 2.4. In table 33 the luminosity for each nucleus is presented. The different parameters that are needed to calculate the luminosity are also explained in equations (37) and (38) in section 2.4. The beam current is $I = 150 \mu\text{A}$. We have to chose the length of the targets individually for each nucleus to take the different scattering cross sections into account. Heavier nuclei have a larger cross section because the cross section scales with Z^2 . If we would have chosen the same length for ^{208}Pb as for ^{12}C the radiation levels would be to high in the experiment hall.

Before we can calculate the measuring time we need to determine how many scattering events take place. This depends on how precise we want to calculate the asymmetry. For this calculations we chose a precision of $\frac{\Delta A}{A} = 0.01$, $\frac{\Delta A}{A} = 0.005$, $\frac{\Delta A}{A} = 0.003$ and $\frac{\Delta A}{A} = 0.001$. To calculate the number of events equation (33) from section 2.4 is used.

Nucleus	Density [$\frac{\text{g}}{\text{cm}^3}$]	Length [cm]	Luminosity [$\frac{1}{\text{cm}^2 \cdot \text{s}}$]
^{12}C	2.26	2.2	$2.34 \cdot 10^{38}$
^{40}Ca	1.55	0.2	$4.81 \cdot 10^{37}$
^{42}Ca	1.55	0.2	$4.58 \cdot 10^{37}$
^{48}Ca	1.55	0.2	$4.01 \cdot 10^{37}$
^{208}Pb	11.342	0.025	$6.76 \cdot 10^{37}$

Table 33: Luminosity for the different nuclei

Equation (33) can be solved for the number of scattering events:

$$N = \frac{1}{\Delta A^2}. \quad (43)$$

Usually not all the electrons in the beam are polarized. This can be taken into account if we calculate:

$$N = \frac{1}{P^2 \cdot \Delta A^2}. \quad (44)$$

The parameter P is the polarization of the beam.

Now the total amount of events can be calculated if we assume a 100% polarized electron beam as well as an electron beam with a polarization of 80%. In table 34 the number of events for fixed Q^2 at $P = 100\%$ and $P = 80\%$ are displayed.

The number of events are independent of the parameterisation because we just look at the asymmetry at fixed Q^2 . We get the same numbers of events for ^{40}Ca as for ^{12}C because both nuclei have the same asymmetry.

Nucleus	Precision	$N, P = 100\%$	$N, P = 80\%$
^{12}C	$0.1\% \cdot A$	$7.1 \cdot 10^{18}$	$1.1 \cdot 10^{19}$
^{12}C	$0.3\% \cdot A$	$7.9 \cdot 10^{17}$	$1.2 \cdot 10^{18}$
^{12}C	$0.5\% \cdot A$	$2.9 \cdot 10^{17}$	$4.5 \cdot 10^{17}$
^{12}C	$1\% \cdot A$	$7.1 \cdot 10^{16}$	$1.1 \cdot 10^{17}$
^{40}Ca	$0.1\% \cdot A$	$7.1 \cdot 10^{18}$	$1.1 \cdot 10^{19}$
^{40}Ca	$0.3\% \cdot A$	$7.9 \cdot 10^{17}$	$1.2 \cdot 10^{18}$
^{40}Ca	$0.5\% \cdot A$	$2.9 \cdot 10^{17}$	$4.5 \cdot 10^{17}$
^{40}Ca	$1\% \cdot A$	$7.1 \cdot 10^{16}$	$1.1 \cdot 10^{17}$
^{42}Ca	$0.1\% \cdot A$	$5.8 \cdot 10^{18}$	$9.1 \cdot 10^{18}$
^{42}Ca	$0.3\% \cdot A$	$6.5 \cdot 10^{17}$	$1.0 \cdot 10^{18}$
^{42}Ca	$0.5\% \cdot A$	$2.3 \cdot 10^{17}$	$3.6 \cdot 10^{17}$
^{42}Ca	$1\% \cdot A$	$5.8 \cdot 10^{16}$	$9.1 \cdot 10^{16}$
^{48}Ca	$0.1\% \cdot A$	$3.5 \cdot 10^{18}$	$5.4 \cdot 10^{18}$
^{48}Ca	$0.3\% \cdot A$	$3.9 \cdot 10^{17}$	$6.0 \cdot 10^{17}$
^{48}Ca	$0.5\% \cdot A$	$1.4 \cdot 10^{17}$	$2.2 \cdot 10^{17}$
^{48}Ca	$1\% \cdot A$	$3.5 \cdot 10^{16}$	$5.4 \cdot 10^{16}$
^{208}Pb	$0.1\% \cdot A$	$2.9 \cdot 10^{18}$	$4.5 \cdot 10^{18}$
^{208}Pb	$0.3\% \cdot A$	$3.2 \cdot 10^{17}$	$5.0 \cdot 10^{17}$
^{208}Pb	$0.5\% \cdot A$	$1.1 \cdot 10^{17}$	$1.8 \cdot 10^{17}$
^{208}Pb	$1\% \cdot A$	$2.9 \cdot 10^{16}$	$4.5 \cdot 10^{16}$

Table 34: Number of Events N needed to reach a given precision with a beam polarisation of $P = 100\%$ and $P = 80\%$ electron beam for the non averaged asymmetry A

The rate of the scattered electrons is:

$$\dot{N} = L \cdot \int \frac{d\sigma}{d\Omega} d\Omega. \quad (45)$$

The rate of the scattered electrons can be found in table 35. The integral was evaluated using equation (30) from section 2.4 and the angle acceptance of the P2-experiment ($\theta = 25^\circ - \theta = 45^\circ$).

The cross section averaged number of events can be found in table 36 and table 37.

If we want to calculate the measuring time we have to use equation (35) from section 2.4. We assume that the luminosity is a time independent parameter. The measuring time estimation is done for all conditions mentioned before for the different nuclei. In table 38 and table 39 the measuring times for the non averaged asymmetries are displayed. Table 40 and table 41 display the cross section averaged measuring times.

Nucleus	$\dot{N} [\frac{1}{s}]$	Parameterisation
^{12}C	$2.1 \cdot 10^{11}$	Polynomial
^{12}C	$2.5 \cdot 10^{11}$	Gaussian
^{12}C	$2.1 \cdot 10^{11}$	Helm
^{12}C	$2.2 \cdot 10^{11}$	Sum of Gaussian
^{12}C	$2.1 \cdot 10^{11}$	Fourier-Bessel
^{40}Ca	$3.1 \cdot 10^{10}$	Polynomial
^{40}Ca	$3.1 \cdot 10^{10}$	Gaussian
^{40}Ca	$3.0 \cdot 10^{10}$	Helm
^{40}Ca	$3.2 \cdot 10^{10}$	Sum of Gaussian
^{40}Ca	$3.1 \cdot 10^{10}$	Fourier-Bessel
^{42}Ca	$3.0 \cdot 10^{10}$	Polynomial
^{42}Ca	$2.7 \cdot 10^{10}$	Gaussian
^{42}Ca	$2.8 \cdot 10^{10}$	Helm
^{42}Ca	$3.0 \cdot 10^{10}$	Sum of Gaussian
^{42}Ca	$3.0 \cdot 10^{10}$	Fourier-Bessel
^{48}Ca	$2.6 \cdot 10^{10}$	Polynomial
^{48}Ca	$2.6 \cdot 10^{10}$	Gaussian
^{48}Ca	$2.5 \cdot 10^{10}$	Helm
^{48}Ca	$2.6 \cdot 10^{10}$	Sum of Gaussian
^{48}Ca	$2.6 \cdot 10^{10}$	Fourier-Bessel
^{208}Pb	$3.4 \cdot 10^{10}$	Gaussian

Table 35: Rate \dot{N} of the scattered electrons for different form factor parameterisations. These values were calculated using equation (45). The luminosity was taken from table 33. The integral was calculated using equation (30). The angle acceptance of the P2-experiment was used as limits for the integral.

Nucleus	Precision	$N_{averaged}, P = 100\%$	$N_{averaged}, P = 80\%$	Parameterisation
^{12}C	0.1% · A	$2.8 \cdot 10^{18}$	$4.4 \cdot 10^{18}$	Polynomial
^{12}C	0.3% · A	$3.1 \cdot 10^{17}$	$4.8 \cdot 10^{17}$	Polynomial
^{12}C	0.5% · A	$1.1 \cdot 10^{17}$	$1.7 \cdot 10^{17}$	Polynomial
^{12}C	1% · A	$2.8 \cdot 10^{16}$	$4.4 \cdot 10^{16}$	Polynomial
^{12}C	0.1% · A	$2.9 \cdot 10^{18}$	$4.6 \cdot 10^{18}$	Gaussian
^{12}C	0.3% · A	$3.2 \cdot 10^{17}$	$5.1 \cdot 10^{17}$	Gaussian
^{12}C	0.5% · A	$1.2 \cdot 10^{17}$	$1.8 \cdot 10^{17}$	Gaussian
^{12}C	1% · A	$2.9 \cdot 10^{16}$	$4.6 \cdot 10^{16}$	Gaussian
^{12}C	0.1% · A	$2.8 \cdot 10^{18}$	$4.4 \cdot 10^{18}$	Helm
^{12}C	0.3% · A	$3.1 \cdot 10^{17}$	$4.9 \cdot 10^{17}$	Helm
^{12}C	0.5% · A	$1.1 \cdot 10^{17}$	$1.8 \cdot 10^{17}$	Helm
^{12}C	1% · A	$2.8 \cdot 10^{16}$	$4.4 \cdot 10^{16}$	Helm
^{12}C	0.1% · A	$2.8 \cdot 10^{18}$	$4.4 \cdot 10^{18}$	Sum of Gaussian
^{12}C	0.3% · A	$3.1 \cdot 10^{17}$	$4.9 \cdot 10^{17}$	Sum of Gaussian
^{12}C	0.5% · A	$1.1 \cdot 10^{17}$	$1.8 \cdot 10^{17}$	Sum of Gaussian
^{12}C	1% · A	$2.8 \cdot 10^{16}$	$4.4 \cdot 10^{16}$	Sum of Gaussian
^{12}C	0.1% · A	$2.8 \cdot 10^{18}$	$4.4 \cdot 10^{18}$	Fourier-Bessel
^{12}C	0.3% · A	$3.1 \cdot 10^{17}$	$4.9 \cdot 10^{17}$	Fourier-Bessel
^{12}C	0.5% · A	$1.1 \cdot 10^{17}$	$1.8 \cdot 10^{17}$	Fourier-Bessel
^{12}C	1% · A	$2.8 \cdot 10^{16}$	$4.4 \cdot 10^{16}$	Fourier-Bessel
Nucleus	Precision	$N_{averaged}, P = 100\%$	$N_{averaged}, P = 80\%$	Parameterisation
^{40}Ca	0.1% · A	$3.2 \cdot 10^{18}$	$5.0 \cdot 10^{18}$	Polynomial
^{40}Ca	0.3% · A	$3.5 \cdot 10^{17}$	$5.5 \cdot 10^{17}$	Polynomial
^{40}Ca	0.5% · A	$1.3 \cdot 10^{17}$	$2.0 \cdot 10^{17}$	Polynomial
^{40}Ca	1% · A	$3.2 \cdot 10^{16}$	$5.0 \cdot 10^{16}$	Polynomial
^{40}Ca	0.1% · A	$3.1 \cdot 10^{18}$	$4.9 \cdot 10^{18}$	Gaussian
^{40}Ca	0.3% · A	$3.5 \cdot 10^{17}$	$5.4 \cdot 10^{17}$	Gaussian
^{40}Ca	0.5% · A	$1.3 \cdot 10^{17}$	$2.0 \cdot 10^{17}$	Gaussian
^{40}Ca	1% · A	$3.1 \cdot 10^{16}$	$4.9 \cdot 10^{16}$	Gaussian
^{40}Ca	0.1% · A	$3.1 \cdot 10^{18}$	$4.8 \cdot 10^{18}$	Helm
^{40}Ca	0.3% · A	$3.4 \cdot 10^{17}$	$5.4 \cdot 10^{17}$	Helm
^{40}Ca	0.5% · A	$1.2 \cdot 10^{17}$	$1.9 \cdot 10^{17}$	Helm
^{40}Ca	1% · A	$3.1 \cdot 10^{16}$	$4.8 \cdot 10^{16}$	Helm
^{40}Ca	0.1% · A	$3.1 \cdot 10^{18}$	$4.9 \cdot 10^{18}$	Sum of Gaussian
^{40}Ca	0.3% · A	$3.5 \cdot 10^{17}$	$5.4 \cdot 10^{17}$	Sum of Gaussian
^{40}Ca	0.5% · A	$1.3 \cdot 10^{17}$	$2.0 \cdot 10^{17}$	Sum of Gaussian
^{40}Ca	1% · A	$3.1 \cdot 10^{16}$	$4.9 \cdot 10^{16}$	Sum of Gaussian
^{40}Ca	0.1% · A	$3.0 \cdot 10^{18}$	$4.8 \cdot 10^{18}$	Fourier-Bessel
^{40}Ca	0.3% · A	$3.4 \cdot 10^{17}$	$5.3 \cdot 10^{17}$	Fourier-Bessel
^{40}Ca	0.5% · A	$1.2 \cdot 10^{17}$	$1.9 \cdot 10^{17}$	Fourier-Bessel
^{40}Ca	1% · A	$3.0 \cdot 10^{16}$	$4.8 \cdot 10^{16}$	Fourier-Bessel

Table 36: Number of Events N needed to reach a given precision with a beam polarisation of $P = 100\%$ and $P = 80\%$ electron beam for the averaged asymmetry $\langle A \rangle$

Nucleus	Precision	$N_{averaged} P = 100\%$	$N_{averaged} P = 80\%$	Parameterisation
^{42}Ca	0.1% · A	$2.6 \cdot 10^{18}$	$4.1 \cdot 10^{18}$	Polynomial
^{42}Ca	0.3% · A	$2.9 \cdot 10^{17}$	$4.6 \cdot 10^{17}$	Polynomial
^{42}Ca	0.5% · A	$1.1 \cdot 10^{17}$	$1.7 \cdot 10^{17}$	Polynomial
^{42}Ca	1% · A	$2.6 \cdot 10^{16}$	$4.1 \cdot 10^{16}$	Polynomial
^{42}Ca	0.1% · A	$2.5 \cdot 10^{18}$	$3.8 \cdot 10^{18}$	Gaussian
^{42}Ca	0.3% · A	$2.7 \cdot 10^{17}$	$4.3 \cdot 10^{17}$	Gaussian
^{42}Ca	0.5% · A	$9.8 \cdot 10^{16}$	$1.5 \cdot 10^{17}$	Gaussian
^{42}Ca	1% · A	$2.5 \cdot 10^{16}$	$3.8 \cdot 10^{16}$	Gaussian
^{42}Ca	0.1% · A	$2.5 \cdot 10^{18}$	$3.9 \cdot 10^{18}$	Helm
^{42}Ca	0.3% · A	$2.8 \cdot 10^{17}$	$4.4 \cdot 10^{17}$	Helm
^{42}Ca	0.5% · A	$1.0 \cdot 10^{17}$	$1.6 \cdot 10^{17}$	Helm
^{42}Ca	1% · A	$2.5 \cdot 10^{16}$	$3.9 \cdot 10^{16}$	Helm
^{42}Ca	0.1% · A	$2.6 \cdot 10^{18}$	$4.0 \cdot 10^{18}$	Sum of Gaussian
^{42}Ca	0.3% · A	$2.9 \cdot 10^{17}$	$4.5 \cdot 10^{17}$	Sum of Gaussian
^{42}Ca	0.5% · A	$1.0 \cdot 10^{17}$	$1.6 \cdot 10^{17}$	Sum of Gaussian
^{42}Ca	1% · A	$2.6 \cdot 10^{16}$	$4.0 \cdot 10^{16}$	Sum of Gaussian
^{42}Ca	0.1% · A	$2.5 \cdot 10^{18}$	$3.9 \cdot 10^{18}$	Fourier-Bessel
^{42}Ca	0.3% · A	$2.8 \cdot 10^{17}$	$4.3 \cdot 10^{17}$	Fourier-Bessel
^{42}Ca	0.5% · A	$9.9 \cdot 10^{16}$	$1.6 \cdot 10^{17}$	Fourier-Bessel
^{42}Ca	1% · A	$2.5 \cdot 10^{16}$	$3.9 \cdot 10^{16}$	Fourier-Bessel
Nucleus	Precision	$N_{averaged} P = 100\%$	$N_{averaged} P = 80\%$	Parameterisation
^{48}Ca	0.1% · A	$1.6 \cdot 10^{18}$	$2.4 \cdot 10^{18}$	Polynomial
^{48}Ca	0.3% · A	$1.7 \cdot 10^{17}$	$2.7 \cdot 10^{17}$	Polynomial
^{48}Ca	0.5% · A	$6.2 \cdot 10^{16}$	$9.7 \cdot 10^{16}$	Polynomial
^{48}Ca	1% · A	$1.6 \cdot 10^{16}$	$2.4 \cdot 10^{16}$	Polynomial
^{48}Ca	0.1% · A	$1.5 \cdot 10^{18}$	$2.4 \cdot 10^{18}$	Gaussian
^{48}Ca	0.3% · A	$1.7 \cdot 10^{17}$	$2.7 \cdot 10^{17}$	Gaussian
^{48}Ca	0.5% · A	$6.1 \cdot 10^{16}$	$9.6 \cdot 10^{16}$	Gaussian
^{48}Ca	1% · A	$1.5 \cdot 10^{16}$	$2.4 \cdot 10^{16}$	Gaussian
^{48}Ca	0.1% · A	$1.5 \cdot 10^{18}$	$2.3 \cdot 10^{18}$	Helm
^{48}Ca	0.3% · A	$1.7 \cdot 10^{17}$	$2.6 \cdot 10^{17}$	Helm
^{48}Ca	0.5% · A	$6.0 \cdot 10^{16}$	$9.3 \cdot 10^{16}$	Helm
^{48}Ca	1% · A	$1.5 \cdot 10^{16}$	$2.3 \cdot 10^{16}$	Helm
^{48}Ca	0.1% · A	$1.5 \cdot 10^{18}$	$2.4 \cdot 10^{18}$	Sum of Gaussian
^{48}Ca	0.3% · A	$1.7 \cdot 10^{17}$	$2.6 \cdot 10^{17}$	Sum of Gaussian
^{48}Ca	0.5% · A	$6.1 \cdot 10^{16}$	$9.5 \cdot 10^{16}$	Sum of Gaussian
^{48}Ca	1% · A	$1.5 \cdot 10^{16}$	$2.4 \cdot 10^{16}$	Sum of Gaussian
^{48}Ca	0.1% · A	$1.5 \cdot 10^{18}$	$2.3 \cdot 10^{18}$	Fourier-Bessel
^{48}Ca	0.3% · A	$1.7 \cdot 10^{17}$	$2.6 \cdot 10^{17}$	Fourier-Bessel
^{48}Ca	0.5% · A	$5.9 \cdot 10^{16}$	$9.3 \cdot 10^{16}$	Fourier-Bessel
^{48}Ca	1% · A	$1.5 \cdot 10^{16}$	$2.3 \cdot 10^{16}$	Fourier-Bessel
Nucleus	Precision	$N_{averaged} P = 100\%$	$N_{averaged} P = 80\%$	Parameterisation
^{208}Pb	0.1% · A	$1.4 \cdot 10^{18}$	$2.3 \cdot 10^{18}$	Gaussian
^{208}Pb	0.3% · A	$1.6 \cdot 10^{17}$	$2.5 \cdot 10^{17}$	Gaussian
^{208}Pb	0.5% · A	$5.8 \cdot 10^{16}$	$9.1 \cdot 10^{16}$	Gaussian
^{208}Pb	1% · A	$1.4 \cdot 10^{16}$	$2.3 \cdot 10^{16}$	Gaussian

Table 37: Number of Events N needed to reach a given precision with a beam polarisation of $P = 100\%$ and $P = 80\%$ electron beam for the averaged asymmetry $\langle A \rangle$

Nucleus	Precision	$T, P = 100\%$ [h]	$T, P = 80\%$ [h]	Parameterisation
^{12}C	0.1% · A	9294	14522	Polynomial
^{12}C	0.3% · A	1033	1614	Polynomial
^{12}C	0.5% · A	372	581	Polynomial
^{12}C	1% · A	93	145	Polynomial
^{12}C	0.1% · A	7965	12445	Gaussian
^{12}C	0.3% · A	885	1383	Gaussian
^{12}C	0.5% · A	319	498	Gaussian
^{12}C	1% · A	80	124	Gaussian
^{12}C	0.1% · A	9398	14684	Helm
^{12}C	0.3% · A	1044	1632	Helm
^{12}C	0.5% · A	376	587	Helm
^{12}C	1% · A	94	147	Helm
^{12}C	0.1% · A	9129	14264	Sum of Gaussian
^{12}C	0.3% · A	1014	1646	Sum of Gaussian
^{12}C	0.5% · A	379	593	Sum of Gaussian
^{12}C	1% · A	91	143	Sum of Gaussian
^{12}C	0.1% · A	9285	14507	Fourier-Bessel
^{12}C	0.3% · A	1032	1585	Fourier-Bessel
^{12}C	0.5% · A	371	580	Fourier-Bessel
^{12}C	1% · A	93	145	Fourier-Bessel
Nucleus	Precision	$T, P = 100\%$ [h]	$T, P = 80\%$ [h]	Parameterisation
^{40}Ca	0.1% · A	64473	100738	Polynomial
^{40}Ca	0.3% · A	7164	11193	Polynomial
^{40}Ca	0.5% · A	2579	4030	Polynomial
^{40}Ca	1% · A	645	1007	Polynomial
^{40}Ca	0.1% · A	64015	100024	Gaussian
^{40}Ca	0.3% · A	7113	11114	Gaussian
^{40}Ca	0.5% · A	2561	4001	Gaussian
^{40}Ca	1% · A	640	1000	Gaussian
^{40}Ca	0.1% · A	67128	104888	Helm
^{40}Ca	0.3% · A	7459	11654	Helm
^{40}Ca	0.5% · A	2685	4196	Helm
^{40}Ca	1% · A	671	1049	Helm
^{40}Ca	0.1% · A	62912	98300	Sum of Gaussian
^{40}Ca	0.3% · A	6990	10922	Sum of Gaussian
^{40}Ca	0.5% · A	2516	3948	Sum of Gaussian
^{40}Ca	1% · A	632	987	Sum of Gaussian
^{40}Ca	0.1% · A	63677	99496	Fourier-Bessel
^{40}Ca	0.3% · A	7075	11055	Fourier-Bessel
^{40}Ca	0.5% · A	2547	3932	Fourier-Bessel
^{40}Ca	1% · A	637	995	Fourier-Bessel

Table 38: Estimated measuring time T needed to reach a given precision with a beam polarisation of $P = 100\%$ and $P = 80\%$ for the non averaged asymmetry A

Nucleus	Precision	$T, P = 100\%$ [h]	$T, P = 80\%$ [h]	Parameterisation
^{42}Ca	$0.1\% \cdot A$	53394	83428	Polynomial
^{42}Ca	$0.3\% \cdot A$	5933	9270	Polynomial
^{42}Ca	$0.5\% \cdot A$	2136	3337	Polynomial
^{42}Ca	$1\% \cdot A$	534	834	Polynomial
^{42}Ca	$0.1\% \cdot A$	58794	91866	Gaussian
^{42}Ca	$0.3\% \cdot A$	6533	10207	Gaussian
^{42}Ca	$0.5\% \cdot A$	2352	3675	Gaussian
^{42}Ca	$1\% \cdot A$	588	919	Gaussian
^{42}Ca	$0.1\% \cdot A$	56930	88954	Helm
^{42}Ca	$0.3\% \cdot A$	6326	9884	Helm
^{42}Ca	$0.5\% \cdot A$	2277	3558	Helm
^{42}Ca	$1\% \cdot A$	569	890	Helm
^{42}Ca	$0.1\% \cdot A$	53284	83257	Sum of Gaussian
^{42}Ca	$0.3\% \cdot A$	5920	9251	Sum of Gaussian
^{42}Ca	$0.5\% \cdot A$	2131	3330	Sum of Gaussian
^{42}Ca	$1\% \cdot A$	533	833	Sum of Gaussian
^{42}Ca	$0.1\% \cdot A$	53858	84154	Fourier-Bessel
^{42}Ca	$0.3\% \cdot A$	5984	9350	Fourier-Bessel
^{42}Ca	$0.5\% \cdot A$	2154	3366	Fourier-Bessel
^{42}Ca	$1\% \cdot A$	539	842	Fourier-Bessel
Nucleus	Precision	$T, P = 100\%$ [h]	$T, P = 80\%$ [h]	Parameterisation
^{48}Ca	$0.1\% \cdot A$	37652	58832	Polynomial
^{48}Ca	$0.3\% \cdot A$	4184	6537	Polynomial
^{48}Ca	$0.5\% \cdot A$	1506	2353	Polynomial
^{48}Ca	$1\% \cdot A$	377	588	Polynomial
^{48}Ca	$0.1\% \cdot A$	37126	58009	Gaussian
^{48}Ca	$0.3\% \cdot A$	4125	6445	Gaussian
^{48}Ca	$0.5\% \cdot A$	1485	2320	Gaussian
^{48}Ca	$1\% \cdot A$	371	580	Gaussian
^{48}Ca	$0.1\% \cdot A$	38187	59667	Helm
^{48}Ca	$0.3\% \cdot A$	4243	6630	Helm
^{48}Ca	$0.5\% \cdot A$	1527	2387	Helm
^{48}Ca	$1\% \cdot A$	382	597	Helm
^{48}Ca	$0.1\% \cdot A$	37337	58339	Sum of Gaussian
^{48}Ca	$0.3\% \cdot A$	4149	6482	Sum of Gaussian
^{48}Ca	$0.5\% \cdot A$	1493	2334	Sum of Gaussian
^{48}Ca	$1\% \cdot A$	373	583	Sum of Gaussian
^{48}Ca	$0.1\% \cdot A$	37118	57997	Fourier-Bessel
^{48}Ca	$0.3\% \cdot A$	4124	6444	Fourier-Bessel
^{48}Ca	$0.5\% \cdot A$	1485	2320	Fourier-Bessel
^{48}Ca	$1\% \cdot A$	371	580	Fourier-Bessel
Nucleus	Precision	$T, P = 100\%$ [h]	$T, P = 80\%$ [h]	Parameterisation
^{208}Pb	$0.1\% \cdot A$	23310	36422	Gaussian
^{208}Pb	$0.3\% \cdot A$	2590	4047	Gaussian
^{208}Pb	$0.5\% \cdot A$	932	1457	Gaussian
^{208}Pb	$1\% \cdot A$	233	364	Gaussian

Table 39: Estimated measuring time T needed to reach a given precision with a beam polarisation of $P = 100\%$ and $P = 80\%$ for the non averaged asymmetry A

Nucleus	Precision	$T_{averaged}, P = 100\%$ [h]	$T_{averaged}, P = 80\%$ [h]	Parameterisation
^{12}C	0.1% · A	3635	5680	Polynomial
^{12}C	0.3% · A	404	631	Polynomial
^{12}C	0.5% · A	145	227	Polynomial
^{12}C	1% · A	36	57	Polynomial
^{12}C	0.1% · A	3260	5094	Gaussian
^{12}C	0.3% · A	362	566	Gaussian
^{12}C	0.5% · A	130	204	Gaussian
^{12}C	1% · A	33	51	Gaussian
^{12}C	0.1% · A	3721	5815	Helm
^{12}C	0.3% · A	413	646	Helm
^{12}C	0.5% · A	149	233	Helm
^{12}C	1% · A	37	58	Helm
^{12}C	0.1% · A	3625	5664	Sum of Gaussian
^{12}C	0.3% · A	403	629	Sum of Gaussian
^{12}C	0.5% · A	151	236	Sum of Gaussian
^{12}C	1% · A	36	57	Sum of Gaussian
^{12}C	0.1% · A	3667	5730	Fourier-Bessel
^{12}C	0.3% · A	407	637	Fourier-Bessel
^{12}C	0.5% · A	147	229	Fourier-Bessel
^{12}C	1% · A	37	57	Fourier-Bessel
Nucleus	Precision	$T_{averaged}, P = 100\%$ [h]	$T_{averaged}, P = 80\%$ [h]	Parameterisation
^{40}Ca	0.1% · A	28681	44815	Polynomial
^{40}Ca	0.3% · A	3187	4979	Polynomial
^{40}Ca	0.5% · A	1147	1793	Polynomial
^{40}Ca	1% · A	287	448	Polynomial
^{40}Ca	0.1% · A	28112	43926	Gaussian
^{40}Ca	0.3% · A	3124	4881	Gaussian
^{40}Ca	0.5% · A	1124	1757	Gaussian
^{40}Ca	1% · A	281	439	Gaussian
^{40}Ca	0.1% · A	28989	45295	Helm
^{40}Ca	0.3% · A	3221	5033	Helm
^{40}Ca	0.5% · A	1160	1812	Helm
^{40}Ca	1% · A	290	453	Helm
^{40}Ca	0.1% · A	27658	43215	Sum of Gaussian
^{40}Ca	0.3% · A	3073	4801	Sum of Gaussian
^{40}Ca	0.5% · A	1106	1728	Sum of Gaussian
^{40}Ca	1% · A	277	432	Sum of Gaussian
^{40}Ca	0.1% · A	27189	42483	Fourier-Bessel
^{40}Ca	0.3% · A	3021	4722	Fourier-Bessel
^{40}Ca	0.5% · A	1088	1699	Fourier-Bessel
^{40}Ca	1% · A	272	425	Fourier-Bessel

Table 40: Estimated measuring time T needed to reach a given precision with a beam polarisation of $P = 100\%$ and $P = 80\%$ for the averaged asymmetry $\langle A \rangle$

Nucleus	Precision	$T_{averaged}, P = 100\% [h]$	$T_{averaged}, P = 80\% [h]$	Parameterisation
^{42}Ca	$0.1\% \cdot A$	24314	37991	Polynomial
^{42}Ca	$0.3\% \cdot A$	2702	4221	Polynomial
^{42}Ca	$0.5\% \cdot A$	973	1520	Polynomial
^{42}Ca	$1\% \cdot A$	243	380	Polynomial
^{42}Ca	$0.1\% \cdot A$	24869	38858	Gaussian
^{42}Ca	$0.3\% \cdot A$	2763	4318	Gaussian
^{42}Ca	$0.5\% \cdot A$	995	1554	Gaussian
^{42}Ca	$1\% \cdot A$	249	389	Gaussian
^{42}Ca	$0.1\% \cdot A$	24539	38342	Helm
^{42}Ca	$0.3\% \cdot A$	2727	4260	Helm
^{42}Ca	$0.5\% \cdot A$	982	1534	Helm
^{42}Ca	$1\% \cdot A$	245	383	Helm
^{42}Ca	$0.1\% \cdot A$	23693	37021	Sum of Gaussian
^{42}Ca	$0.3\% \cdot A$	2633	4113	Sum of Gaussian
^{42}Ca	$0.5\% \cdot A$	948	1481	Sum of Gaussian
^{42}Ca	$1\% \cdot A$	237	370	Sum of Gaussian
^{42}Ca	$0.1\% \cdot A$	22985	35914	Fourier-Bessel
^{42}Ca	$0.3\% \cdot A$	2554	3990	Fourier-Bessel
^{42}Ca	$0.5\% \cdot A$	919	1437	Fourier-Bessel
^{42}Ca	$1\% \cdot A$	230	359	Fourier-Bessel
Nucleus	Precision	$T_{averaged}, P = 100\% [h]$	$T_{averaged}, P = 80\% [h]$	Parameterisation
^{48}Ca	$0.1\% \cdot A$	16865	26351	Polynomial
^{48}Ca	$0.3\% \cdot A$	1874	2928	Polynomial
^{48}Ca	$0.5\% \cdot A$	675	1054	Polynomial
^{48}Ca	$1\% \cdot A$	169	263	Polynomial
^{48}Ca	$0.1\% \cdot A$	16362	25566	Gaussian
^{48}Ca	$0.3\% \cdot A$	1818	2841	Gaussian
^{48}Ca	$0.5\% \cdot A$	654	1023	Gaussian
^{48}Ca	$1\% \cdot A$	164	256	Gaussian
^{48}Ca	$0.1\% \cdot A$	16392	25613	Helm
^{48}Ca	$0.3\% \cdot A$	1821	2846	Helm
^{48}Ca	$0.5\% \cdot A$	656	1025	Helm
^{48}Ca	$1\% \cdot A$	164	256	Helm
^{48}Ca	$0.1\% \cdot A$	16337	25526	Sum of Gaussian
^{48}Ca	$0.3\% \cdot A$	1815	2836	Sum of Gaussian
^{48}Ca	$0.5\% \cdot A$	653	1021	Sum of Gaussian
^{48}Ca	$1\% \cdot A$	163	255	Sum of Gaussian
^{48}Ca	$0.1\% \cdot A$	15849	24763	Fourier-Bessel
^{48}Ca	$0.3\% \cdot A$	1761	2751	Fourier-Bessel
^{48}Ca	$0.5\% \cdot A$	634	991	Fourier-Bessel
^{48}Ca	$1\% \cdot A$	158	248	Fourier-Bessel
Nucleus	Precision	$T_{averaged} P = 100\% [h]$	$T_{averaged} P = 80\% [h]$	Parameterisation
^{208}Pb	$0.1\% \cdot A$	11822	18473	Gaussian
^{208}Pb	$0.3\% \cdot A$	1314	2053	Gaussian
^{208}Pb	$0.5\% \cdot A$	473	739	Gaussian
^{208}Pb	$1\% \cdot A$	118	185	Gaussian

Table 41: Estimated measuring time T needed to reach a given precision with a beam polarisation of $P = 100\%$ and $P = 80\%$ for the averaged asymmetry $\langle A \rangle$

6 Results and discussion

6.1 Summary of the parity-violating asymmetry and measuring time

In this thesis the estimated measuring times of parity-violating electron scattering for different nuclei at the P2-experiment in Mainz were calculated. The selected nuclei are ^{12}C , ^{40}Ca , ^{42}Ca , ^{48}Ca and ^{208}Pb .

To do this different parameterisations are used in order to get an analytical expression for the electric form factor. This was achieved by calculating the form factor from various electron nuclei cross section data sets and using a fit function to describe the form factor data points. As parameterisations for the form factor the Helm parameterisation, the Sum of Gaussian functions parameterisation, the Fourier-Bessel parameterisation, the polynomial function parameterisation and the Gaussian function parameterisation were used. Only for ^{208}Pb we were only able to find a fit solution for the Gaussian function parameterisation. This is because the form factor values deviate from each other for $Q^2 > 30 \cdot 10^3 \frac{\text{MeV}^2}{c^2}$ which is not the case for the other nuclei.

The inelastic electron scattering is neglected for the calculation of the asymmetry and measuring time because for forward scattering the cross section and form factor values are smaller by a factor ≈ 1000 compared to elastic scattering. Because the angular range of the P2-experiment is from 25° to 45° only the forward scattering values are important to take into account.

Generally, the parity-violating asymmetry becomes larger for heavier nuclei. We also see that the cross section averaged asymmetry is between 1.4 and 1.6 times larger for the nuclear targets than the parity-violating asymmetry calculated with the Q^2 -value for the P2-experiment from using a hydrogen target. The reason for the different values for the cross section averaged asymmetry is that the different parameterisations are taken into account. The differences in parameterisation is particularly noticeable if we look at figures 33, 41, 49, 57 and 65. We can see that for ^{42}Ca the fit functions for the form factor differ from each other. This is because we have the fewest data points for ^{42}Ca . Therefore, the fitting tool of ROOT has problems finding good fit solutions for the data points.

The biggest difference in measuring time between parameterisation for a given precision were calculated for ^{40}Ca and ^{42}Ca . The reason for this is that the parameterisation differ from each other in the Q^2 -interval from $Q^2 \approx 4.5 \cdot 10^3 \frac{\text{MeV}^2}{c^2}$ to $Q^2 \approx 15 \cdot 10^3 \frac{\text{MeV}^2}{c^2}$.

The measuring time for ^{12}C ranges from $T \approx 15000$ h to $T \approx 33$ h dependent on which parameterisation is used, which precision is desired and if we use the non averaged or the cross section averaged asymmetry. For ^{40}Ca the measuring time ranges from $T \approx 105000$ h to $T \approx 272$ h and for ^{42}Ca the measuring time is between $T \approx 92000$ h and $T \approx 230$ h. The measuring time for ^{48}Ca is between $T \approx 59700$ h and $T \approx 158$ h and for ^{208}Pb we get measuring times from $T \approx 36421$ h to $T \approx 118$ h. It is important to remember that the tar-

gets of the different nuclei have different lengths. The target for ^{12}C was 2.2 cm long, those for $^{40,42,48}\text{Ca}$ were 0.2 cm long and that for ^{208}Pb was 0.025 cm long.

6.2 Discussion of the parity-violating asymmetry and measuring time

Generally, the order of magnitude of the estimated measuring time seems realistic. Nevertheless there are some inaccuracies that happen during the calculations.

First of all it is important to note that not all of the cross section data sets have radiative corrections applied. Furthermore the angular acceptance of the different detectors are unknown. Because there were no corrections made in retrospect for the analysis in this thesis, this can lead to inaccuracies for the cross section data which further influences the form factor values. These inaccuracies influence the further calculations because every set of data is treated equally.

This leads to inaccuracies for the fit functions found by ROOT. What also has to be taken into account is that the starting parameters for the fitting tool of ROOT influences the outcome for the fitting function. There is a possibility that for different starting parameters other fit functions can be found that describe the data points better. This has an influence on the calculations that depend on the fit parameters.

For the calculations of the luminosity for the different targets we assumed that we only have one target with a specific length. In reality the target consists of many smaller targets. This assumption leads to a small inaccuracies. One minor source of uncertainties is that we used only one density for ^{40}Ca , ^{42}Ca and ^{48}Ca .

It is also important to note that the formula that was used to calculate the parity-violating asymmetry is not completely accurate. The formula is only accurate in leading order. Nevertheless the calculated result seem to be realistic.

7 References

- [1] Povh et al, Teilchen und Kerne: Eine Einführung in die physikalischen Konzepte 9.Auflage
- [2] Gintaras Dda et al, JCAP04(2007)012
- [3] T.D. Lee, C.N. Yang, Question of Parity Conservation in Weak Interactions, Physical Review **104** 254 (1956)
- [4] C.S. Wu, E. Ambler, R.W. Hayward, D.D. Hoppes, R.P. Hudson, Experimental Test of Parity Conservation in Beta Decay, Physical Review **105** 1413 (1957)
- [5] Dominik Becker et al, The P2-experiment: A future high precision measurement of the elektroweak mixing angle at low momentum transfer, The European Physical Journal **A54** 208 (2018)
- [6] Oleksander Koshchii, Jens Erler and Mikhail Gorchtein, Weak charge and weak radius of ^{12}C , Physical Review C **102** 022501 (2020)
- [7] <https://www.nndc.bnl.gov/nudat2/>
- [8] <https://inspirehep.net/>
- [9] <https://root.cern.ch/>
- [10] H.L. Crannell and T.A. Griffy, Determination of radiative transition Widths of excited states in ^{12}C , Physical Review **136** B 1580 (1964)
- [11] Jerome H. Fregeau, Elastic and inelastic scattering of 187-MeV electrons from ^{12}C , Physical Review **104** 225 (1956)
- [12] I. Sick and J.S. McCarthy, Elastic electron scattering from ^{12}C and ^{16}O , Nuclear Physics **A150** 631 (1970)
- [13] F.J. Kline, Hall Crannell and James T. O'Brien, Elastic electron scattering from ^{14}C , Nuclear Physics **A209** 381 (1973)
- [14] E.A.J.M Offermann, L.S. Cardman and C.W. de Jager, Energy dependence of the form factor for elastic electron scattering from ^{12}C , Physical Review C **44** 1096 (1991)
- [15] Jerome H. Fregeau and Robert Hofstadter, High-Energy electron scattering and nuclear structure determinations III Carbon-12 nucleus, Physical Review **99** 1503 (1955)
- [16] W. Reuter, G.Fricke, K.Merle and H.Miska, Nuclear charge distribution and rms radius of ^{12}C from absolute elastic electron scattering measurements, Physical Review **26** 806 (1982)
- [17] R.F. Frosch, R. Hofstadter and J.S. McCarthy, Electron scattering studies of calcium and titanium isotopes, Physical Review **174** 1380 (1968)
- [18] R.A. Eisenstein, D.W. Madsen and H. Theissen, Electron-Scattering studies on ^{40}Ca and ^{48}Ca , Physical Review **188** 1815 (1969)
- [19] B.B.P. Sinah, G.A. Peterson and R.R. Whitney, Nuclear charge distributions of isotone pairs II ^{39}K and ^{40}Ca , Physical Review **7** 1930 (1973)
- [20] H. Crannell, R.Helm and H.Kendall, Scattering of high-energy electrons from ^{40}Ca , ^{51}V , ^{59}Co , ^{115}In , ^{121}Sb , ^{123}Sb , ^{209}Bi , Physical Review **121** 183 (1961)
- [21] H.D. Gräf, H. Feldmeier and P. Manakos, Study of electric monopole transitions between the ground state and the first excited 0^+ -state in ^{40}Ca , ^{42}Ca , ^{44}Ca , ^{48}Ca with high resolution inelastic electron scattering, Nuclear Physics **A295** 319 (1978)
- [22] J.B. Bellicard and K.J van Oostrum, Elastic electron scattering from lead 208 at 175 MeV and 250 MeV, Physical Review Letters **19** 242 (1967)
- [23] J. Friedrich and F. Lenz, Elastic electron scattering from ^{208}Pb at moderate momentum transfer and model-independent description of the nuclear charge distribution, Nuclear Physics **A183** 523 (1971)

- [24] J. Friedrich, Investigation of some low lying states in ^{208}Pb by inelastic electron scattering, Nuclear Physics **A191** 118 (1972)
- [25] J.L. Friar and J.W. Negele, The determination of the nuclear charge distribution of ^{208}Pb from elastic electron scattering and muonic X-rays, Nuclear Physics **A212** 93 (1973)
- [26] H. De Vries, C.W. De Jager and C. De Vries, Nuclear charge distribution parameters from elastic electron scattering, Atomic Data and Nuclear Data Tables **36** 495 (1987)

8 Personal Acknowledgements

First of all I want to thank Prof. Dr. Frank Maas for giving me the opportunity to write my bachelor thesis on a topic related to current research at the Johannes Gutenberg-University. Furthermore I would like to thank Malte Wilfert who supported me on all the questions and problems that have arisen during my work on the bachelor thesis.

I would also like to thank all my fellow students who accompanied me during my bachelor and with whom I worked on the solutions to the exercise sheets and lab courses.

I also want to thank my family and friends who always believed and supported me in all circumstances during my bachelor.

9 Appendix

9.1 C++ code used for the calculations

Code:

```
#include <iostream>
#include <fstream>
#include <sstream>
#include <string>
#include <vector>
#include <math.h>
#include "Constants.hh"
/*****
using std::ios;
using std::cout;
using std::cerr;
using std::endl;
using std::stringstream;
using std::vector;
using std::string;
using std::ifstream;

/*****
void read_data(string dateiname, vector<double> &Energie, vector<double> &Winkel, vector<double>
               &Wirkungsquerschnitt, vector<double> &FehlerWirkungsquerschnitt, vector<double>
               &FehlerWinkel){
    ifstream stream;

    double Energietemp, Winkeltemp, Wirkungsquerschnitttemp, FehlerWinkeltemp
    ,FehlerWirkungsquerschnitttemp;

    stringstream nn;
    stream.open(dateiname.c_str(), ios::in);

    string line;

    if(!stream.good()) { cerr << "Warning: No data file found." << endl; return;}

    getline(stream, line);

    while(true){
        if (stream.eof()) break;
        getline(stream, line);
        if( line[0] != '#' && !line.empty() ) {

            nn.str("");
            nn.clear();
            nn.str(line);
            nn >> Energietemp >> Winkeltemp >> Wirkungsquerschnitttemp >>
            FehlerWirkungsquerschnitttemp >> FehlerWinkeltemp ;
            //cout << "Energietemp " << Energietemp << "Winkeltemp " << Winkeltemp
            << "Wirkungsquerschnitttemp " << Wirkungsquerschnitttemp
            << "FehlerWirkungsquerschnitttemp "
            << FehlerWirkungsquerschnitttemp <<
            " FehlerWinkeltemp " << FehlerWinkeltemp << endl;

            Energie.push_back(Energietemp); // run
            Winkel.push_back(Winkeltemp);
            Wirkungsquerschnitt.push_back(Wirkungsquerschnitttemp);
            FehlerWirkungsquerschnitt.push_back(FehlerWirkungsquerschnitttemp);
            FehlerWinkel.push_back(FehlerWinkeltemp);

        }
    }
    stream.close();
}

double Sum_of_Gauß(double *x, double *par){
```

```

double q = sqrt(x[0]);
const int N = 3;
double parQ[N];
double parR[N];
double parGamma = par[0]*fm;
q /= hquerc;
double SumQ = 0;
for(int i=0;i<N;i++){
    parQ[i]=par[2*i+2];
    parR[i]=par[2*i+1]*fm;
}
double Formfaktor = exp(-pow(q*parGamma,2)/4);
double Summe = 0;
for(int i=0;i<N;i++){
    double T1=parQ[i]/(1+2*pow(parR[i]/parGamma,2));
    double T2=cos(q*parR[i]);
    double T3=(2*pow(parR[i]/parGamma,2));
    double T4=sin(q*parR[i]/(q*parR[i]));
    Summe += T1*(T2+T3*T4);
}
Formfaktor *= Summe;
return pow(Formfaktor,2);
}

double Fourier_Bessel(double *x,double *par){

    double q = sqrt(x[0]);
    const int N = 3;
    double parA[N];
    double parR = par[0]*fm;
    q /= hquerc;
    double Sum1 = 0;
    double Sum2 = 0;
    double Formfaktor = sin(q*parR)/(q*parR);
    for(int i=0;i<N;i++){
        parA[i] = par[i+1];
    }
    for(int i=1;i<=N;i++){
        double T1=pow((-1),i)*parA[i-1]/(pow(i,2)*pow(M_PI,2)-pow(q,2)*pow(parR,2));
        double T2=pow((-1),i)*parA[i-1]/(pow(i,2)*pow(M_PI,2));
        Sum1 += T1;
        Sum2 += T2;
    }

    Formfaktor *= Sum1/Sum2;
    return pow(Formfaktor,2);
}

double Sigma(double *x,double *par){

    double Z=6;
    double M_Kern=12;
    double Energie = 155*MeV;

    double Geschwindigkeit= sqrt(1-pow(((M_Elektron)/(Energie-M_Elektron)),2));
    double Faktor1=1/(1+Energie/(M_Kern*931.4936)*(1-cos(x[0]*deg)));
    double neuer_Mott= pow(((Z*hquerc*alpha)/(2*Energie)),2)*(1/ pow(sin(x[0]*deg/(2)),4))
        *(Faktor1)*(1- pow((Geschwindigkeit),2)* pow(sin(x[0]*deg/(2)),2));
    double Q_squared[1] = {4*Energie*Faktor1*Energie*pow(sin(x[0]*deg/(2)),2)};
    double Formfaktor = Fourier_Bessel(Q_squared,par);
    //double Formfaktor = Sum_of_Gauß(Q_squared,par);
    //double Formfaktor = pow(3*(sin(sqrt(Q_squared[0])*par[0])/pow(
        sqrt(Q_squared[0])*par[0],3)-cos(sqrt(Q_squared[0])*par[0])/pow(
        sqrt(Q_squared[0])*par[0],2)),2)*exp(-1*pow(sqrt(
        Q_squared[0],2)*pow(par[1],2)));
    //double Formfaktor = pow(par[0]*exp(par[1]*pow(Q_squared[0]-par[2],2))+par[3]*exp(
        par[4]*pow(Q_squared[0]-par[5],2))+par[6]*exp(par[7]*pow(
        Q_squared[0]-par[8],2)),2);

```

```

//double Formfaktor = pow(exp(-par[0]*Q_squared[0]) * ( par[1] + par[2]*Q_squared[0]
+par[3]*pow(Q_squared[0],2)+par[4]*pow(Q_squared[0],3)+par[5]
*pow(Q_squared[0],4)+par[6]*pow(Q_squared[0],5)),2);

return Formfaktor*2*M.PI*sin(x[0]*deg)*neuer_Mott;
}

double Asymetrie(double *x, double *par){

double Z = 6;
double M_Kern = 12;
double Beam_Energy = 155*MeV; //in GeV

double Faktor1=1/(1+Beam_Energy/(M_Kern*u)*(1-cos(x[0]*deg)));
double Q_squared = 4*Beam_Energy*Faktor1*Beam_Energy*pow(sin(x[0]*deg/(2)),2);
double Q_w = Z*(1-4*weak_mixing_angle)-(M_Kern-Z);
double Asym = -(G_f*Q_squared*137)/(4*sqrt(2)*M.PI)*Q_w/Z;

return Asym;
}

double AsymInt(double *x, double *par){

return Asymetrie(x, par)*Sigma(x, par);
}

void PlotC12(){
const int nex=9;
vector<double> Energie[nex], Winkel[nex], Wirkungsquerschnitt[nex], FehlerWinkel[nex],
FehlerWirkungsquerschnitt[nex], Mott[nex], Formfaktor[nex], Impulsübertrag[nex],
Formfaktor_Fehler[nex], Impulsübertrag_Fehler[nex];
vector<double> Impulsübertrag_alle, Impulsübertrag_Fehler_alle, Formfaktor_alle,
Formfaktor_Fehler_alle, Winkel_alle,
Wirkungsquerschnitt_alle, Winkel_Fehler_alle, Wirkungsquerschnitt_Fehler_alle;
double Geschwindigkeit, Masse_e, Lichtgeschw, epsilon0, Z, Faktor1, M_Kern, neuer_Mott,
neuer_Formfaktor, neuer_Impulsübertrag, neuer_Formfaktor_Fehler,
neuer_Impulsübertrag_Fehler;

string Datei[9]={ "Determination of Radiative Transition widths of C12 elastic
and inelastic (elastic scattering 250MeV).txt", "Elastic and Inelastic Electron
Scattering for 187-MeV Electrons from C12(Elastic) 187MeV.txt", "Elastic Electron
Scattering from C12 and O16 1970 (21.11.2020)(E0=374.5MeV).txt", "Elastic Electron
Scattering from C14 and C12(E0=374.6MeV).txt", "High-Energy Electron Scattering
and Nuclear structure Determinations of C12(elastic) 187MeV.txt", "Energy dependence
of the form factor for elastic electron scattering from C12(E0=238MeV).txt", "Energy
dependence of the form factor for elastic electron scattering from C12(E0=243MeV).txt",
"Nuclear Charge Distribution and rms Radius of C12 from absolute elastic
electron scattering (E0=240.17MeV).txt", "Nuclear Charge Distribution and rms Radius
of C12 from absolute elastic electron scattering (E0=300.52MeV).txt" };
for (int i=0; i<nex; i++){
read_data (Datei[i], Energie[i], Winkel[i], Wirkungsquerschnitt[i],
FehlerWirkungsquerschnitt[i], FehlerWinkel[i]);
}

Z=6; //muss an den jeweiligen Kern angepasst werden
M_Kern=12; //muss an den jeweiligen Kern angepasst werden
for (int j=0; j<nex; j++){
for (int i=0; i<Energie[j].size(); i++){
Geschwindigkeit= sqrt(1-pow(((M_Elektron)/(Energie[j][i]-M_Elektron)), 2));
Faktor1=1/(1+Energie[j][i]/(M_Kern*u)*(1-cos(Winkel[j][i]*deg)));
neuer_Mott= pow(((Z*hquerc*alpha)/(2*Energie[j][i])), 2)*
(1/ pow( sin(Winkel[j][i]*deg/(2)), 4))*(Faktor1)*(1- pow((Geschwindigkeit), 2)
* pow( sin(Winkel[j][i]*deg/(2)), 2));
Mott[j].push_back(neuer_Mott);
neuer_Formfaktor=Wirkungsquerschnitt[j][i]/Mott[j][i];
Formfaktor[j].push_back(neuer_Formfaktor);
}
}
}

```

```

neuer_Formfaktor_Fehler=FehlerWirkungsquerschnitt[j][i]/Mott[j][i];
Formfaktor_Fehler[j].push_back(neuer_Formfaktor_Fehler);
neuer_Impulsübertrag=4*Energie[j][i]*Faktor1*Energie[j][i]*
pow(sin(Winkel[j][i]*deg/(2)),2);
Impulsübertrag[j].push_back(neuer_Impulsübertrag);
neuer_Impulsübertrag_Fehler=(4*Energie[j][i]*Faktor1*Energie[j][i]*
cos(Winkel[j][i]*deg/(2))*sin(Winkel[j][i]*deg/(2))+4*Energie[j][i]*
pow(sin(Winkel[j][i]*deg/(2)),2)*(Energie[j][i]*sin(Winkel[j][i]*deg)/M.Kern*u)
/pow(((Energie[j][i]/M.Kern*u)*(1-cos(Winkel[j][i]*deg))+1),2))
*FehlerWinkel[j][i]*deg;
Impulsübertrag_Fehler[j].push_back(neuer_Impulsübertrag_Fehler);
Impulsübertrag_alle.push_back(neuer_Impulsübertrag);
Impulsübertrag_Fehler_alle.push_back(neuer_Impulsübertrag_Fehler);
Formfaktor_alle.push_back(neuer_Formfaktor);
Formfaktor_Fehler_alle.push_back(neuer_Formfaktor_Fehler);
Wirkungsquerschnitt_alle.push_back(Wirkungsquerschnitt[j][i]);
Winkel_alle.push_back(Winkel[j][i]);
Wirkungsquerschnitt_Fehler_alle.push_back(FehlerWirkungsquerschnitt[j][i]);
Winkel_Fehler_alle.push_back(FehlerWinkel[j][i]);
}
}
TCanvas* c1 [nexp];
TGraphErrors *gr [nexp];
TGraph *gr1 [nexp];
string Legende[nexp]={"E=250MeV","E=187MeV","E=374.5MeV","E=374.6MeV","E=187MeV",
"E=238MeV","E=243MeV","E=240.17MeV","E=300.52MeV"};

for (int i=0;i<nexp;i++){
string tname = "c_" + to_string(i);
c1[i] = new TCanvas(tname.c_str(),"Elastische Streuung C12",1500,1000);
gr[i] = new TGraphErrors(Winkel[i].size(),&Winkel[i][0],&Wirkungsquerschnitt[i][0],
&FehlerWinkel[i][0],&FehlerWirkungsquerschnitt[i][0]);
gr1[i] = new TGraph(Winkel[i].size(),&Winkel[i][0],&Mott[i][0]);
gr[i]->SetTitle("#theta [xB0];d#sigma/d#Omega [cm^2/sr]");
gr[i]->GetYaxis()->SetTitleOffset(1.5);
gr[i]->SetMarkerStyle(20);
gr[i]->SetMarkerColor(kRed-2);
gr[i]->SetLineColor(kRed-2);
gr[i]->Draw("AP");
gr1[i]->SetMarkerStyle(21);
gr1[i]->SetMarkerColor(kCyan-2);
gr1[i]->SetLineColor(kCyan-2);
gr1[i]->Draw("P");

TLegend* legend = new TLegend(.9,1,.9,1);
legend->SetHeader(Legende[i].c_str(),"C");
legend->AddEntry(gr[i],"Experimentally measured cross section","ep");
legend->AddEntry(gr1[i],"Mott cross section","p");
legend->Draw();
}

TCanvas* c3 = new TCanvas("c3","Wirkungsquerschnitt",1500,1000);
TGraphErrors* gr5 = newTGraphErrors(Impulsübertrag_alle.size(),&Winkel_alle[0],
&Wirkungsquerschnitt_alle[0],
&Winkel_Fehler_alle[0],&Wirkungsquerschnitt_Fehler_alle[0]);
gr5->Draw("AP");
gr5->SetTitle("#theta [xB0];d#sigma/d#Omega [cm^2/sr]");
int Marker2[nexp]={20,34,22,23,33,29,8,43,45};
int Color2[nexp]={6,9,42,1,7,8,34,20,46};

TGraphErrors *gr4 [nexp];
TLegend* legend3 = new TLegend(0.2,0.7,0.6,0.9);
legend3->SetNColumns(2);
for (int i=0;i<nexp;i++){
gr4[i] = new TGraphErrors(Impulsübertrag[i].size(),&Winkel[i][0],
&Wirkungsquerschnitt[i][0],&FehlerWinkel[i][0],&FehlerWirkungsquerschnitt[i][0]);
gr4[i]->Draw("P");
}

```

```

gr4 [i] -> SetMarkerStyle (Marker2 [i]);
gr4 [i] -> SetMarkerColor (Color2 [i]);
gr4 [i] -> SetMarkerSize (0.9);
legend3 -> AddEntry (gr4 [i], Legende [i].c_str (), "ep");
}
legend3 -> Draw ();

TCanvas* c2 = new TCanvas ("c2", "Formfaktor", 1500, 1000);
TGraphErrors* gr2 = new TGraphErrors (Impulsübertrag_alle.size (),
&Impulsübertrag_alle [0],
&Formfaktor_alle [0], &Impulsübertrag_Fehler_alle [0], &Formfaktor_Fehler_alle [0]);
gr2 -> SetMarkerStyle (22);
gr2 -> SetMarkerColor (kBlack);
gr2 -> SetLineColor (kBlack);
gr2 -> SetTitle ("  $Q^2$  [MeV $^2$ ]/c $^2$ ]; |F(Q $^2$ )|^ $2$ ");

//TF1 *f = new TF1 ("f", "pow(exp(-[0]*x) * ([1] + [2]*x + [3]*pow(x,2) + [4]*pow(x,3) +
[5]*pow(x,4) + [6]*pow(x,5)), 2)");
//TF1 *f = new TF1 ("f", "pow([0]*exp([1]*pow(x-[2],2)) + [3]*exp([4]*pow(x-[5],2)) + [6]*
exp([7]*pow(x-[8],2)), 2)");
//TF1 *f = new TF1 ("f", "pow(3*(sin(sqrt(x)*[0])/pow(sqrt(x)*[0],3) -
cos(sqrt(x)*[0])/pow(sqrt(x)*[0],2), 2)*exp(-1*pow(sqrt(x),2)*pow([1],2))");
//TF1 *f = new TF1 ("f", "Sum_of_Gauß, 0, 200e3, 7);
TF1 *f = new TF1 ("f", "Fourier_Bessel, 0, 200e3, 4);
f -> SetNpx (5000);
//f -> SetParNames ("a_{0}", "a_{1}", "a_{2}", "a_{3}", "a_{4}", "a_{5}", "a_{6}", "a_{7}");
//f -> SetParNames ("a_{1}", "a_{2}", "a_{3}", "a_{4}", "a_{5}", "a_{6}", "a_{7}", "a_{8}", "a_{9}");
//f -> SetParNames ("effective nuclear radius", "nuclear skin thickness");
//f -> SetParNames ("#gamma", "R_{1}", "Q_{1}", "R_{2}", "Q_{2}", "R_{3}", "Q_{3}");
f -> SetParNames ("R", "a_{1}", "a_{2}", "a_{3}");
gStyle -> SetOptFit (); // gibt fit parameter an
//f -> SetParameters (9.629e-6, 0.931, 5.174e-6, 2.645e-10, -5.275e-15, 3.989e-20, -1.104e-25);
//f -> SetParameters (0.3632, -1.498e-10, -1.078e4, 1.133e-6, 4.684e-11, 5.365e5,
-0.1055, -6.828e-12, -3.182e5);
//f -> SetParameters (0.01273, 0.0039);
//f -> SetParameters (1.501, 1.189, 0.6242, 1.163, 0.3971, 3.022, 4.668e-9);
f -> SetParameters (4, 0.035, 0.018, -0.0077);
//f -> SetRange (0, 126e3);
gr2 -> Fit (f);
gr2 -> Draw ("AP");

int Marker [nexp] = {20, 34, 22, 23, 33, 29, 8, 43, 45};
int Color [nexp] = {6, 9, 42, 1, 7, 8, 34, 20, 46};

TGraphErrors *gr3 [nexp];
TLegend* legend1 = new TLegend (0.2, 0.7, 0.6, 0.9);
//legend1 -> SetHeader (" ", "C");
legend1 -> AddEntry (f, "fit function", "l");
legend1 -> SetNColumns (2);
for (int i=0; i<nexp; i++){
gr3 [i] = new TGraphErrors (Impulsübertrag [i].size (), &Impulsübertrag [i][0],
&Formfaktor [i][0], &Impulsübertrag_Fehler [i][0], &Formfaktor_Fehler [i][0]);
gr3 [i] -> Draw ("P");
gr3 [i] -> SetMarkerStyle (Marker [i]);
gr3 [i] -> SetMarkerColor (Color [i]);
gr3 [i] -> SetMarkerSize (0.9);
legend1 -> AddEntry (gr3 [i], Legende [i].c_str (), "ep");
}
legend1 -> Draw ();

double Q_squared = 4.5e-3*GeV*GeV;
double Dichte_Graphit = 2.26*g/cm3;
double Dichte_Diamant = 3.51*g/cm3;
double Strom = 150*muA;
double Länge_Target = 2.2*cm;
double Molare_Masse = 12;
double Beam_Energy = 155*MeV;

```

```

double Polarisation = 0.8;
double Integral;

double Q_w = Z*(1-4*weak_mixing_angle)-(M_Kern-Z);
double Asym = -(G_f*Q_squared)/(4*sqrt(2)*M_PI*alpha)*Q_w/Z;
double Fehler_Asym = 0.001*Asym;
double Events = 1/(pow(Fehler_Asym,2));
double Events_pol = 1/(pow(Fehler_Asym*Polarisation,2));
cout << "Events: " << Events << "Events polarisiert: " << Events_pol << endl;

double Luminosität_Graphit = (Strom/Ladung)*Dichte_Graphit*Länge_Target*
Avogadro/Molare_Masse;
double Luminosität_Diamant = (Strom/Ladung)*Dichte_Diamant*Länge_Target*
Avogadro/Molare_Masse;
cout << "Strom: " << Strom << " Avogadro: " << Avogadro << " Dichte_Graphit: "
<< Dichte_Graphit << " Laenge: " << Länge_Target << " Molare Masse: " << Molare_Masse <<
" Ladung: " << Ladung << endl;
cout << "Luminositaet_Graphit: " << Luminosität_Graphit << " Luminositaet_Diamant: "
<< Luminosität_Diamant << endl;
cout << "Asymmetrie: " << Asym << endl;
TF1 *f_sigma = new TF1("f_sigma",Sigma,0,180,4);
TF1 *f_Asym = new TF1("f_Asym",AsymInt,0,180,4);

for (int i=0;i<4;i++){
    f_sigma->SetParameter(i,f->GetParameter(i));
    f_Asym->SetParameter(i,f->GetParameter(i));
}

Integral = f_sigma->Integral(25,45);
Integral *= deg;
cout << "Integral: " << Integral << endl;
double AsymIntegral = f_Asym->Integral(25,45);
AsymIntegral *= deg;
cout << "AsymIntegral: " << AsymIntegral << endl;
double Asym_gemittelt = AsymIntegral/Integral;
double Testwinkel[3] = {25,35,45};
for (int i=0;i<3;i++){
    Faktor1=1/(1+Beam_Energy/(M_Kern*u)*(1-cos(Testwinkel[i]*deg)));
    neuer_Impulsübertrag=4*Beam_Energy*Faktor1*Beam_Energy*pow(sin(Testwinkel[i]*deg/(2)),2);
    cout << "Testwinkel: " << Testwinkel[i] << " Q_squared: " << neuer_Impulsübertrag
<< " Formfaktor: " << f->Eval(neuer_Impulsübertrag) << " Sigma: " <<
f_sigma->Eval(Testwinkel[i]) << endl;
}
double T_Messzeit_Graphit = Events/(Luminosität_Graphit*Integral*3600);
double T_Messzeit_Graphit_pol = Events_pol/(Luminosität_Graphit
*Integral*3600);
cout << "Vermutete Messzeit: " << T_Messzeit_Graphit << "Vermutete Messzeit polarisiert: "
<< T_Messzeit_Graphit_pol << endl;

double Fehler_Asym_gemittelt = 0.001*Asym_gemittelt;
double Events_gemittelt = 1/(pow(Fehler_Asym_gemittelt,2));
double Events_gemittelt_pol = 1/(pow(Fehler_Asym_gemittelt*Polarisation,2));
double T_Messzeit_Graphit_gemittelt = Events_gemittelt/(Luminosität_Graphit
*Integral*3600);
double T_Messzeit_Graphit_gemittelt_pol = Events_gemittelt_pol/(Luminosität_Graphit
*Integral*3600);
cout << "Events_gemittelt: " << Events_gemittelt << "Events_gemittelt_pol: "
<< Events_gemittelt_pol << endl;
cout << "Asymmetrie gemittelt: " << Asym_gemittelt << endl;
cout << "Vermutete Messzeit gemittelt: " << T_Messzeit_Graphit_gemittelt
<< "Vermutete Messzeit gemittelt polarisiert: " << T_Messzeit_Graphit_gemittelt_pol << endl;

double Rate = Luminosität_Graphit * Integral;
cout << "Rate: " << Rate << endl;
cout << muA << endl;
}
/*****
"Constants.hh":

```

```

#ifndef PHYS.CONST
#define PHYS.CONST 1
#include <math.h>

const double MeV = 1;
const double s = 1;
const double rad = 1;
const double deg = M_PI/180;
const double A = 1;
const double cm = 1;
const double g = 1;

const double m = 1e2*cm;
const double fm = 1e-15*m;
const double nm = 1e-3*m;

const double cm2 = cm*cm;
const double cm3 = cm*cm*cm;
const double m2 = m*m;
const double m3 = m*m*m;
const double fm2 = fm*fm;
const double fm3 = fm*fm*fm;
const double barn = 1e-28*m2;
const double mbarn = 1e-3*barn;

const double muA = 1e-6*A;

const double GeV = 1e3*MeV;

const double c = 299792458*m/s;
const double alpha = 1/137.035999;
const double hquerc = 197.326980*MeV*fm;
const double G_f = 1.166378e-5/(GeV*GeV);
const double M_Elektron = 0.510998950*MeV;
const double u = 931.494102*MeV;
const double weak_mixing_angle = 0.2312;
const double Avogadro = 6.02214076e23;
const double Ladung = 1.602176634e-19*A*s;

const double minute = 60*s;
const double h = 60*minute;
const double d = 24*h;

#endif

```

9.2 Plots of the measured cross sections for different nuclei

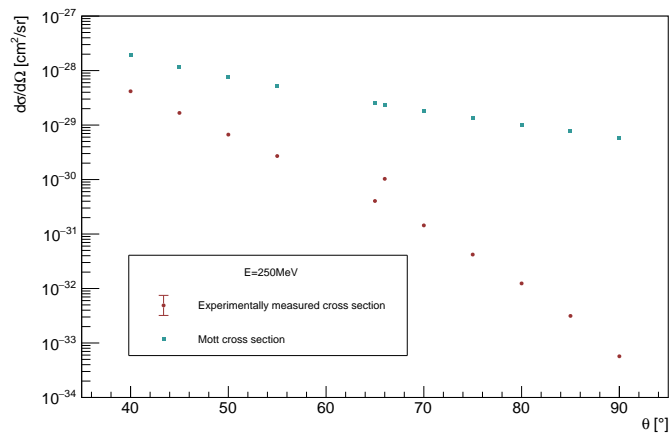


Figure 80: Cross section for elastic electron scattering off the ground state of ^{12}C , [10]

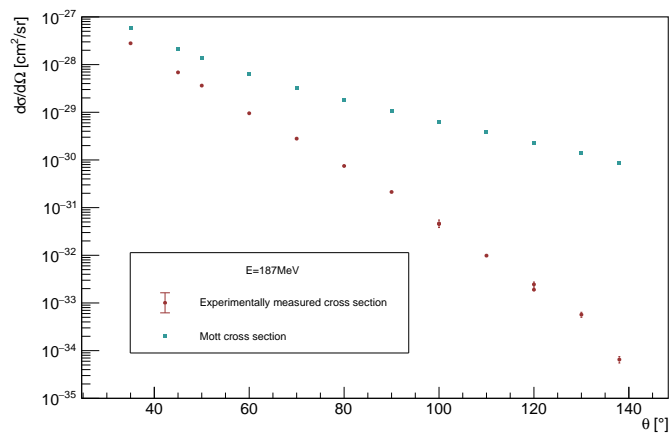


Figure 81: Cross section for elastic electron scattering off the ground state of ^{12}C , [11]

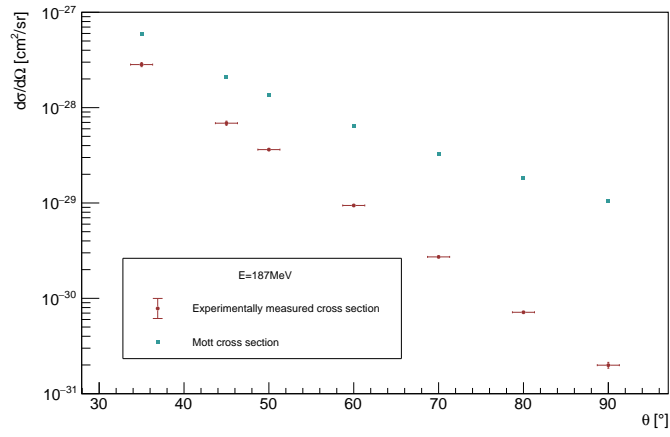


Figure 82: Cross section for elastic electron scattering off the ground state of ^{12}C , [15]

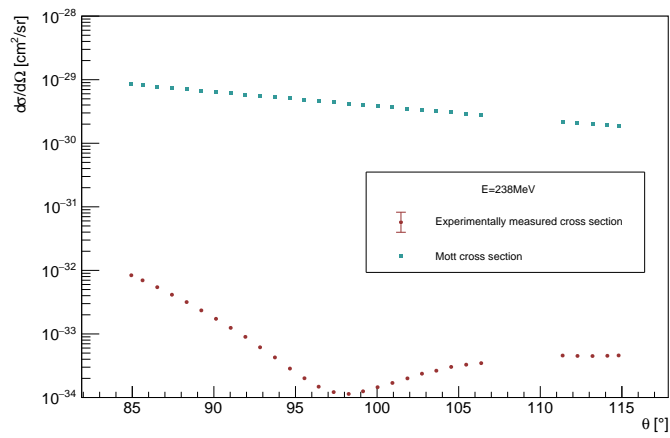


Figure 83: Cross section for elastic electron scattering off the ground state of ^{12}C , [14]

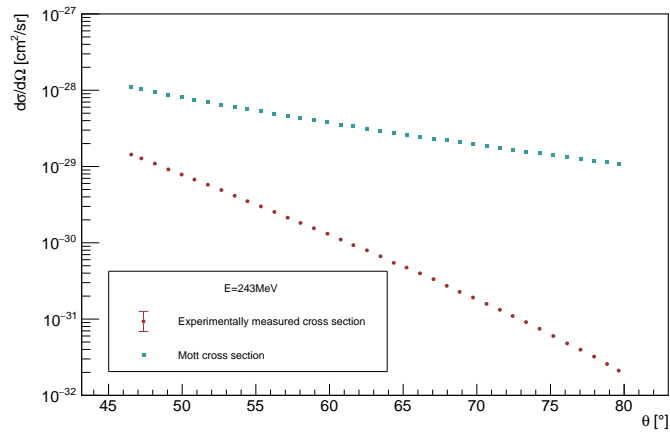


Figure 84: Cross section for elastic electron scattering off the ground state of ^{12}C , [14]

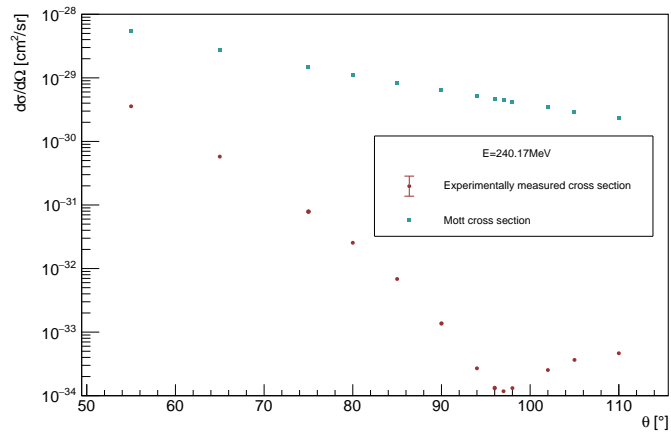


Figure 85: Cross section for elastic electron scattering off the ground state of ^{12}C , [16]

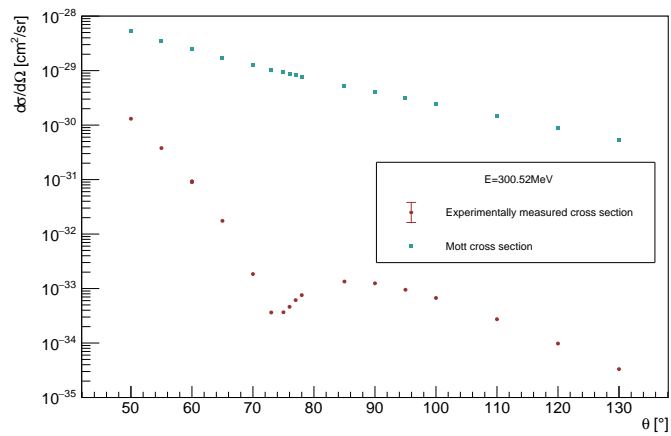


Figure 86: Cross section for elastic electron scattering off the ground state of ^{12}C , [16]

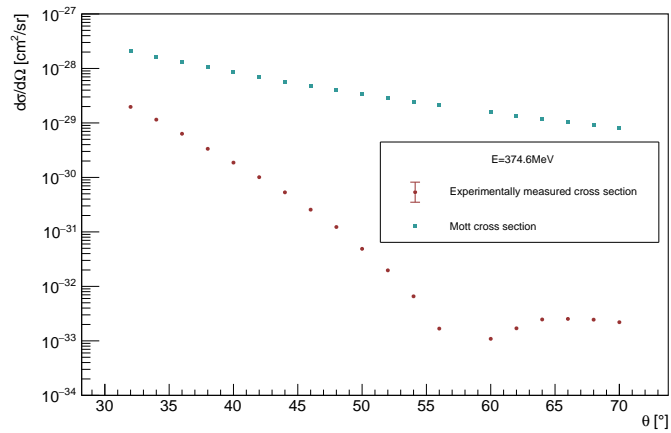


Figure 87: Cross section for elastic electron scattering off the ground state of ^{12}C , [13]

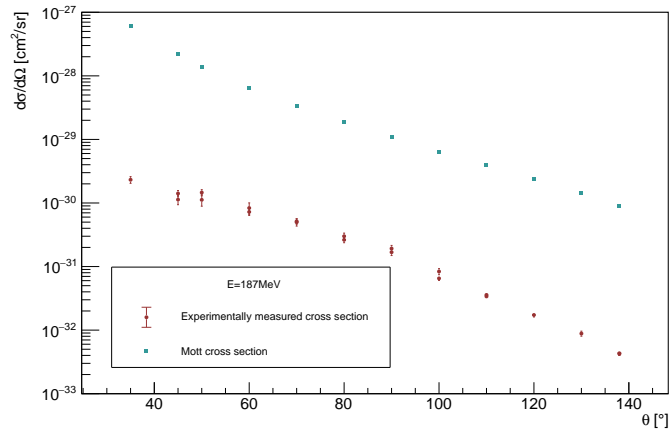


Figure 88: Cross section for inelastic electron scattering off the first excited state $E_x = 4.43$ MeV of ^{12}C , [11]

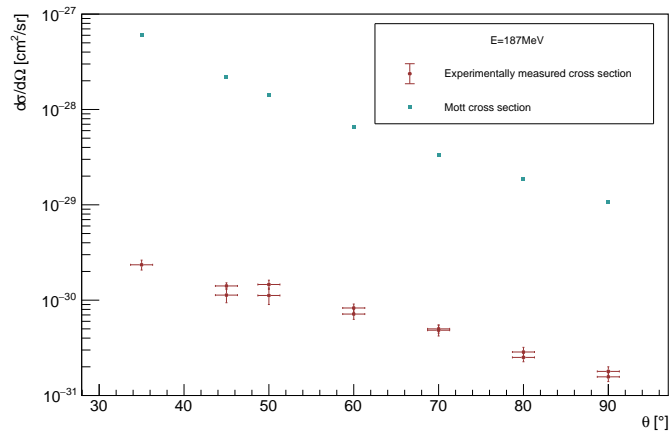


Figure 89: Cross section for inelastic electron scattering off the first excited state $E_x = 4.43$ MeV of ^{12}C , [15]

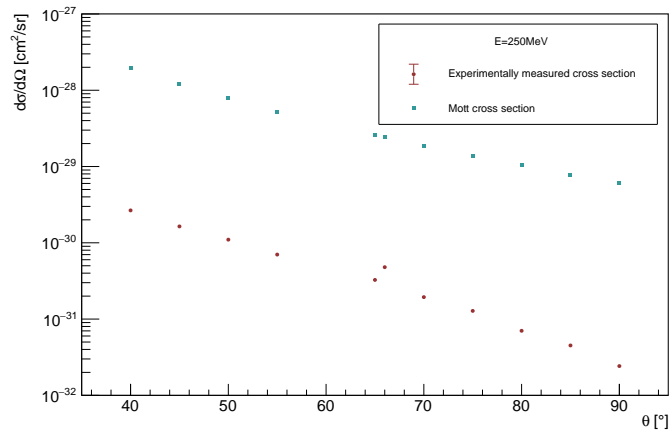


Figure 90: Cross section for inelastic electron scattering off the first excited state $E_x = 4.43$ MeV of ^{12}C , [10]

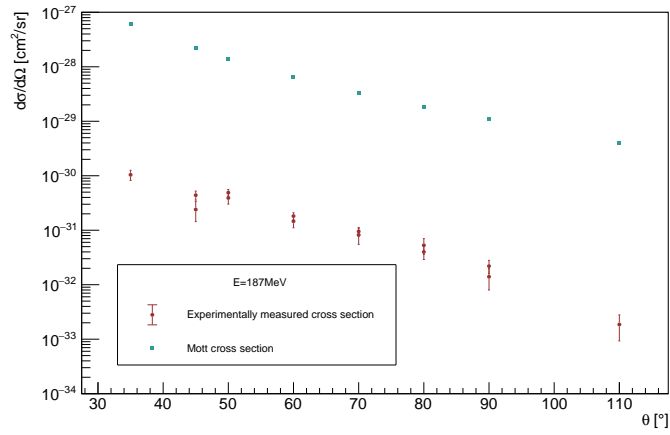


Figure 91: Cross section for inelastic electron scattering off the second excited state $E_x = 7.66$ MeV of ^{12}C , [11]

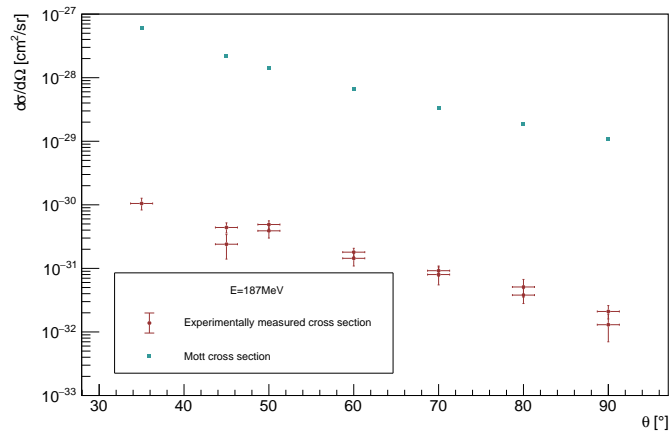


Figure 92: Cross section for inelastic electron scattering off the second excited state $E_x = 7.66$ MeV of ^{12}C , [15]

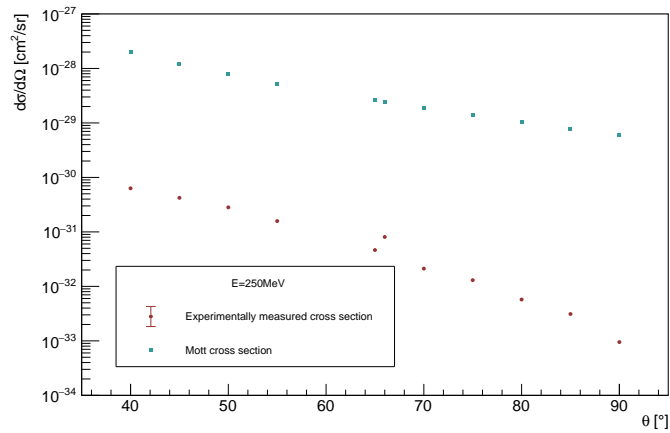


Figure 93: Cross section for inelastic electron scattering off the second excited state $E_x = 7.66$ MeV of ^{12}C , [10]

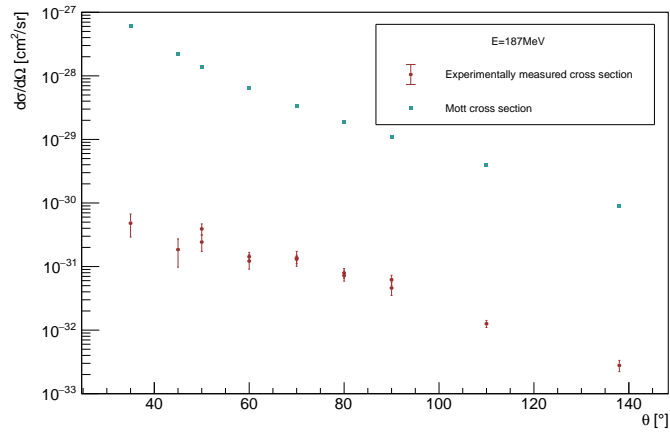


Figure 94: Cross section for inelastic electron scattering off the third excited state $E_x = 9.64$ MeV of ^{12}C , [11]

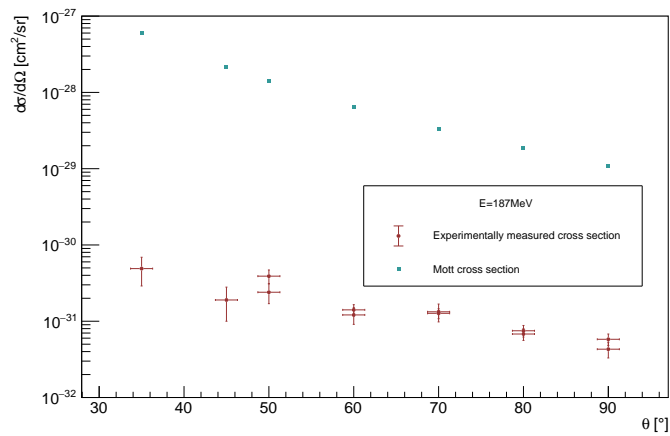


Figure 95: Cross section for inelastic electron scattering off the third excited state $E_x = 9.64$ MeV of ^{12}C , [15]

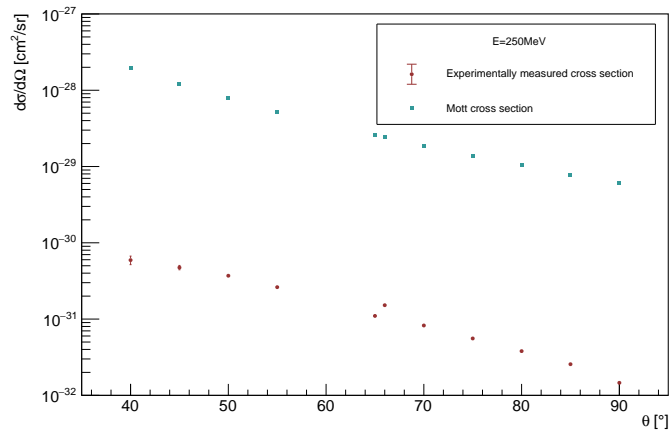


Figure 96: Cross section for inelastic electron scattering off the third excited state $E_x = 9.64$ MeV ^{12}C , [10]

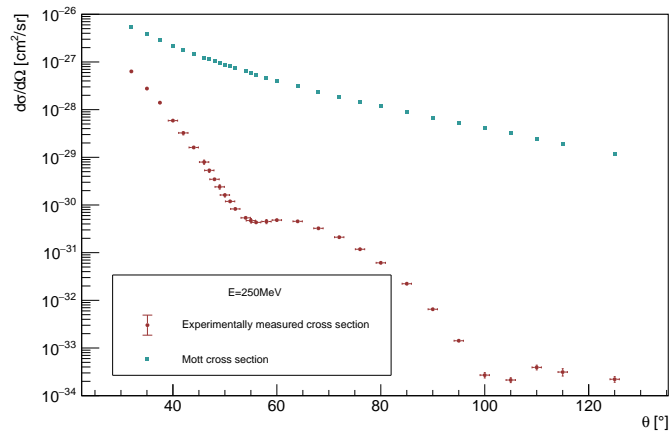


Figure 97: Cross section for elastic electron scattering off the ground state of ^{40}Ca , [17]

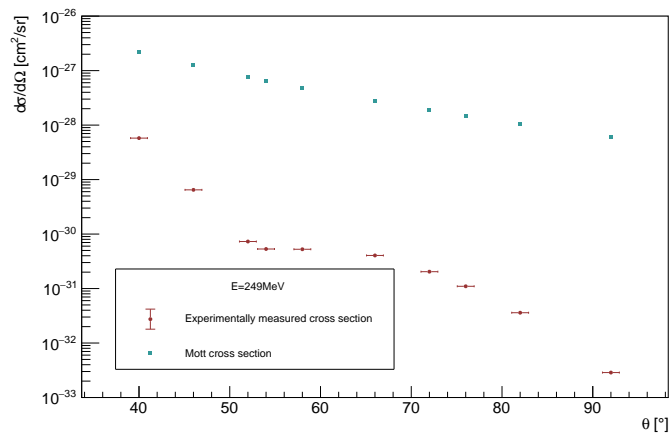


Figure 98: Cross section for elastic electron scattering off the ground state of ^{40}Ca , [19]

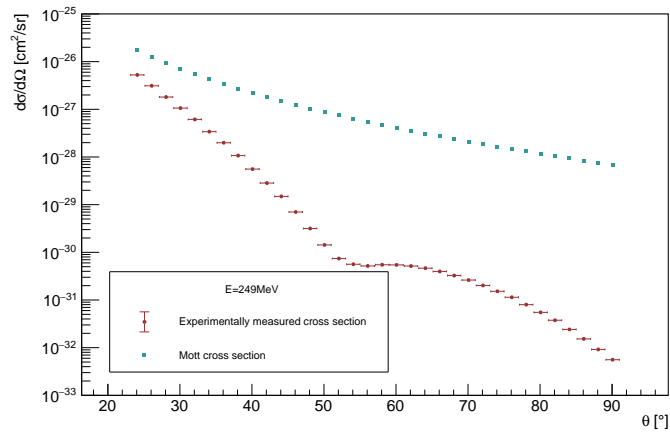


Figure 99: Cross section for elastic electron scattering off the ground state of ^{40}Ca , [19]

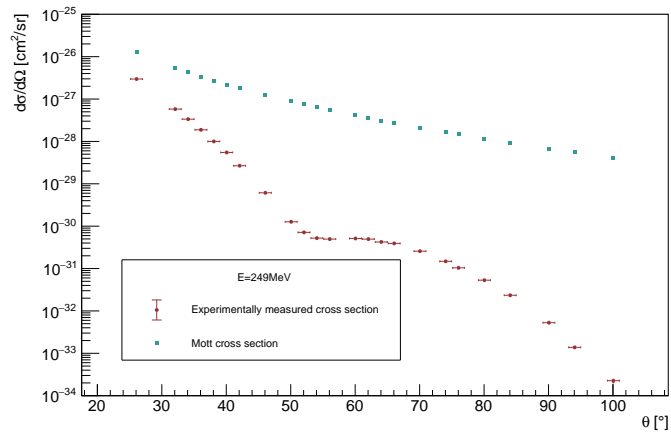


Figure 100: Cross section for elastic electron scattering off the ground state of ^{40}Ca , [19]

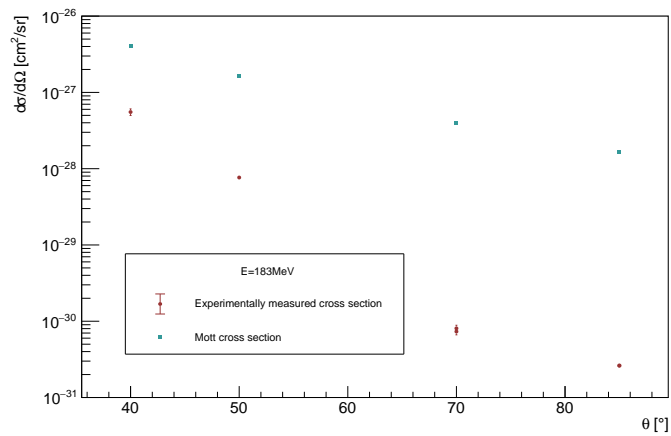


Figure 101: Cross section for elastic electron scattering off the ground state of ^{40}Ca , [20]

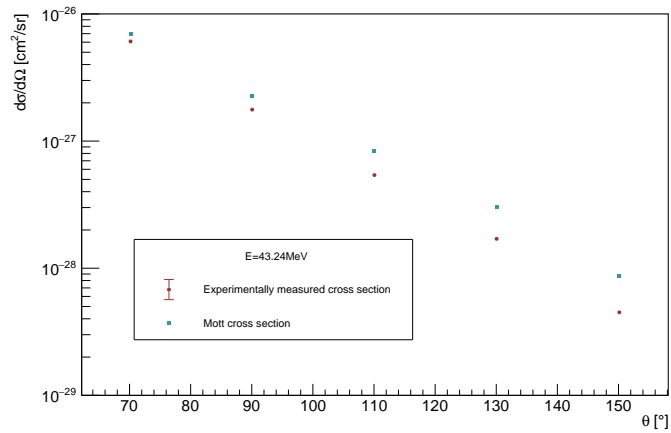


Figure 102: Cross section for elastic electron scattering off the ground state of ^{40}Ca , [18]

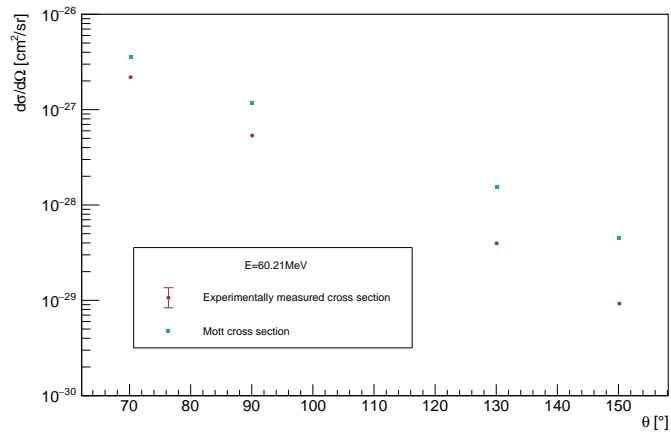


Figure 103: Cross section for elastic electron scattering off the ground state of ^{40}Ca , [18]

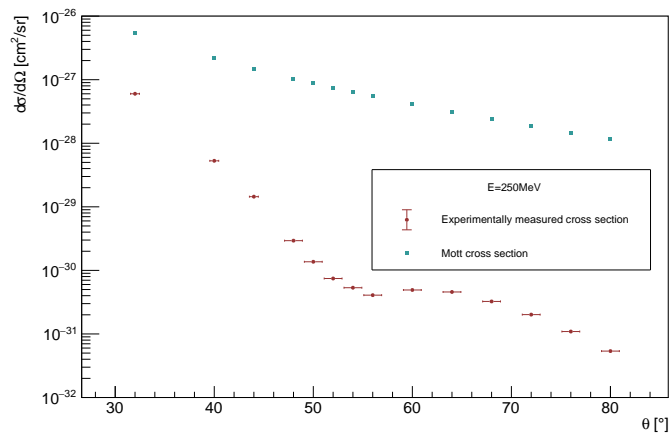


Figure 104: Cross section for elastic electron scattering off the ground state of ^{42}Ca , [17]

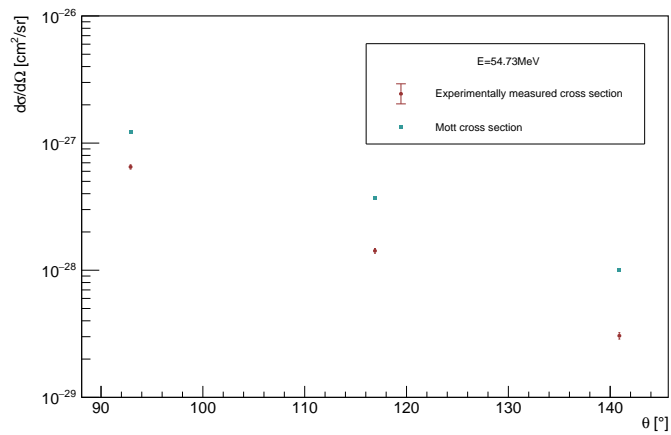


Figure 105: Cross section for elastic electron scattering off the ground state of ^{42}Ca , [21]

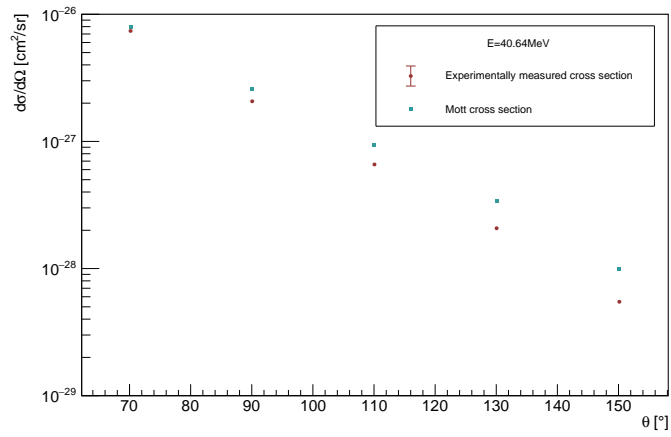


Figure 106: Cross section for elastic electron scattering off the ground state of ^{48}Ca , [17]

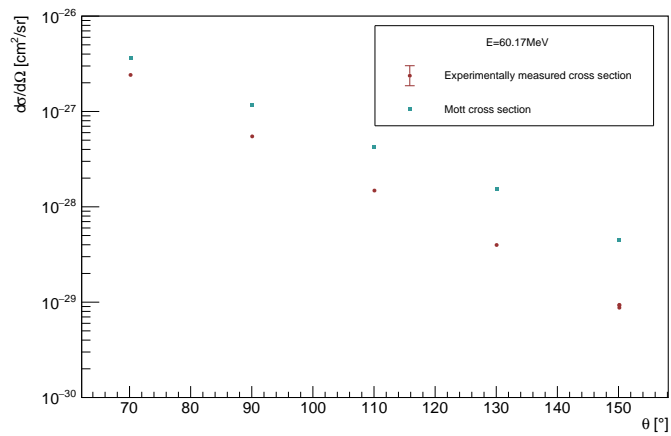


Figure 107: Cross section for elastic electron scattering off the ground state of ^{48}Ca , [18]

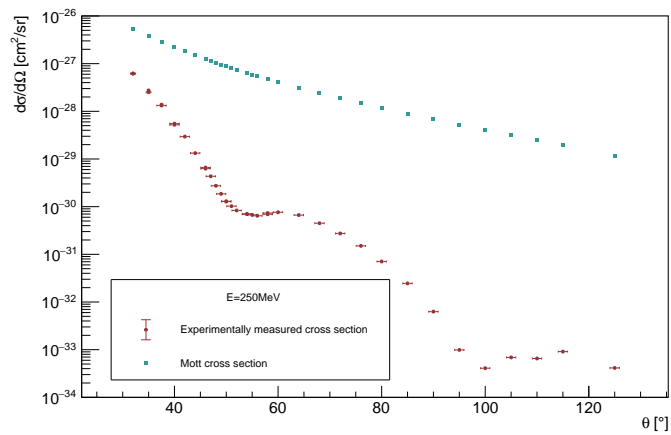


Figure 108: Cross section for elastic electron scattering off the ground state of ^{48}Ca , [17]

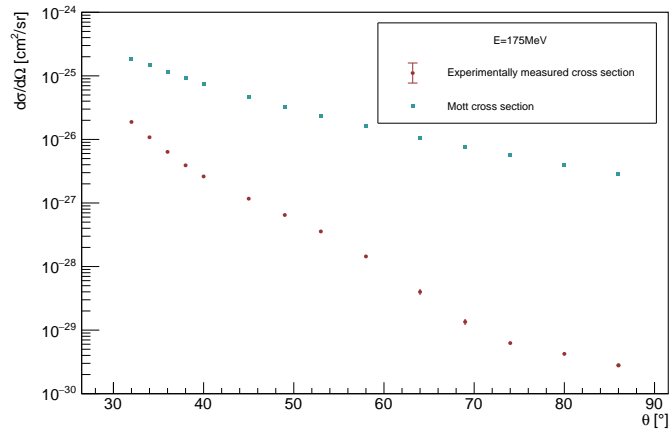


Figure 109: Cross section for elastic electron scattering off the ground state of ^{208}Pb , [22]

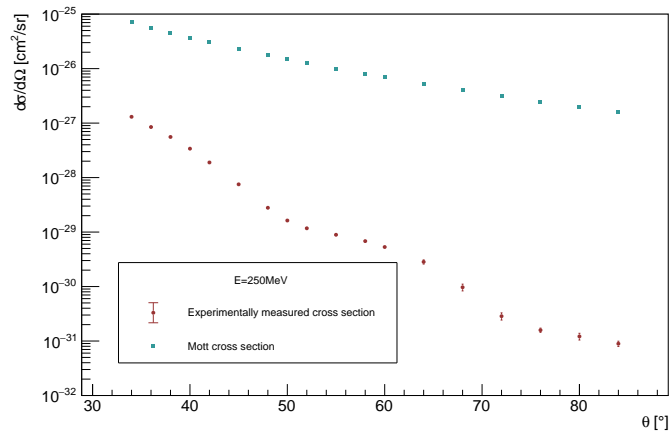


Figure 110: Cross section for elastic electron scattering off the ground state of ^{208}Pb , [22]

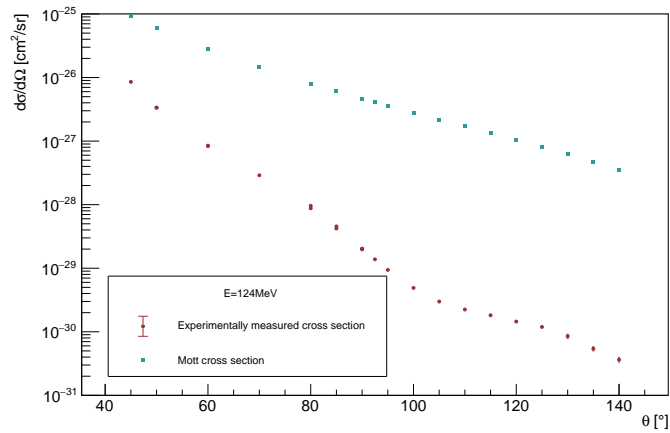


Figure 111: Cross section for elastic electron scattering off the ground state of ^{208}Pb , [23]

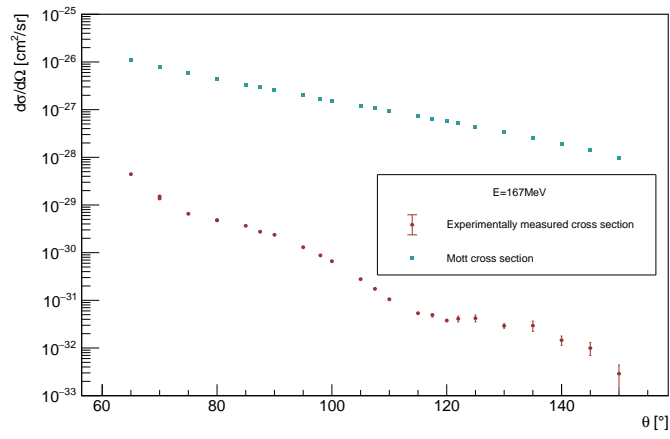


Figure 112: Cross section for elastic electron scattering off the ground state of ^{208}Pb , [23]

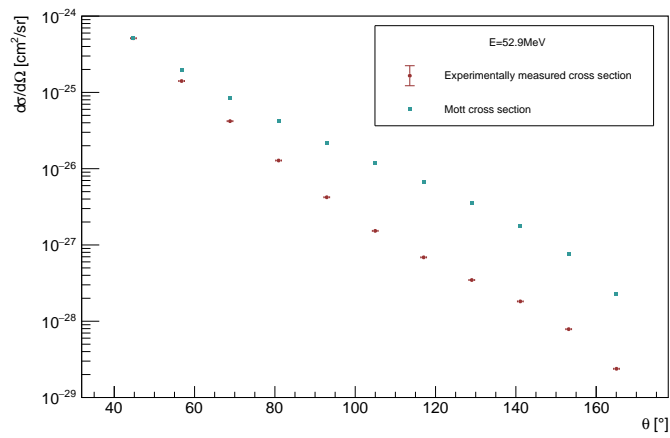


Figure 113: Cross section for elastic electron scattering off the ground state of ^{208}Pb , [25]

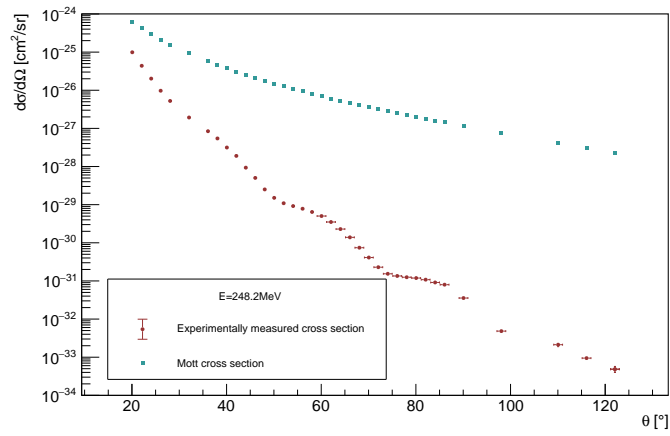


Figure 114: Cross section for elastic electron scattering off the ground state of ^{208}Pb , [25]

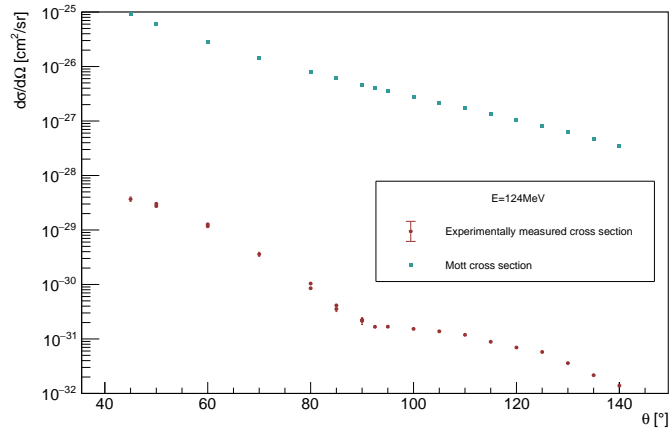


Figure 115: Cross section for inelastic electron scattering off the first excited state $E_x = 2.6$ MeV of ^{208}Pb , [24]

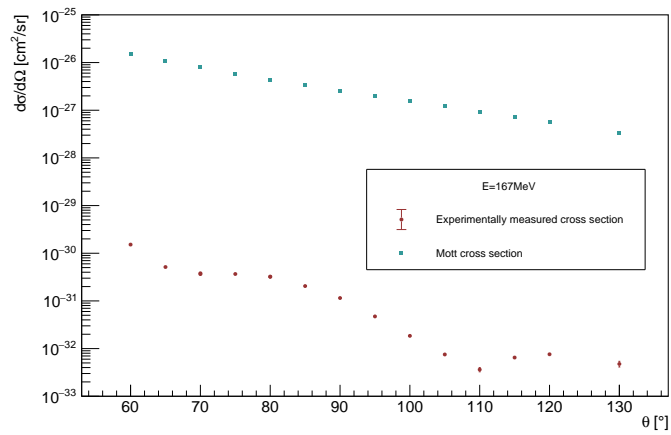


Figure 116: Cross section for inelastic electron scattering off the first excited state $E_x = 2.6$ MeV of ^{208}Pb , [24]

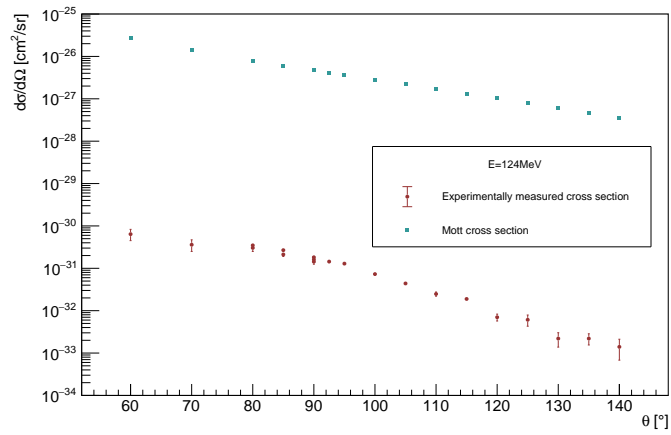


Figure 117: Cross section for inelastic electron scattering off the second excited state of $E_x = 3.2$ MeV of ^{208}Pb , [24]

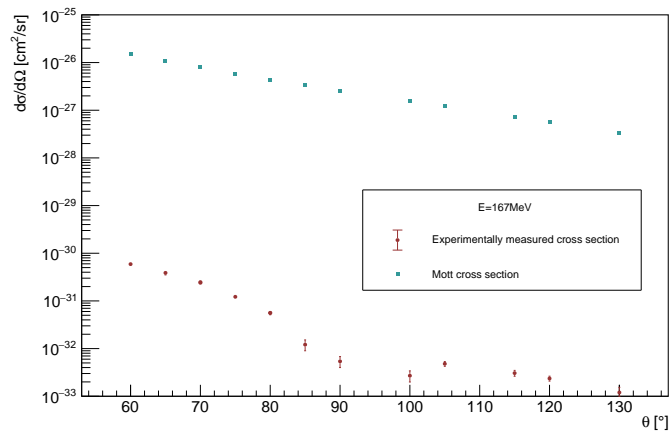


Figure 118: Cross section for inelastic electron scattering off the second excited state $E_x = 3.2$ MeV of ^{208}Pb , [24]